US Army Corps
of Engineers®
Engineer Research and
Development Center

Study of Complex Flows in the Lower San Bernard River, Texas

Jose A. Sanchez and Trimbak M. Parchure

September 2001

20020305 182

Study of Complex Flows in the Lower San Bernard River, Texas

by   Jose A. Sanchez, Trimbak M. Parchure

Coastal and Hydraulics Laboratory
U.S. Army Engineer Research and Development Center
3909 Halls Ferry Road
Vicksburg, MS 39180-6199

Final report

Prepared for   U.S. Army Corps of Engineers
Washington, DC 20314-1000

Contents

Preface

A numerical model study of the complex flow pattern in the vicinity of the mouth of San Bernard River, Texas, was conducted at the Coastal and Hydraulics Laboratory (CHL) of the U. S. Army Engineer Research and Development Center (ERDC), Vicksburg, MS, during 1999 - 2000. The U. S. Army Engineer District, Galveston, provided funding for this study. Dr. Trimbak M. Parchure, research hydraulic engineer, was the principal investigator for the project. Dr. Parchure prepared this report jointly with Mr. Jose Sanchez. Mr. Timothy Fagerburg and Mr. Howard Benson of CHL collected and provided the field data required for this study.

Dr. Parchure and Mr. Jose Sanchez conducted the work under general supervision of Dr. Robert McAdory, Chief, Tidal Hydraulics Branch, Mr. Thomas W. Richardson, Acting Director, CHL, Mr. Thomas J. Pokrefke, Acting Deputy Director, CHL, and and Dr. James R. Houston, former Director, CHL.

During the preparation and publication of this report, Dr. James R. Houston was the Director of ERDC, and COL John W. Morris III, EN, was Commander and Executive Director.

1   Introduction

Background

The San Bernard River, Texas, joins the Gulf of Mexico between the mouths of the Colorado River on the west and the Brazos River on the east (Figure 1). The Gulf Intracoastal Waterway (GIWW) runs roughly parallel to the shore and intersects all the three rivers. Two floodgates have been provided on the Brazos River and a navigation lock has been provided on the Colorado River at the respective intersections of the rivers with the GIWW. The floodgates are 22.86 m (75 ft) wide. The construction of these gates was completed in September 1943. Hauck (1992) has reported hydrodynamics at the mouth of the Colorado River. The two Brazos River floodgates are called the west and east gate referring to their respective locations on the riverbank. These floodgates have been in existence for the past 50 years. Both floodgates are supposed to be kept closed most of the time so as to arrest sediments from the rivers getting into the GIWW and thus reduce the cost of maintenance dredging. The gates are opened only when a barge wants to pass through and then closed immediately thereafter. Routine small craft traffic exists through the upper part of San Bernard River and through the GIWW.

The reach of the San Bernard River south of the intersection of GIWW up to its mouth has silted up substantially over the last few years, and very few pleasure boats, if any, use this reach because the heavy sedimentation has made it hazardous for safe navigation. The U.S. Army Corps of Engineers is responsible for maintaining adequate navigable depths in the GIWW. However, the Corps is not responsible for navigation in other reaches of the rivers. Hence, the reach of the San Bernard River south of GIWW has never been dredged in the recent past. The mouth of the San Bernard River does not have any manmade structures such as jetties, and the river mouth has been shifting its location towards the west over the past few years of heavy sediment transport in the westerly direction, perhaps from the mouth of the Brazos River.

The Problem

Water levels and currents along the coastal inlet waters of Texas are influenced by the astronomical tide, wind, and river flows. Often, the river flows and wind-induced currents dominate the hydrodynamics of the shallow-water bays

and channels in Texas, particularly during times of high river discharges and during passage of weather fronts that occur from October through May. The Texas portion of GIWW is 685.58 km (426 miles) long and runs through many constricted areas, including approximately 6.43-km- (4-mile-) long segment between the Brazos River and the San Bernard River (Figure 2). This area is the focus of this study. River discharges significantly increase the currents in the river channel and through the GIWW in such constricted areas.

Although there are no written records, the barge navigators have been complaining for about 15 years that they experience a strong west to east current through the Brazos west gate, primarily during high discharge in the San Bernard River. It is presumed that when the gates are open, high river flow from the San Bernard is diverted to sea through the GIWW and the Brazos River causing increased west to east flow velocity at the west gate. It is not known why the complaints have occurred only over the past 15 years while the gates have been there for more than 50 years. Increased length and width of barges over the recent years may be partly responsible for the situation; however, changes in the hydro-dynamic conditions are suspected to be the major reason. Two large shallow lakes on the south are connected to the GIWW, and marshlands on the east are connected to the San Bernard River through McNeal Bayou. McNeal Bayou has two lakes, namely McNeal Lake and Pelican Lake along its course (Figure 2). The hydraulic site conditions are complicated due to storage and release of floodwater in these water bodies. Studies to investigate the problem were performed by the Coastal and Hydraulics Laboratory (CHL) of the U.S. Army Engineer Research and Development Center (ERDC) for the U.S. Army Engineer District, Galveston.

Objective

The main objective of the study was to construct a verified, working numeri-cal model of the relevant water bodies that are hydraulically connected and make an attempt to correctly simulate the unusual hydraulic conditions experienced at the site. Field data and information obtained from the site on the hydrodynamic parameters relevant to the study were used for model verification. In addition to investigating preliminary plans for improving flow conditions in the area of interest, this model will also be useful in the future investigation of inlet hydro-dynamics and evaluation of alternative remedial measures for improving the flow pattern.

Scope of Model Study

The scope of the model study mainly included development of a two-dimensional (depth-averaged) hydrodynamic model covering the relevant area with an appropriate grid resolution, which will run using RMA2 code (Appendix A). Investigations were focused on two important sites, namely the west floodgate at the Brazos River and the intersection of the GIWW with the San Bernard River.

New field data collected by ERDC were analyzed and results were used for model verification.

Study of coastal processes and stability of the San Bernard River mouth were outside the scope of work for this report. Development of restoration plans for Jones Lake and the sedimentation aspects of any river mouth modification were not included in the scope of work.

2   Field Data

Introduction

Attempts were made to obtain field data already available in literature. Mason (1981) has described hydraulics and stability of five coastal inlets. This report covers Freeport Harbor entrance, San Louis pass, Galveston Bay entrance, Rollover pass and Sabine pass. It does not include San Bernard River entrance. This inlet has not been the subject of investigations probably because it is not significant in the context of any commercial or recreational traffic. Other reports or papers were not found in literature. Data on routine atmospheric and hydrologic parameters are available from the National Oceanic and Atmospheric Administration. Since required field data were not available, the Galveston District requested ERDC-CHL to collect the necessary data for use of the numerical model study.

Site Conditions

During major floods, the San Bernard River overflows its banks into a wide floodplain, which is typical for Texas coastal streams. The manmade development at several places along the river has apparently encroached on the floodplains confining more water in the river channel with less escaping into the flat overland areas. Dredged material disposal sites were located near the river mouth in the past years, which may be preventing natural floodplain overland flow between the GIWW and the sea, thus forcing the flow elsewhere, probably eastward into the GIWW. Two large and shallow lakes, known as Cedar Lakes, are located between the GIWW and the shoreline on the west side of the San Bernard River. These are connected to the GIWW at least at two locations through narrow channels. Hence, they participate in attenuation of tides as well as floodwater.

Redfish Bayou, McNeal Bayou, and Jones Creek are three small drains joining the San Bernard River on the north side of the GIWW. McNeal Bayou has McNeal Lake, and Pelican Lake and Jones Creek has Jones Lake along their respective paths leading to the San Bernard River (Figure 2). Extensive marshlands in the area are also indirectly connected to the San Bernard River. The resulting hydraulic conditions at the site are extremely complicated due to storage and release of floodwater in these water bodies.

Objective and Scope

The purpose of the field investigation was to obtain information, which will best describe the hydrodynamic parameters relevant to navigation through the study area. The field data have been used for a better understanding of site conditions and also for the verification of the numerical model.

The following field data were collected:

a. Tides: Tidal data were collected at nine stations at and around the intersection of the San Bernard River with the GIWW, along the San Bernard River and along the GIWW.

b. Currents: Current velocity was measured along five transects on August 26, 1999, using Acoustic Doppler Current Profiler (ADCP), which gave complete distribution of velocity over the cross section and also the bathymetry of each transect.

c. Bathymetry: About 1-mile reach on the north, west, and east sides of the intersection of the San Bernard River with the GIWW were surveyed. The entire reach of San Bernard River south of the GIWW along with a portion of the shoreline on each side of the mouth of the San Bernard River was surveyed. In addition, bathymetric transects were conducted for covering the northern part of the San Bernard River, Cedar Lake, and other areas that were included in the numerical model.

d. Suspended sediment and salinity: Water samples were collected at the locations of velocity transects at the deepest point of transect. Samples were collected near surface, middepth, and near-bottom, which were analyzed for salinity and total suspended matter.

e. Bottom sediment: Surface bed sediment samples were collected at 22 locations, which were analyzed for particle size distribution.

All the field data were processed at ERDC-CHL, and a report on the same is under preparation. Results of additional analysis of the field data relevant to the numerical model study are given in this report.

3 Field Data Analysis

Tides

Tide recorders were installed at nine stations at and around the intersection of the San Bernard River with the GIWW, along the San Bernard River and along the GIWW. The locations are shown in Figure 3 by serial numbers 1 through 8 and 10. The gage at location 9 was on land. It was not a tide gage but a barometric gage for recording atmospheric pressure. Totally submersible sensors that internally record water temperature and total (hydrostatic plus atmospheric) pressure were used. Water level changes were worked out for all the gages by subtracting atmospheric pressure from the total pressure.

The installation of gages was done prior to the hydrographic survey work, and they were left at site for about 3 months. The gages were serviced once a month and data were retrieved during each visit. Locations of these gages were as follows:

a. Sta 1: About 800 m inside the mouth of the San Bernard River

b. Sta 2: On San Bernard River about 400 m (1,312 ft) south of the intersection.

c. Sta 3: On San Bernard River about 1.6 km (1 mile) north of the intersection.

d. Sta 4: In San Bernard River about 9 km (5.6 miles) north of the intersection.

e. Sta 5: In GIWW about 7 km (4.3 miles) west of the intersection.

f. Sta 5A: About 2 km (1.24 miles) west of tide Gage 5 location (Figure 4).

g. Sta 6: At the intersection with GIWW.

h. Sta 6A: About 1 km (0.62 miles) east of tide Gage 6 location (Figure 4).

i. Sta 7: In GIWW about 1.2 km (0.75 miles) east of the intersection.

j. Sta 8: In GIWW about 500 m (1,640 ft) west of the west floodgate on the Brazos River.

k. Sta 10: On the east bank of Brazos River, 15.24 m (50 ft) south of its intersection.

All the tide gages, 1 through 8 were installed on July 13-14, 1999. Gage 10 on the Brazos River was installed on August 25. The barges plying in the vicinity knocked down recorders at stations 5 and 6 soon after their installation. Hence, they were replaced by installing tide recorders at stations 5A and 6A (Figure 4). Tidal data were obtained over the period August 1999 through October 1999 or more (Table 1). All the gages were pulled out on 16 November 1999. Tide gage at only one station, namely sta 3, was left operating at the site in anticipation of a second field data collection effort during a high river flow. It has recorded data until July 2000 with a few interruptions. As an illustration, tides observed at all the stations are plotted in Figures 5 through 9 for August 1999.

River Flows

The San Bernard River and the Brazos River are connected to each other by the GIWW close to their mouths. Hence, a considerable quantity of water is exchanged between the two rivers, requiring them to be considered as one system. The San Bernard River, located in Fort Bend County, has a drainage area of 1,882.9 sq km (727 square miles) (Figure 10). Brazos River, also located in Fort Bend County, has a drainage area of 117,430 sq km (45,340 square miles), which is more than 60 times that of San Bernard River.

U. S. Geological Survey has maintained gages near Boling, TX, for the San Bernard River and near Rosharon, TX, for the Brazos River. The gage data are converted into daily mean discharge data by using an established correlation. The daily mean discharge data were retrieved from the National Water Information System files called ADAPS. Daily average discharges for the San Bernard River for 10 years from 1990 through 1999 are plotted in Figures 11 through 15. Daily average discharges for the Brazos River for 10 years from 1990 through 1999 are plotted in Figures 16 through 20. Five-day moving averages were worked out for the Brazos River for the years 1990, 1991, and 1992. These are shown in Figures 21 and 22. A comparison of daily plots and corresponding moving average plots did not show any significant change.

It was necessary to select pattern and discharge magnitudes of the San Bernard and the Brazos Rivers for simulation in the numerical model. In the absence of measured water levels and currents under high discharge in the San Bernard River, discharge data over the past 10 years from 1990 to 1999 were examined to get the order of magnitude of high flows. It was seen that the daily maximum river discharge varied between 178 to 549 cu m/s (6,290 to 19,400 cfs). Such high flows in San Bernard River did not sustain for more than a day or two. The catchment area of San Bernard River is relatively small and narrow. Hence, the pattern of high flows in the river is closer to flash flows lasting over a short

time. The numerical model was run with tides over a 6-day duration. Hence, river flows were also required over the same duration. Based on the 10-year data, the maximum discharge values of 28.3, 141.5, 283, and 566 cu m/s (1,000, 5,000, 10,000 and 20,000 cfs) were selected for San Bernard River. The simultaneous maximum values of 254.7, 1,924, 2,122, and 2,377 cu m/s (9,000, 68,000, 75,000, and 84,000 cfs) were selected for the Brazos River. A 6-day hydrograph was constructed for each maximum discharge based on the past data. These hydrographs, which were used for running the numerical model for four sets of high discharge runs, are given in Figures 23 through 26.

Inlet

Jetties have been constructed at the mouth of the Brazos River; hence the inlet has stabilized at the designated location. On the other hand, San Bernard Inlet has been shifting its location over the past several years. No measures have been taken for stabilizing its position. Inlet geometry in 1971 is shown in Figure 27. An old (circa 1971) aerial photo (Figure 28) of the inlet shows heavy accumulation of sediment on the east side and a relatively perpendicular alignment of the lower segment of the river to the general shoreline. Figure 29 shows the river mouth in 1984. A recent (circa 1998) aerial photograph (Figure 30) shows significant changes at the mouth. Net direction of littoral drift from east to west is clearly shown by the heavy sediment accumulation on the east side of the inlet and beach erosion on the west side. The inlet alignment has significantly changed; its location has shifted several hundred meters to the west of its earlier position on the shoreline. Figure 31 shows an aerial photo of the recent alignment of the mouths of the San Bernard and Brazos Rivers. It is seen that the jetties at the mouth of the Brazos River have been effective in preventing migration of its mouth along the shoreline.

The practical problem of estimating net sand transport through a tidal inlet in the absence of direct, long-term measurements was handled by Bales and Holly (1989) for the Rollover Pass Inlet, TX. However, measures for ensuring inlet stability are best evaluated from physical or numerical model studies. Such studies need to take into account the relative impacts of river discharge, inlet hydraulics, and littoral drift. It also includes design of an optimum inlet cross section, which would maintain essentially through tidal action alone. Field data collected specifically for this type of study is crucial for model verification. Aspects related to the stability of the San Bernard River mouth will not be considered here.

Bed Sediment

Surface bed samples were collected at 22 locations within the study area. These were analyzed to determine particle-size distribution. The results of analyses are listed in Table 2 and plotted in Figure 32. An illustration of the size distribution curve is given in Figure 33.

Based on the median diameter, the samples may be classified as follows:

Less than 4 microns (clay)	5 samples
Between 4 and 64 microns (silt)	12 samples
Between 64 and 125 microns (very fine sand)	3 samples
Between 125 and 250 microns (fine sand)	2 samples

The samples are predominantly in the silt category.

Suspended Sediment

Water samples were collected at 5 transects shown in Figure 34. The samples were collected at 2 ft below surface, middepth and close to bottom at approximately 1-hour intervals. Standard filtration procedure was used to determine the weight of total suspended solids in each sample. The results for the five transects are given in Table 3 through Table 7 respectively. An illustration of variation in suspended sediment concentration with time is plotted in Figure 35.

The following conclusions are drawn from the limited data given in Table 3 through Table 7:

a. The suspended sediment concentration varied between 19 and 149 mg/L near surface, 21 and 209 mg/L at middepth, and between 27 and 402 mg/L near bed.

b. Variation in sediment concentration over the vertical within the water column was noticed.

c. As would be expected, the near-bottom suspension concentration is always higher than that at middepth and near surface.

Salinity

Water samples were collected at 5 transects shown in Figure 34. The samples were collected on August 26, 1999, 0.61 m (2 ft) below surface, middepth and close to bottom at approximately 1-hr intervals. Standard equipment was used to determine the salinity of each sample. The results for the five transects are given in Table 8 through Table 12 respectively. An illustration of variation in salinity with time is plotted in Figure 36.

The following conclusions are drawn from the limited data:

a. Substantial variation in surface and bottom salinities was noticed at transect R1 (from 25 to 35 ppt), transect R4 (from 22 to 33 ppt), and

transect R5 (from 18 to 28 ppt). These three locations are in the San Bernard River.

b. The maximum salinity decreases with increasing distance upstream of the San Bernard River from the river mouth, but the difference in salinity from bottom to surface remained about 10 ppt. The values at R1, R4, and R5 were 35, 33, and 28 respectively. This clearly shows the effect of freshwater flow in the river, which is plotted in Figure 37 for the month of August 1999. The residual effect of rain over the first 25 days before taking salinity measurements resulted in lower salinity within the river.

c. Such a large variation was not seen at transects R2 and R3, which are located within the GIWW.

Currents

The Acoustic Doppler Current Profiler (ADCP) was installed aboard a boat furnished by ERDC-CHL and was operated by its personnel. The current velocities at five transects were monitored over about 12 hr with simultaneous tidal levels. Velocity measurements were conducted on August 26, 1999, when the river discharge was relatively low. A second visit was planned for short-duration measurements during high discharge in the San Bernard River; however, the opportunity did not arise because the period August 1999 to August 2000 was exceptionally dry.

ADCP measures current speed, current direction, and local water depth. Under data processing, local cross-sectional area is computed and the discharge through the section is computed. Figure 38 shows the water level, Figure 39 shows the average velocity, Figure 40 shows the average current direction, Figure 41 shows the inlet cross section, and Figure 42 shows the tidal discharge at transect 1 on 26 August 1999.

4 Geometry of Modified Inlet

It is seen from earlier maps and aerial photographs that the San Bernard River Inlet has been shoaling over the past few years. An attempt was made with the help of the Galveston District officials to determine the width and depth of inlet section prevailing about 30 to 40 years ago. However, this information could not be obtained from records. Hence, we computed the approximate dimensions of a stable inlet by applying the area versus tidal prism method and used that cross section for examining its effect on tides and currents. The equation is as follows:

$$A_E = C P^n \tag{1}$$

where

A_E = equilibrium cross-sectional area

P = tidal prism

C = empirical parameter

n = empirical parameter

Jarett (1976) has given the values of C and n for the Gulf Coast, which are $C = 6.992 \times 10^{-4}$, and $n = 0.86$. The tidal influx worked out to 2.26 million cu m (80 million cu ft). Substitution in the formula gives the equilibrium cross-sectional area as 407 sq m (4,377 sq ft), which was rounded off to 418.5 sq m (4,500 sq ft). Consistent with the width of the present river channel, a width of 182.9 m (600 ft) was assumed for the new outlet. To get the cross-sectional area of 418.5 sq m (4,500 sq ft), it requires a depth of 2.28 m (7.5 ft), which is also consistent with the depths in the existing channel. Hence, a 183-m- (600-ft-) wide, 2.28-m- (7.5-ft-) deep channel is recommended for the new outlet, which is shown in Figure 43. This configuration was adopted for running the numerical model to examine the effect of providing new inlet geometry.

5 Numerical Hydrodynamic Model

Description

In this study the changes in water surface elevation and water velocities that would result by providing a new outlet for the San Bernard River were tested using a two-dimensional, vertically averaged numerical hydrodynamic model. The hydrodynamic model used in this study employs the Garlekin finite element formulation to solve the vertically-averaged Reynolds form of the Navier-Stokes equations with hydrostatic assumption applied. These equations are commonly known as the vertically integrated shallow-water equation. The hydrodynamic model, known as RMA2-WES, was originally written by Dr. Ian King and Mr. William Norton of Resource Management Associates (RMA) in Lafayette, CA, under contract to the U.S. Army Corps of Engineers (USACE). The model is maintained and has been enhanced by personnel of ERDC's Waterways Experiment Station (WES) in Vicksburg, MS. The version used in this study was RMA2-WES, Version 4.52.

The numerical model RMA2-WES was chosen for this study for several reasons. First, the finite element method permits the modeler to develop an unstructured mesh to define the channel geometry. The study area has many channels and marsh areas that are difficult to discretize in the sense of a structured, index-based grid. The finite element method uses freely connected three-sided and four-sided elements that are knitted together by means of an element connection table, thus permitting the modeler more flexibility to resolve important geometric features that may be required to accurately compute the flow field. Second, a vertically-averaged description of the hydrodynamics was sufficient to answer the questions that were posed concerning the relative impacts of the engineering plan on water velocities at the intersections of the GIWW with the San Bernard and Brazos Rivers. Third, RMA2-WES has been successfully applied in over 100 estuarine and riverine modeling studies by the Corps. (See Appendix A for details).

Mesh

The numerical mesh (Figure 44) is composed of 9,568 nodes and 3,120 quadratic elements, 795 are triangular elements and 2,198 are quadrilaterals. The mesh includes a rectangular portion of the Gulf of Mexico 35.4 km (22 miles) long that extends 20.9 km (13 miles) offshore where the tidal boundary is applied. The portion of the GIWW represented in the model begins in the northeast at Road 1495, located halfway between the Freeport Harbor channel and the Brazos River, and extends southwest to Dead Caney Lake. The San Bernard and Brazos Rivers were included in the mesh. Both rivers were represented with two-dimensional elements and high resolution in the lower portion where the GIWW is intersected. The upper reaches were represented by one-dimensional elements. The portion of each river included in the mesh extends approximately 45 km (28 miles) upstream from their respective outlets at the Gulf of Mexico. All the marsh areas adjacent to the San Bernard/Brazos/GIWW system were also included in the mesh using the wetting and drying by marsh porosity capability of RMA2.

Bathymetry

An elevation contour map of the study area is shown in Figure 45. Bathymetric information for the offshore part of the model was digitized from NOAA nautical charts. Elevations vary from -0.305 m (-1.0 ft) mllw at the shoreline to -21.9 m (-72.0 ft) mllw at the tidal boundary. Detailed survey data, provided by the U.S. Army Engineer District, Galveston, and by ERDC's field group, included the GIWW starting 4.83 km (3 miles) southwest from San Bernard River and ending more than 1.61 km (1 mile) northeast from the Brazos River. The average depth for the ICWW channel was 4.94 m (16.2 ft) mllw. Detailed bathymetric data was also obtained from ERDC's field group survey for the San Bernard River outlet. The maximum water depth at some San Bernard outlet cross sections corresponded to a bed elevation of -1.37 m (-4.5 ft) mllw. Minimum bed elevations for the lower reaches of San Bernard River and Brazos River corresponded to -3.05 m (-10.0 ft) mllw and -2.74 m (-9.0 ft), respectively. The elevation assigned to the marsh areas was 0.46 m (1.5 ft) mllw as a result of model calibration. Survey data was not available for the marshes.

Boundary conditions

The measured water surface elevation at NOAA tide sta 8772440 located in Freeport, TX, was applied at the offshore boundary of the mesh (Figure 46). No adjustment to the amplitude or phase of the tidal signal was necessary. The period covered by the tidal signal was 144 hr (6 days) from August 21, 1999, to August 26, 1999. This period was selected to accommodate model spin-off time as well as the verification period. The first two days of the simulation were used to eliminate any initial condition effect and the last day (August 26) was used for verification of the model against prototype water discharge measurements.

Water discharge was applied at the upstream end of the San Bernard River as well as the Brazos River. The discharge data for the Brazos River was obtained from the U.S. Geological Survey sta 08116650 near Rosharon, TX, and varied between 20.43 and 32 cu m/s (722 and 1,130 cfs). The discharge for San Bernard River was obtained from USGS sta 08117500 near Boling, TX, with values between 2.66 and 3.45 cu m/s (94 and 122 cfs).

6 Hydrodynamic Model Verification

The parameters available to adjust the model are channel bed roughness and eddy viscosity. The roughness is controlled by means of the correct spatial assignment of the Manning's n coefficient values. The assignment of the coefficient values is accomplished by associating a material type with each of the elements in the mesh. Several different material types can be defined to describe the different physiographic regions of the estuary. The eddy viscosity or turbulent exchange coefficients E describe the degree to which small scale turbulent flow features dissipate energy in the flow field. A high eddy viscosity coefficient indicates high levels of turbulent energy dissipation. This parameter accounts for small scale flow features that are not specifically resolved by the numerical mesh. Therefore, the value of eddy viscosity is a function of both the local flow field and the local grid size. As a rule of thumb, eddy viscosity is often assigned according to a grid Peclet number criterion. The grid Peclet number is defined (BYU 1994) as:

$$P = (\rho \, V \, \Delta x)/E_{ij} \tag{2}$$

where

ρ = density, slugs/ft^3

V = velocity along a particular streamline, ft/s

Δx = mesh spacing, ft

E_{ij} = eddy viscosity where i is momentum turbulent exchange in j-direction, lbf•s/ft^2

A Peclet number less than 50 is desirable for numerical stability. During model calibration it was found that a Manning's roughness coefficient of 0.025 and a turbulent exchange coefficient of 50 applied over the entire domain were the optimum combination to reproduce prototype conditions while keeping the numerical stability of the model.

Information about the Brazos River floodgate operation was obtained from the lockmaster. The information contained in the log was mainly the time and

description of the vessels passing through the gate. There is no record about the time when the floodgate is actually open for traffic and closed. During a phone conversation with the floodgate operator more detailed information was obtained. The floodgate is supposed to start opening 5 min before the arrival of a vessel. The floodgate is immediately closed once the vessel passes through, unless there is another incoming vessel within 10 min of arrival. Investigation of the system was performed following the operation guidelines described by the floodgate operator and the times recorded in the floodgate log. From the comparison between modeled and prototype discharges, it was concluded that the gate remained open during the period covered by the intensive data survey on August 26, 2000, not following the operation guidelines already described. Due to the uncertainty of the gate operation, verification of the model was performed using two scenarios, open and closed floodgate.

Verification for Tide

Tide data were obtained by eight gages strategically placed in the study area by ERDC personnel (Figure 3). Figures 47 to 54 show the prototype tide plotted against the modeled tide with the west Brazos River floodgate open and closed. All stations show high frequency fluctuations in the prototype signal that could be affected by a combination of barge traffic as well as the floodgate operation. These fluctuations are minimal at Gage 10. As expected, the prototype tidal signal is enclosed between the two simulated extreme scenarios. This behavior is observed in all gages but Gage 10, located in Brazos River where water flow is less restricted. Part of the water discharge from the San Bernard River is diverted through the open west Brazos River floodgate instead of flowing through the San Bernard River outlet. When the gate is closed, water interchange between the San Bernard River, the GIWW, and the Gulf of Mexico is limited to the shallow San Bernard River outlet. This condition maintains inland water surface elevations higher than when the floodgate is open. By observation of the model results at sta 10, used as the control tide gauge, we conclude that the verification of the model for water-surface elevation was good. However, a good match between prototype and modeled water-surface elevations at the other tide gages was difficult due to the uncertainty of the floodgate operation.

Verification for Discharge

Discharge data were collected by ERDC personnel at five cross sections within the area of study (Figure 34). The survey took place on August 26, 1999, for approximately 10 hr between flood and ebb tide, therefore, verification of the model against peak flood and ebb discharges could not be performed. Nevertheless, comparison between the model and prototype trends was achieved. Figures 55 to 59 show prototype discharges plotted against the modeled discharges with the floodgate open as well as closed. Discharges at Range 3, located in the ICWW between the San Bernard and Brazos Rivers, clearly show the fact that the floodgate remained open during the survey period instead of remaining mostly closed as it would by following the floodgate operation guidelines. The other

ranges also show a marked difference in modeled discharges when the floodgate is open or closed, as the open floodgate scenario is one that resembles prototype conditions the most. A secondary peak in discharges occurring in the prototype is well reproduced by the model at all locations.

7 Model Results

Model runs were performed to investigate the behavior of the system during different flow events. Four simulations were done using a maximum discharge of 28.3, 141.5, 283, and 566 cu m/s (1,000, 5,000, 10,000, and 20,000 cfs) for the San Bernard River. Corresponding discharges at the Brazos River were obtained from historical USGS data. Figures 23 to 26 show the hydrographs used for both rivers. Existing conditions and the new San Bernard River outlet were simulated with the west Brazos River floodgate open as well as closed.

Velocities and water-surface elevations at the west Brazos River floodgate, the intersection of the San Bernard River outlet with the GIWW, and the San Bernard River outlet are plotted in Figures 60 to 87 for all flow conditions.

When the new outlet is provided and the San Bernard River has a flow of 28.3 cu m (1,000 cfs), eastbound water velocities decrease from more than 0.91 m/s (3 ft/sec) to less than 0.61 m/s (2 ft/sec) at the floodgate. During higher flow regimes 141.5 to 283 cu m/s (5,000 to 10,000 cfs) in San Bernard River), velocities at the floodgate are mainly westbound because the larger Brazos River flows 1,924 to 2,122 cu m/s (68,000, to 75,000 cfs) divert through the GIWW. The westbound velocities occur with the existing San Bernard outlet as well as the new outlet, but providing a new outlet generates maximum velocities of 1.83 m/s (6 ft/s) which are higher than the existing maximum velocities by more than 0.61 m/s (2 ft/s). At a San Bernard River discharge of 566 cu m/s (20,000 cfs), the water velocities at the floodgate are mainly eastbound with the existing outlet. The reversal of the flow from west to east is created because the size of the existing San Bernard River outlet is not sufficient to efficiently handle a high flood event. Therefore, water levels increase inland and prevent the diversion of the Brazos River flow into the GIWW. By providing a new outlet, velocities remain westbound during the highest San Bernard River flow.

Crosscurrents at the intersection of the San Bernard River with the GIWW are less than 0.3 m/s (1 ft/s) during low flow conditions for all scenarios. Providing a new outlet, crosscurrents increase to a maximum velocity of 0.61 m/s (2 ft/s) using a San Bernard River discharge of 566 cu m/s (20,000 cfs). Maximum velocities remain slightly above 0.3 m/s (1 ft/s) using the existing outlet.

Velocities around 0.244 m/s (0.8 ft/s) at the existing San Bernard River outlet increase by 50 percent during ebb by keeping the floodgate closed during low flow conditions. A slight increase is also observed during ebb and flood by

keeping the floodgate closed with the new outlet. The new San Bernard River outlet had higher maximum velocities than the existing outlet during all four simulated flow events. The magnitudes of the maximum velocities increase with the magnitude of the flood event to a maximum of almost 1.22 m/s (4 ft/s) with the west Brazos River floodgate open.

The new outlet reduces water-surface elevations throughout the system during all flood events by facilitating the outflow of water to the Gulf of Mexico and increasing tidal flushing. Inland water levels west of the Brazos River are also affected by the operation of the floodgates and both San Bernard and Brazos River stages.

8 Conclusions and Recommendations

A numerical model of the estuary system including the intersections of the GIWW with the San Bernard and Brazos Rivers, was developed by ERDC to investigate the effects of providing a new outlet for the San Bernard River. It was assumed that the old outlet is instantly closed when the new outlet is in place.

During verification of the model against field data it was concluded that the model reasonably reproduces prototype trends in water-surface elevation, velocities, and discharges. Knowledge of the floodgate operation is essential for a better verification of the model. Better recording procedures are necessary at the floodgate to increase the availability of information that will help to fully understand the processes within the system. Marshland bathymetry is also necessary to accurately reproduce the amount of water storage.

Comparison of the model results against the prototype suggest that the west Brazos River floodgate remains open most of the time.

Providing a new outlet for the San Bernard River reduces the velocity of water through the gates when the San Bernard and Brazos Rivers have low flow, 28.3 and 254.7 cu m/s (1,000 and 9,000 cfs), respectively. Maximum eastbound velocities at the floodgates are reduced from higher than 0.91 m/s (3 ft/s) to less than 0.61 m/s (2 ft/s). Maximum velocities at the floodgate increase to 1.83 m/s (6 ft/s), an increase of more than 0.61 m/s (2 ft/s), and remain westbound during high flow events.

The new outlet reduces water-surface elevations throughout the system during all flood events by facilitating the outflow of water to the Gulf of Mexico and increasing tidal flushing.

Velocities around 0.244 m/s (0.8 ft/s) at the existing San Bernard River outlet increase by 50 percent during ebb by keeping the floodgate closed during low flow conditions. A slight increase is also observed during ebb and flood with the new outlet.

Crosscurrent velocities at the intersection of the San Bernard River with the GIWW increase during high flood events with the provision of the new outlet.

Input from barge navigators will be necessary to find out if the magnitude of increase in crosscurrents is a matter of concern.

In general, providing a new outlet is favorable during low flow conditions, but some adverse effects are shown during high flow events. Factors such as the frequency of high flow events, the operation of the floodgates, the drop of water-surface elevation throughout the system, and the cost of keeping the new outlet open should be considered at the time of acceptance or rejection of the proposed plan. The model simulations discussed in this report were based on specific combinations of boundary conditions, especially for the San Bernard River and Brazos River flows. Different combinations of flow from each of these rivers will provide different results. A coastal processes study is recommended to better understand the current behavior of the existing San Bernard River outlet as well as to find ways of achieving inlet stabilization.

The absence of high flow events during the performance of this study made impossible the achievement of a more complete verification. Therefore, it is recommended to revisit the verification as soon as a new set of prototype data covering a higher range of flows is available.

References

Ackers, P., and White, W. R. (1973). "Sediment transport: New approach and analysis," *Journal, Hydraulics Division, American Society of Civil Engineers* 99(HY-11), 2041-2060.

Ariathurai, R., MacArthur, R. D., and Krone, R. C. (1977). "Mathematical model of estuarial sediment transport," Technical Report D-77-12, U.S. Army Engineer Waterways Experiment Station, Vicksburg, MS.

Bales, J. D., and Holley, E. R. (1989). "Sand transport in Texas tidal inlet," *Journal of Waterway, Port, Coastal, and Ocean Engineering* 115(4), 427-443.

Brigham Young University. (1994). "Tabs primer," Brigham Young University Computer Graphics Laboratory, Provo, UT.

Hauck, L. M. (1992). "Hydrodynamics at mouth of Colorado River, TX project, numerical model investigation," Final report, Prepared by the U.S. Army Engineer Waterways Experiment Station, for the U.S. Army Engineer District, Galveston.

Jarett, J. T. (1976). "Tidal prism – inlet area relationships," GITI Report 3, U.S. Army Engineer Waterways Experiment Station, Vicksburg, MS.

King, Ian P., and Richard R. (1989). "Program documentation: A two dimensional water quality model; Version 3.0," Resource Management Associates, Laffayette, CA.

Krone, R. B. (1962). "Flume studies of transport of sediment in estuarial shoaling processes," Final Report, Hydraulics Engineering Research Laboratory, University of California, Berkeley, CA.

Mason C. (1981). Hydraulics and stability of five Texas inlets," Miscellaneous Report No. 81-1, U. S. Army Corps of Engineers, Coastal Engineering Research Center, Fort Belvoir, VA.

Norton, W. R., and King, I. P. (1977). "Operating instructions for the computer Program," Resource Management Associates, Lafayette, CA.

Partheniades, E. (1962). "A study of erosion and deposition of cohesive soils in salt water," Ph.D. diss., University of California, Berkeley, CA.

Swart, D. H. (1976). "Coastal sediment transport, computation of longshore transport," R968, Part 1, Delft Hydraulics Laboratory, The Netherlands.

Thomas, W. A., and McAnally, W. H., Jr. (1985). "User's manual for the generalized computer program system; Open-channel flow and sedimentation, TABS-2," Instruction Report HL-85-1, U.S. Army Engineer Waterways Experiment Station, Vicksburg, MS.

White, W. R., Milli, H., and Crabbe, A. D. (1975). "Sediment transport theories: An appraisal of available methods," Report Int 119, Vols 1 and 2, Hydraulics Research Station, Wallingford, England.

Bibliography

Johnson J. W. (1972). "Tidal inlets on the California, Oregon, and Washington coasts, Technical Report HEL-24-12, Hydraulic Engineering Laboratory, University of California at Berkeley.

Kraus, N. C. (1998). "Inlet cross-sectional area calculated by process-based model," Coastal Engineering, 98, Proceedings of ASCE conference, Copenhagen, Denmark.

O'Brian, M. P. (1931). "Estuary and tidal prisms related to entrance areas," *Civil Engineering* 1(18), 738-739.

_____. (1969). "Equilibrium flow areas of inlets on sandy coasts," *Journal of Waterways and Harbors Division* 95(WW1), 43-52.

Table 1		
Duration of Tide Data Collected for San Bernard River Project		
Station	**Year 1999**	**Comments**
1	July 13 - 31	
	August 1 - 31	
	September 1 - 30	
	October 1 - 31	
	November 1 - 16	
2	July 14 – 31	
	August 1 – 31	
	September 1 - 30	
	October 1 - 31	
	November 1 - 16	
3	July 14 – 31	
	August 1 – 31	
	September 1 - 30	
	October 1 - 16	
	November	No data
	December	No data
	January 11 – 31	
	February 1 - 29	
	March / April	No data
	May 10 - 31	
	June 1 – 30	
	July 1 - 24	
	August 1 - 31	
4	July 14 – 31	
	August 1 – 31	
	September 1 - 30	
	October 1 - 31	
	November 1 - 16	
5A	August 25 – 31	
	September 1 - 30	
	October 1 - 31	
	November 1 - 30	
6A	August 25 - 31	
	September 1 - 30	
	October 1 - 31	
	November 1 - 16	
7	July 13 – 31	
	August 1 – 31	
	September 1 - 30	
	October 1 - 31	
	November 1 - 16	
8	July 13 – 31	
	August 1 – 31	
	September 1 - 30	
	October 1 - 31	
	November 1 - 16	
10	August 25 – 27	
	September 1 - 30	
	October 1 - 31	
	November 1 - 16	

Table 2
Particle Size Analysis of Bed Sediment for San Bernard River Project

San Bernard River - Coulter Particle Size Analyzer Results								
Size - µm	**D50**	**%Finer**						
Sample	Micron	100	90	75	50	25	10	0
1	4.205	200	50.55	14.3	4.205	1.866	0.955	0.4
2	7.536	250	65.62	30.12	7.536	2.533	1.114	0.1
3	9.26	300	80.09	41.1	9.26	2.797	1.192	0.1
4								
5								
6	96.93	900	196.5	135.6	96.93	29.47	3.026	0.4
7	86.71	900	176.1	128.5	86.71	19.92	2.683	0.4
8	4.954	300	104.7	21.68	4.954	1.903	0.938	0.1
9	28.46	700	126.6	85.25	28.46	4.102	1.461	0
10	29.22	750	143.4	89.33	29.22	4.22	1.506	0
11	6.311	250	77.03	27.2	6.311	2.156	0.993	0.1
12	6.036	225	75.93	25.85	6.036	2.147	0.993	0.1
13	4.542	220	42.43	15.18	4.542	1.822	0.909	0.15
14	3.99	180	31.87	11.7	3.99	1.686	0.875	0.2
15	3.948	180	27.72	10.66	3.948	1.736	0.897	0.1
16	3.276	150	15.3	6.69	3.276	1.529	0.829	0.1
17	3.513	200	25.55	9.26	3.513	1.522	0.826	0.15
18	3.821	180	23.62	10.22	3.821	1.59	0.849	0.15
19	8.726	225	76.79	39.55	8.726	2.436	1.066	0.1
20	6.093	220	61.48	25.81	6.093	2.172	1.006	0.1
21	11.77	750	120.2	66.7	11.77	2.948	1.209	0
22	103.3	900	182.6	142.9	103.3	60.08	4.793	0.4
San Bernard River - Sieve Analysis								
Size - mm		**%Finer**						
Sample	D50	100	99.79	90.68	56.16	1.78	0.58	Pan
	mm							
4	0.149	0.84	0.42	0.21	0.149	0.074	0.063	0
Sample	D50	100	99.03	51.15	44.97	2.54	0.65	Pan
5	0.149	0.84	0.42	0.21	0.149	0.074	0.063	0

Note: The D50 for samples 4 and 5 are given in mm. All other samples are in microns.

Table 3
Suspended Sediment Concentration at Transect R1

Date	Station	Time	Suspension Concentration (mg/L)		
			Surface	Middepth	Bottom
8/26/99	R1.0	7:11			61
8/26/99	R1.0	7:13		58	
8/26/99	R1.0	7:14	29		
8/26/99	R1.0	8:07	26		
8/26/99	R1.0	8:07			64
8/26/99	R1.0	8:08		41	
8/26/99	R1.0	9:00	31		
8/26/99	R1.0	9:00			56
8/26/99	R1.0	9:02		44	
8/26/99	R1.0	10:02	25		
8/26/99	R1.0	10:04			61
8/26/99	R1.0	10:05		53	
8/26/99	R1.0	11:05	24		
8/26/99	R1.0	11:05			58
8/26/99	R1.0	11:06		46	
8/26/99	R1.0	12:04	23		
8/26/99	R1.0	12:04			61
8/26/99	R1.0	12:05		40	
8/26/99	R1.0	13:07	23		
8/26/99	R1.0	13:07			103
8/26/99	R1.0	13:08		42	
8/26/99	R1.0	14:07	33		
8/26/99	R1.0	14:07			70
8/26/99	R1.0	14:08		38	
8/26/99	R1.0	15:03	32		
8/26/99	R1.0	15:03			81
8/26/99	R1.0	15:04		37	
8/26/99	R1.0	16:05	38		
8/26/99	R1.0	16:05			51
8/26/99	R1.0	16:06		76	
8/26/99	R1.0	17:05	29		
8/26/99	R1.0	17:05			198
8/26/99	R1.0	17:06		64	
8/26/99	R1.0	17:55	38		
8/26/99	R1.0	17:55			138
8/26/99	R1.0	17:56		67	

Table 4
Suspended Sediment Concentration at Transect R2

Date	Station	Time	Suspended Concentration (mg/L)		
			Surface	Middepth	Bottom
8/26/99	R2.0	7:35			79
8/26/99	R2.0	7:36		62	
8/26/99	R2.0	7:36	29		
8/26/99	R2.0	8:21	51		
8/26/99	R2.0	8:29			76
8/26/99	R2.0	8:30		66	
8/26/99	R2.0	9:14			106
8/26/99	R2.0	9:15	39		
8/26/99	R2.0	9:15		68	
8/26/99	R2.0	10:16	33		
8/26/99	R2.0	10:16			80
8/26/99	R2.0	10:17		50	
8/26/99	R2.0	11:17	36		
8/26/99	R2.0	11:18			65
8/26/99	R2.0	11:19		43	
8/26/99	R2.0	12:14	36		
8/26/99	R2.0	12:14			57
8/26/99	R2.0	12:16		38	
8/26/99	R2.0	13:23	36		
8/26/99	R2.0	13:23			106
8/26/99	R2.0	13:24		75	
8/26/99	R2.0	14:21	64		
8/26/99	R2.0	14:21			144
8/26/99	R2.0	14:22		52	
8/26/99	R2.0	15:16	59		
8/26/99	R2.0	15:16			141
8/26/99	R2.0	15:17		84	
8/26/99	R2.0	16:17	66		
8/26/99	R2.0	16:17			223
8/26/99	R2.0	16:18		145	
8/26/99	R2.0	17:16	50		
8/26/99	R2.0	17:17			202
8/26/99	R2.0	17:18		83	
8/26/99	R2.0	18:08	149		
8/26/99	R2.0	18:08			272
8/26/99	R2.0	18:09		165	

Table 5
Suspended Sediment Concentration at Transect R3

Date	Station	Time	Suspended Concentration (mg/L)		
			Surface	Middepth	Bottom
8/26/99	R3.0	7:54	89		
8/26/99	R3.0	7:55			121
8/26/99	R3.0	7:56		98	
8/26/99	R3.0	8:44	62		
8/26/99	R3.0	8:45			107
8/26/99	R3.0	8:46		87	
8/26/99	R3.0	9:27	50		
8/26/99	R3.0	9:27			105
8/26/99	R3.0	9:28		88	
8/26/99	R3.0	10:29	35		
8/26/99	R3.0	10:30			92
8/26/99	R3.0	10:31		65	
8/26/99	R3.0	11:34	39		
8/26/99	R3.0	11:34			68
8/26/99	R3.0	11:35		57	
8/26/99	R3.0	12:30	27		
8/26/99	R3.0	12:30			48
8/26/99	R3.0	12:31		42	
8/26/99	R3.0	13:37	32		
8/26/99	R3.0	13:38			58
8/26/99	R3.0	13:39		46	
8/26/99	R3.0	14:34	44		
8/26/99	R3.0	14:35			64
8/26/99	R3.0	14:36		61	
8/26/99	R3.0	15:31	61		
8/26/99	R3.0	15:31			100
8/26/99	R3.0	15:32		94	
8/26/99	R3.0	16:30	64		
8/26/99	R3.0	16:30			135
8/26/99	R3.0	16:31		95	
8/26/99	R3.0	17:30	89		
8/26/99	R3.0	17:30			402
8/26/99	R3.0	17:31		209	
8/26/99	R3.0	18:24	114		
8/26/99	R3.0	18:24			356
8/26/99	R3.0	18:25		204	

Table 6
Suspended Sediment Concentration at Transect R4

Date	Station	Time	Suspended Concentration (mg/L)		
			Surface	Middepth	Bottom
8/26/99	R4.0	7:25	33		
8/26/99	R4.0	7:26			75
8/26/99	R4.0	7:27		71	
8/26/99	R4.0	8:26			68
8/26/99	R4.0	8:27		47	
8/26/99	R4.0	8:27	27		
8/26/99	R4.0	9:21	21		
8/26/99	R4.0	9:21			71
8/26/99	R4.0	9:22		71	
8/26/99	R4.0	10:21	22		
8/26/99	R4.0	10:21			71
8/26/99	R4.0	10:22		32	
8/26/99	R4.0	11:22	24		
8/26/99	R4.0	11:22			44
8/26/99	R4.0	11:23		29	
8/26/99	R4.0	12:20	29		
8/26/99	R4.0	12:20			50
8/26/99	R4.0	12:21		26	
8/26/99	R4.0	13:20	30		
8/26/99	R4.0	13:20			55
8/26/99	R4.0	13:21		27	
8/26/99	R4.0	14:27	25		
8/26/99	R4.0	14:27			58
8/26/99	R4.0	14:28		32	
8/26/99	R4.0	15:34	23		
8/26/99	R4.0	15:35			70
8/26/99	R4.0	15:36		24	
8/26/99	R4.0	16:26			48
8/26/99	R4.0	16:27	22		
8/26/99	R4.0	16:27		29	
8/26/99	R4.0	17:25	19		
8/26/99	R4.0	17:26			43
8/26/99	R4.0	17:27		21	
8/26/99	R4.0	18:25	25		
8/26/99	R4.0	18:26			36
8/26/99	R4.0	18:27		23	

Table 7
Suspended Sediment Concentration at Transect R5

| Date	Station	Time	Suspended Concentration (mg/L)		
			Surface	Middepth	Bottom
8/26/99	R5.0	7:07	24		
8/26/99	R5.0	7:08		37	
8/26/99	R5.0	7:08			40
8/26/99	R5.0	8:05	23		
8/26/99	R5.0	8:06			38
8/26/99	R5.0	8:07		37	
8/26/99	R5.0	9:04	23		
8/26/99	R5.0	9:04			29
8/26/99	R5.0	9:05		28	
8/26/99	R5.0	10:03	23		
8/26/99	R5.0	10:04			31
8/26/99	R5.0	10:05		31	
8/26/99	R5.0	11:03	26		
8/26/99	R5.0	11:03			27
8/26/99	R5.0	11:04		28	
8/26/99	R5.0	12:03	23		
8/26/99	R5.0	12:04			30
8/26/99	R5.0	12:05		27	
8/26/99	R5.0	13:02			36
8/26/99	R5.0	13:03		23	
8/26/99	R5.0	13:03	20		
8/26/99	R5.0	14:04	16		
8/26/99	R5.0	14:04			33
8/26/99	R5.0	14:05		25	
8/26/99	R5.0	15:05	20		
8/26/99	R5.0	15:06			28
8/26/99	R5.0	15:07		21	
8/26/99	R5.0	16:04	19		
8/26/99	R5.0	16:05			35
8/26/99	R5.0	16:06		14	
8/26/99	R5.0	17:05	20		
8/26/99	R5.0	17:06			27
8/26/99	R5.0	17:07		21	
8/26/99	R5.0	18:03	17		
8/26/99	R5.0	18:03			28
8/26/99	R5.0	18:04		21	

Table 8
Salinity at Transect R1

Date	Station	Time	Salinity (ppt)		
			Surface	Middepth	Bottom
8/26/99	R1.0	7:11			35.14
8/26/99	R1.0	7:13		35.03	
8/26/99	R1.0	7:14	32.85		
8/26/99	R1.0	8:07	32.53		
8/26/99	R1.0	8:07			35.28
8/26/99	R1.0	8:08		34.95	
8/26/99	R1.0	9:00	33.18		
8/26/99	R1.0	9:00			35.37
8/26/99	R1.0	9:02		35.29	
8/26/99	R1.0	10:02	27.73		
8/26/99	R1.0	10:04			35.37
8/26/99	R1.0	10:05		35.31	
8/26/99	R1.0	11:05	26.28		
8/26/99	R1.0	11:05			35.39
8/26/99	R1.0	11:06		35.17	
8/26/99	R1.0	12:04	24.72		
8/26/99	R1.0	12:04			35.47
8/26/99	R1.0	12:05		34.67	
8/26/99	R1.0	13:07	24.74		
8/26/99	R1.0	13:07			35.31
8/26/99	R1.0	13:08		35.21	
8/26/99	R1.0	14:07	25.83		
8/26/99	R1.0	14:07			35.32
8/26/99	R1.0	14:08		35.21	
8/26/99	R1.0	15:03	27.16		
8/26/99	R1.0	15:03			35.3
8/26/99	R1.0	15:04		35.18	
8/26/99	R1.0	16:05	30.17		
8/26/99	R1.0	16:05			35.19
8/26/99	R1.0	16:06		34.12	
8/26/99	R1.0	17:05	29.77		
8/26/99	R1.0	17:05			34.71
8/26/99	R1.0	17:06		33.99	
8/26/99	R1.0	17:55	30.78		
8/26/99	R1.0	17:55			34.49
8/26/99	R1.0	17:56		33.4	

Table 9
Salinity at Transect R2

Date	Station	Time	Salinity (ppt)		
			Surface	Middepth	Bottom
8/26/99	R2.0	7:35			34.62
8/26/99	R2.0	7:36		34.42	
8/26/99	R2.0	7:36	33.35		
8/26/99	R2.0	8:21	34.19		
8/26/99	R2.0	8:29			34.75
8/26/99	R2.0	8:30		34.48	
8/26/99	R2.0	9:14			34.75
8/26/99	R2.0	9:15	34.22		
8/26/99	R2.0	9:15		34.67	
8/26/99	R2.0	10:16	34.51		
8/26/99	R2.0	10:16			34.79
8/26/99	R2.0	10:17		34.93	
8/26/99	R2.0	11:17	34.76		
8/26/99	R2.0	11:18			34.78
8/26/99	R2.0	11:19		34.8	
8/26/99	R2.0	12:14	34.63		
8/26/99	R2.0	12:14			34.63
8/26/99	R2.0	12:16		34.61	
8/26/99	R2.0	13:23	34.64		
8/26/99	R2.0	13:23			34.66
8/26/99	R2.0	13:24		34.73	
8/26/99	R2.0	14:21	34.62		
8/26/99	R2.0	14:21			34.63
8/26/99	R2.0	14:22		34.64	
8/26/99	R2.0	15:16	34.6		
8/26/99	R2.0	15:16			34.63
8/26/99	R2.0	15:17		34.71	
8/26/99	R2.0	16:17	34.56		
8/26/99	R2.0	16:17			34.59
8/26/99	R2.0	16:18		34.61	
8/26/99	R2.0	17:16	34.42		
8/26/99	R2.0	17:17			34.57
8/26/99	R2.0	17:18		34.45	
8/26/99	R2.0	18:08	34.38		
8/26/99	R2.0	18:08			34.4
8/26/99	R2.0	18:09		34.39	

Table 10
Salinity at Transect R3

Date	Station	Time	Salinity (ppt)		
			Surface	Middepth	Bottom
8/26/99	R3.0	7:54	31.94		
8/26/99	R3.0	7:55			31.93
8/26/99	R3.0	7:56		31.92	
8/26/99	R3.0	8:44	32.19		
8/26/99	R3.0	8:45			32.26
8/26/99	R3.0	8:46		32.26	
8/26/99	R3.0	9:27	32.43		
8/26/99	R3.0	9:27			32.48
8/26/99	R3.0	9:28		32.44	
8/26/99	R3.0	10:29	32.75		
8/26/99	R3.0	10:30			32.77
8/26/99	R3.0	10:31		32.75	
8/26/99	R3.0	11:34	32.7		
8/26/99	R3.0	11:34			33.13
8/26/99	R3.0	11:35		33.04	
8/26/99	R3.0	12:30	32.1		
8/26/99	R3.0	12:30			33.08
8/26/99	R3.0	12:31		32.95	
8/26/99	R3.0	13:37	31.35		
8/26/99	R3.0	13:38			33.06
8/26/99	R3.0	13:39		32.79	
8/26/99	R3.0	14:34	31.8		
8/26/99	R3.0	14:35			32.93
8/26/99	R3.0	14:36		32.67	
8/26/99	R3.0	15:31	31.62		
8/26/99	R3.0	15:31			32.46
8/26/99	R3.0	15:32		32.15	
8/26/99	R3.0	16:30	31.34		
8/26/99	R3.0	16:30			32.26
8/26/99	R3.0	16:31		32	
8/26/99	R3.0	17:30	31.94		
8/26/99	R3.0	17:30			32.47
8/26/99	R3.0	17:31		32.46	
8/26/99	R3.0	18:24	33.39		
8/26/99	R3.0	18:24			33.89
8/26/99	R3.0	18:25		33.56	

Table 11
Salinity at Transect R4

Date	Station	Time	Surface	Middepth	Bottom
				Salinity (ppt)	
8/26/99	R4.0	7:25	31.69		
8/26/99	R4.0	7:26			33.32
8/26/99	R4.0	7:27		33.31	
8/26/99	R4.0	8:26			33.32
8/26/99	R4.0	8:27		33.25	
8/26/99	R4.0	8:27	29.83		
8/26/99	R4.0	9:21	23.9		
8/26/99	R4.0	9:21			33.33
8/26/99	R4.0	9:22		33.28	
8/26/99	R4.0	10:21	22.85		
8/26/99	R4.0	10:21			33.22
8/26/99	R4.0	10:22		32.2	
8/26/99	R4.0	11:22	22.1		
8/26/99	R4.0	11:22			32.99
8/26/99	R4.0	11:23		30.62	
8/26/99	R4.0	12:20	22.23		
8/26/99	R4.0	12:20			33.33
8/26/99	R4.0	12:21		29.26	
8/26/99	R4.0	13:20	22.63		
8/26/99	R4.0	13:20			33.19
8/26/99	R4.0	13:21		26.47	
8/26/99	R4.0	14:27	22.15		
8/26/99	R4.0	14:27			33.12
8/26/99	R4.0	14:28		29.35	
8/26/99	R4.0	15:34	22.3		
8/26/99	R4.0	15:35			33.5
8/26/99	R4.0	15:36		30.29	
8/26/99	R4.0	16:26			33.48
8/26/99	R4.0	16:27	22.17		
8/26/99	R4.0	16:27		26.81	
8/26/99	R4.0	17:25	21.73		
8/26/99	R4.0	17:26			33.69
8/26/99	R4.0	17:27		30.87	
8/26/99	R4.0	18:25	22.39		
8/26/99	R4.0	18:26			33.15
8/26/99	R4.0	18:27		24.55	

Table 12
Salinity at Transect R5

Date	Station	Time	Surface	Salinity (ppt) Middepth	Bottom
8/26/99	R5.0	7:07	18.77		
8/26/99	R5.0	7:08		25.54	
8/26/99	R5.0	7:08			27.4
8/26/99	R5.0	8:05	18.98		
8/26/99	R5.0	8:06			27.51
8/26/99	R5.0	8:07		27.32	
8/26/99	R5.0	9:04	18.81		
8/26/99	R5.0	9:04			27.32
8/26/99	R5.0	9:05		26.38	
8/26/99	R5.0	10:03	18.65		
8/26/99	R5.0	10:04			26.97
8/26/99	R5.0	10:05		23.86	
8/26/99	R5.0	11:03	18.26		
8/26/99	R5.0	11:03			27.12
8/26/99	R5.0	11:04		21.85	
8/26/99	R5.0	12:03	18.3		
8/26/99	R5.0	12:04			27.43
8/26/99	R5.0	12:05		22.67	
8/26/99	R5.0	13:02			28.14
8/26/99	R5.0	13:03		23.81	
8/26/99	R5.0	13:03	17.83		
8/26/99	R5.0	14:04	18.31		
8/26/99	R5.0	14:04			27.2
8/26/99	R5.0	14:05		21.16	
8/26/99	R5.0	15:05	18.12		
8/26/99	R5.0	15:06			27.2
8/26/99	R5.0	15:07		19.05	
8/26/99	R5.0	16:04	18.25		
8/26/99	R5.0	16:05			28.5
8/26/99	R5.0	16:06		19.47	
8/26/99	R5.0	17:05	18.38		
8/26/99	R5.0	17:06			28.21
8/26/99	R5.0	17:07		20.18	
8/26/99	R5.0	18:03	18.45		
8/26/99	R5.0	18:03			28.29
8/26/99	R5.0	18:04		21.1	

Figure 1. Index map of study area
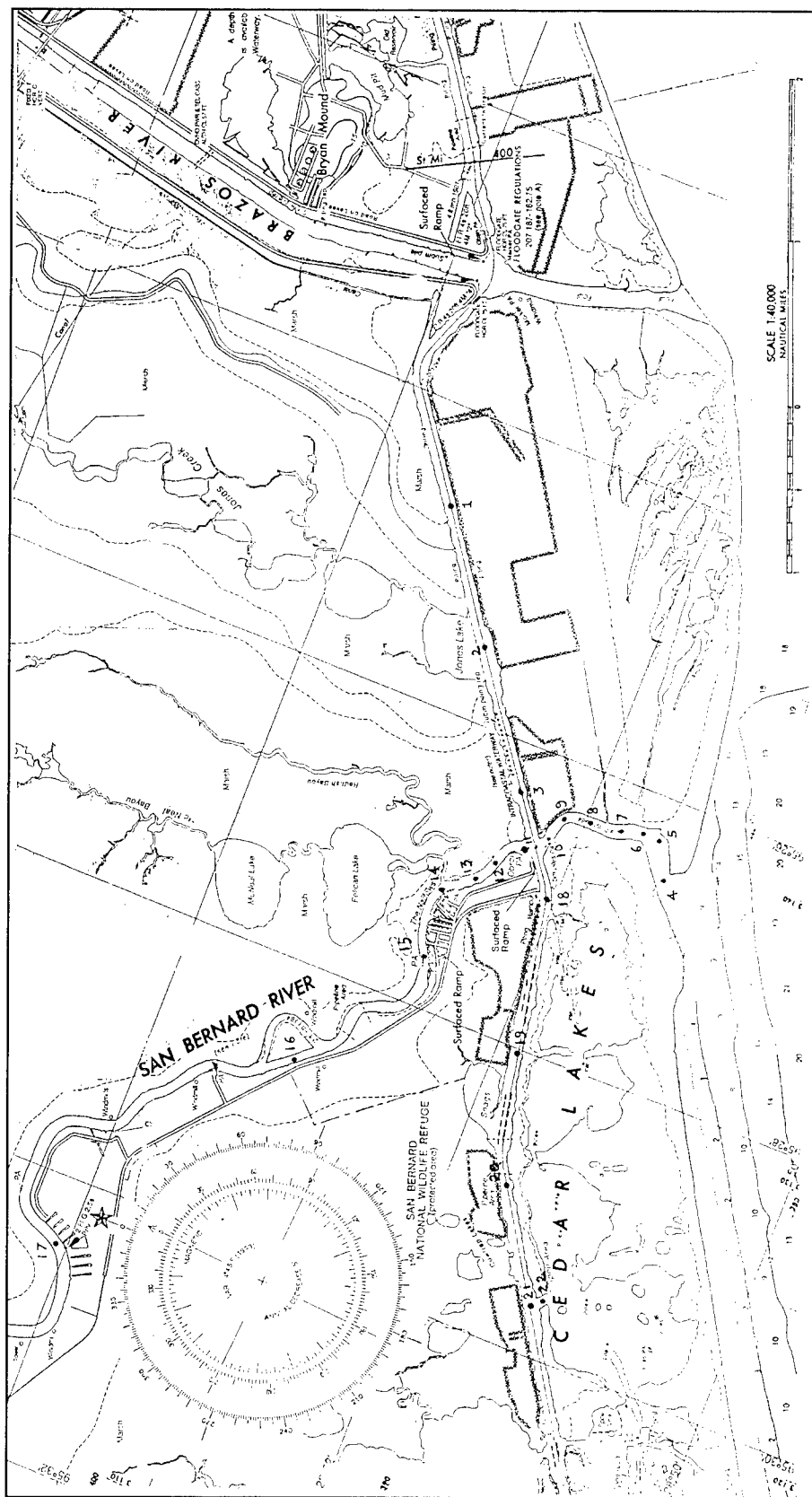
Figure 2. Details of area between San Bernard River and Brazos River (To convert nautical miles to kilometers, multiply by 1.852)
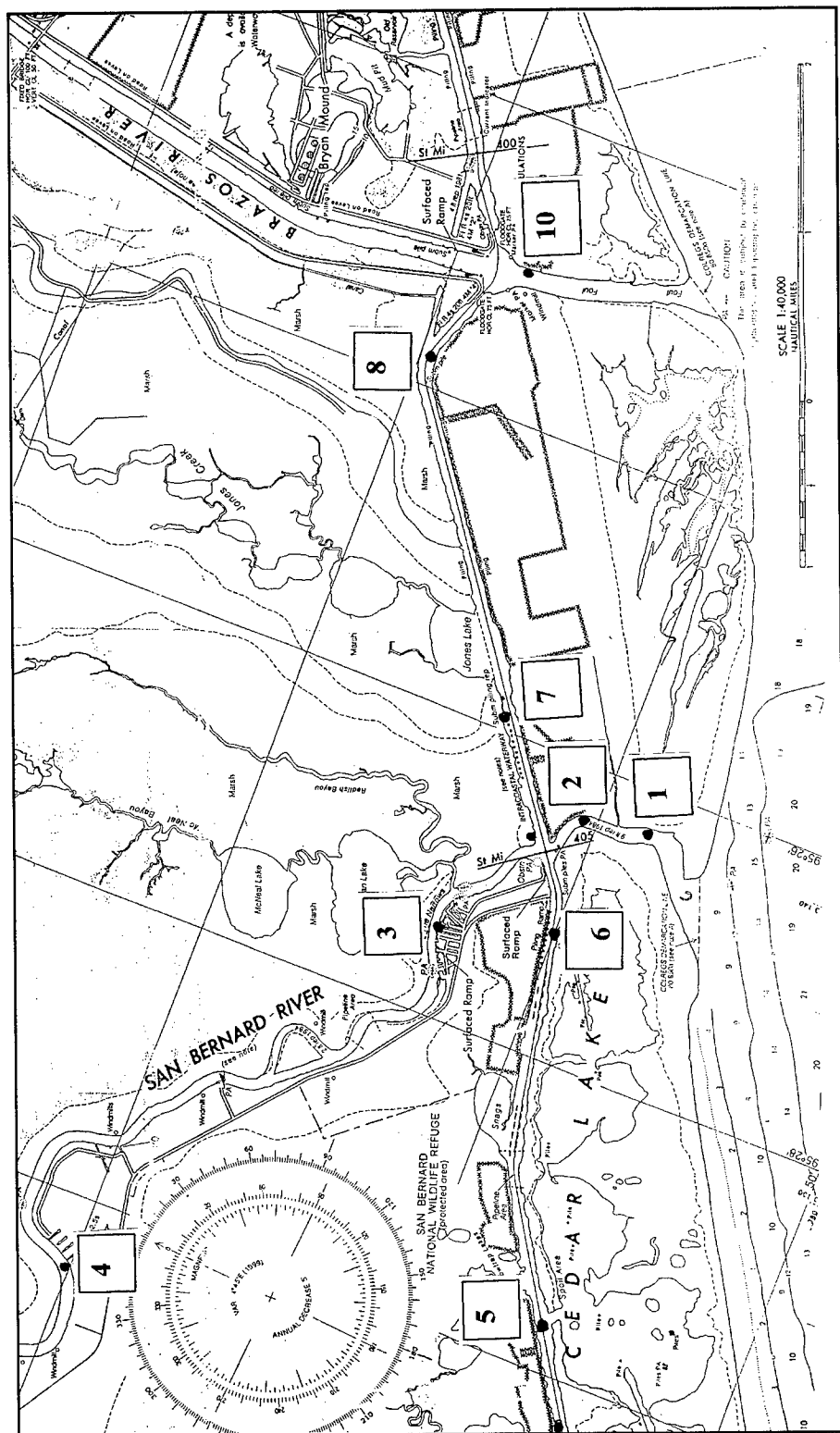
Figure 3.   Locations of tide observation stations (To convert nautical miles to kilometers, multiply by 1.852)
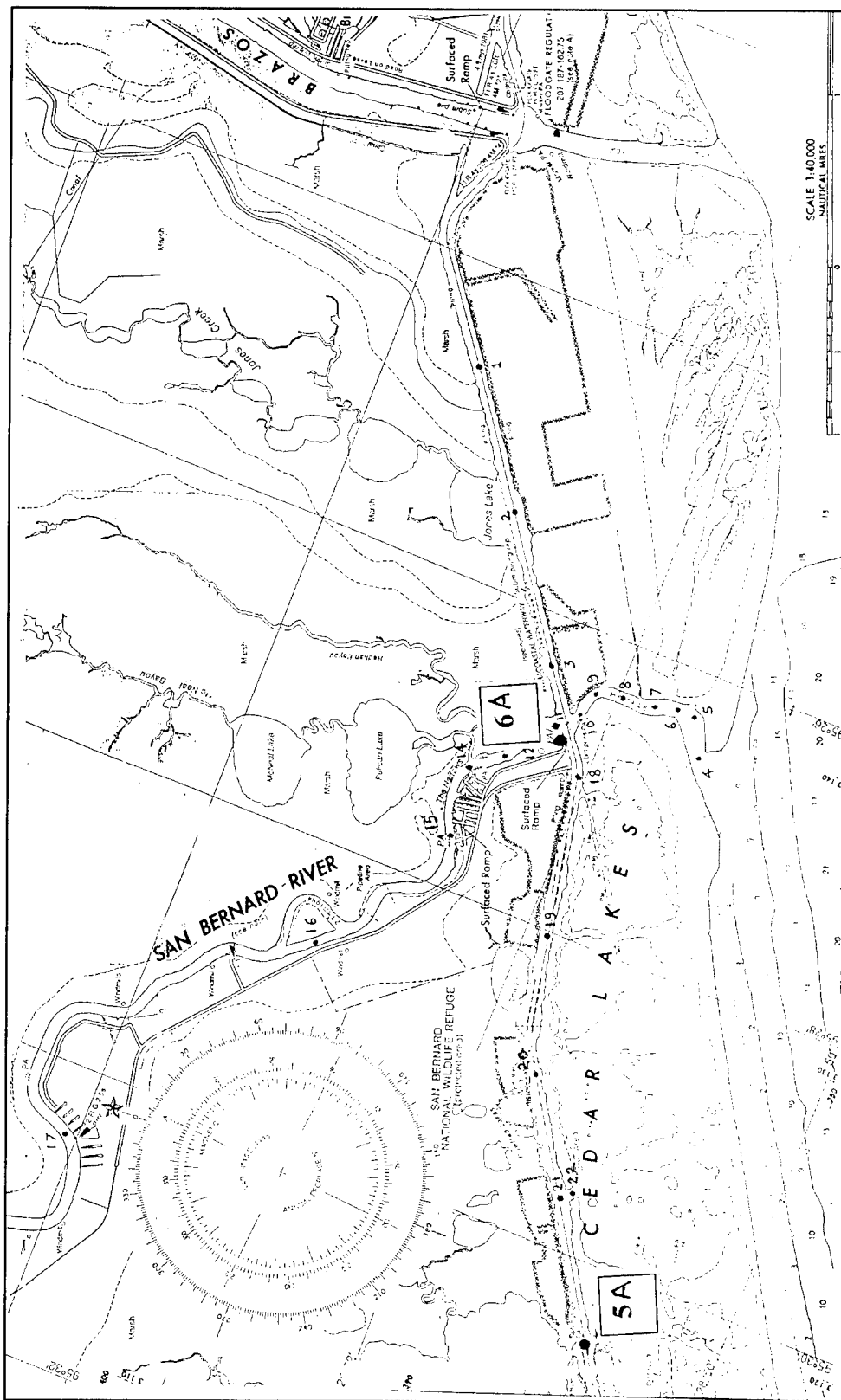
Figure 4.   Locations of tide observation stations 5A and 6A
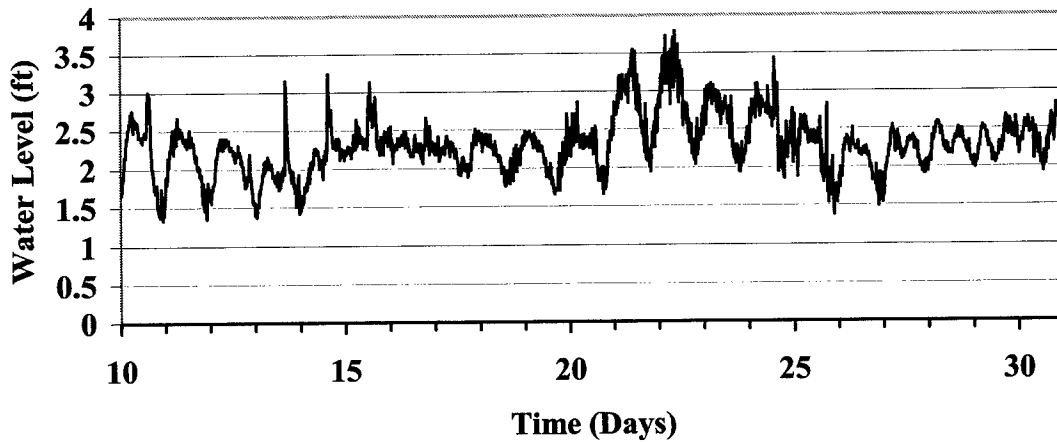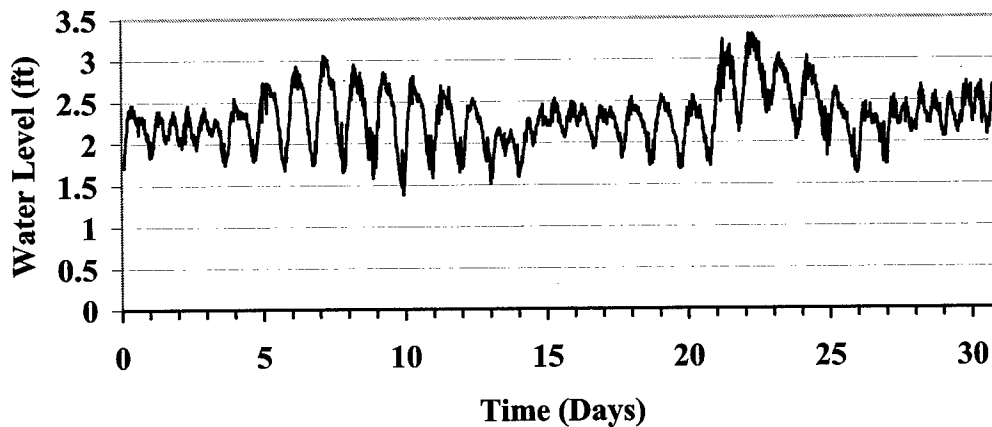
Figure 5. Tides observed at a) sta 1 and b) sta 2 during August 1999 (Water level is in feet, to convert feet to meters, multiply by 0.3048)

Tidal Levels at Sta 3 (North of Intersection)
Field Data of August 1999

Tidal Levels at Sta 4 (North End)
Field Data of August 1999
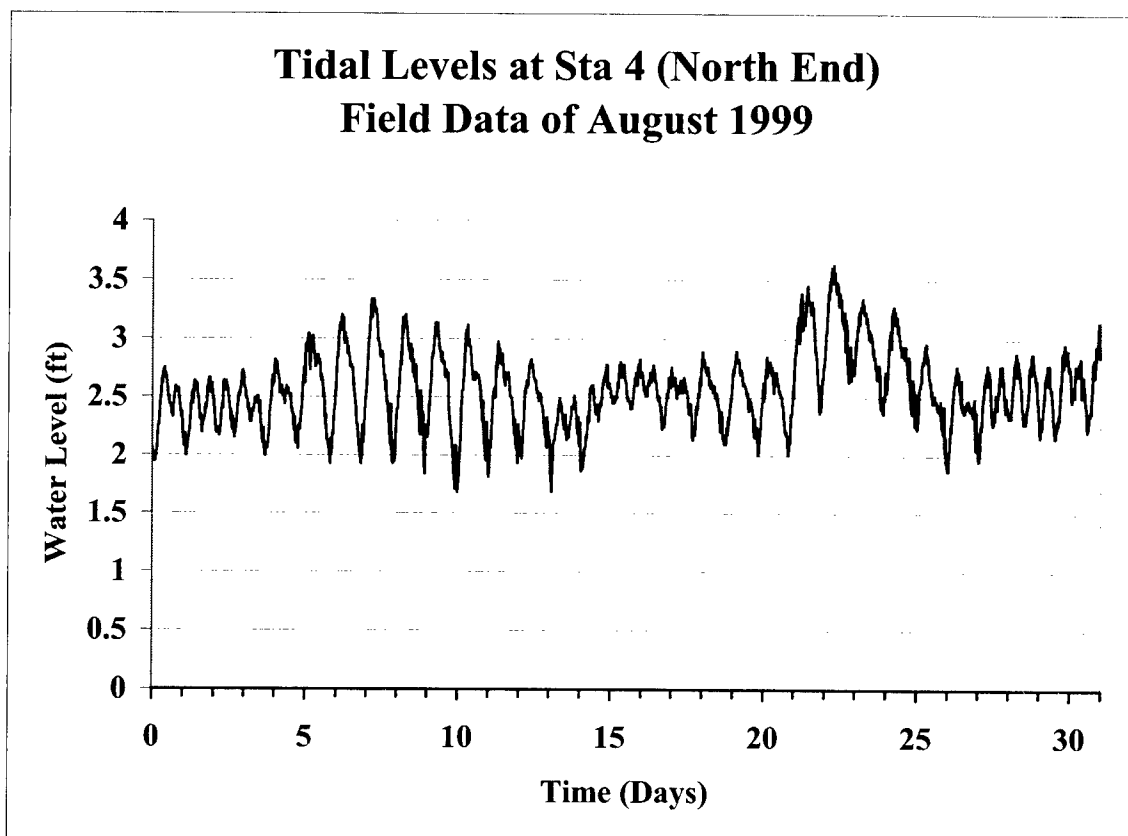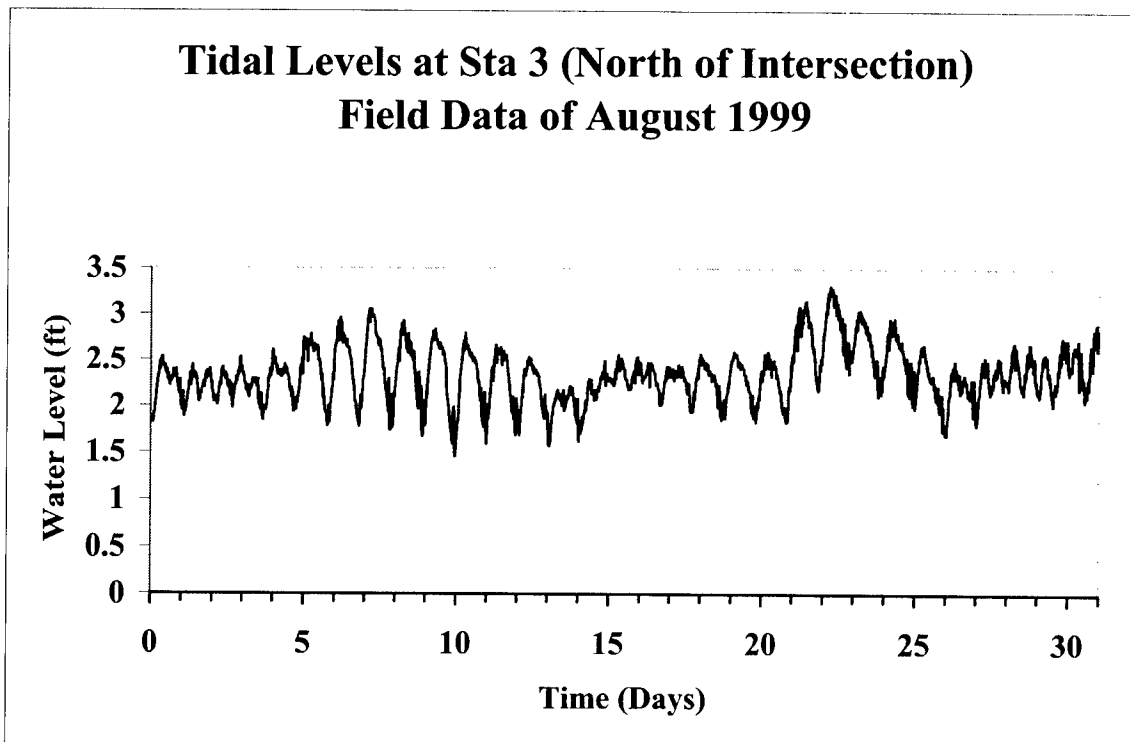
Figure 6.   Tides observed at a) sta 3 and b) sta 4 during August 1999

Tidal Levels at Sta 5A Field Data of August 1999

Water Level (ft) vs Time (Days)

Tidal Levels at Sta 6A
Field Data of August 1999

Water Level (ft) vs Time (Days)
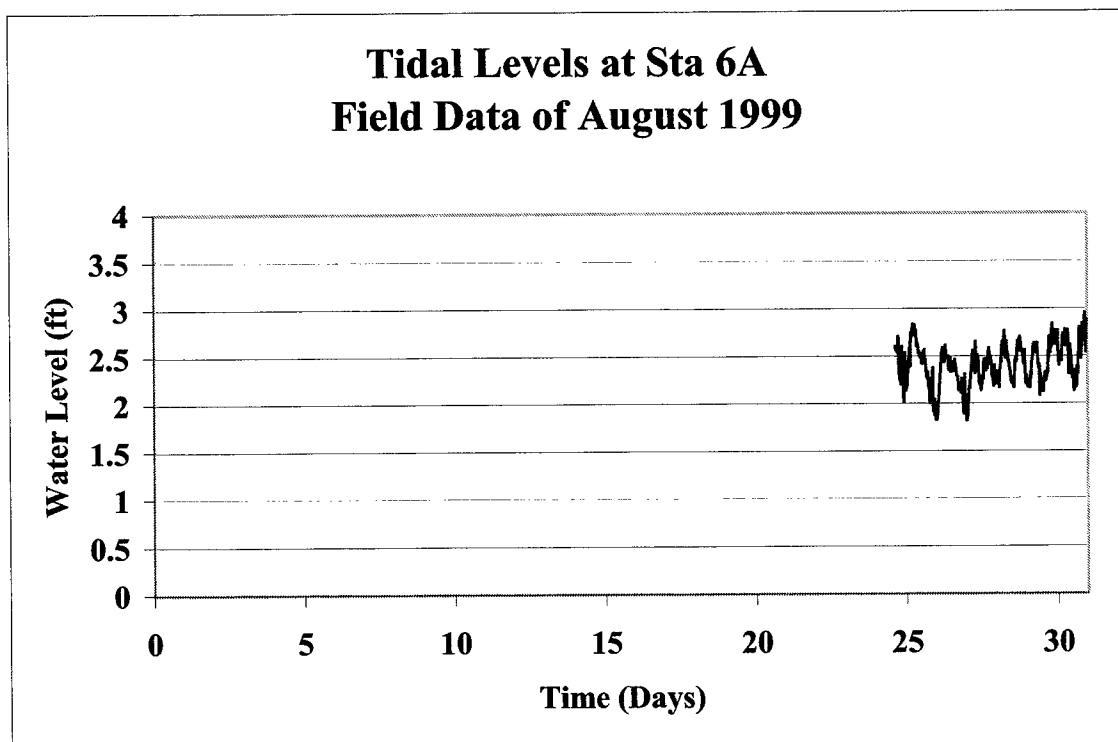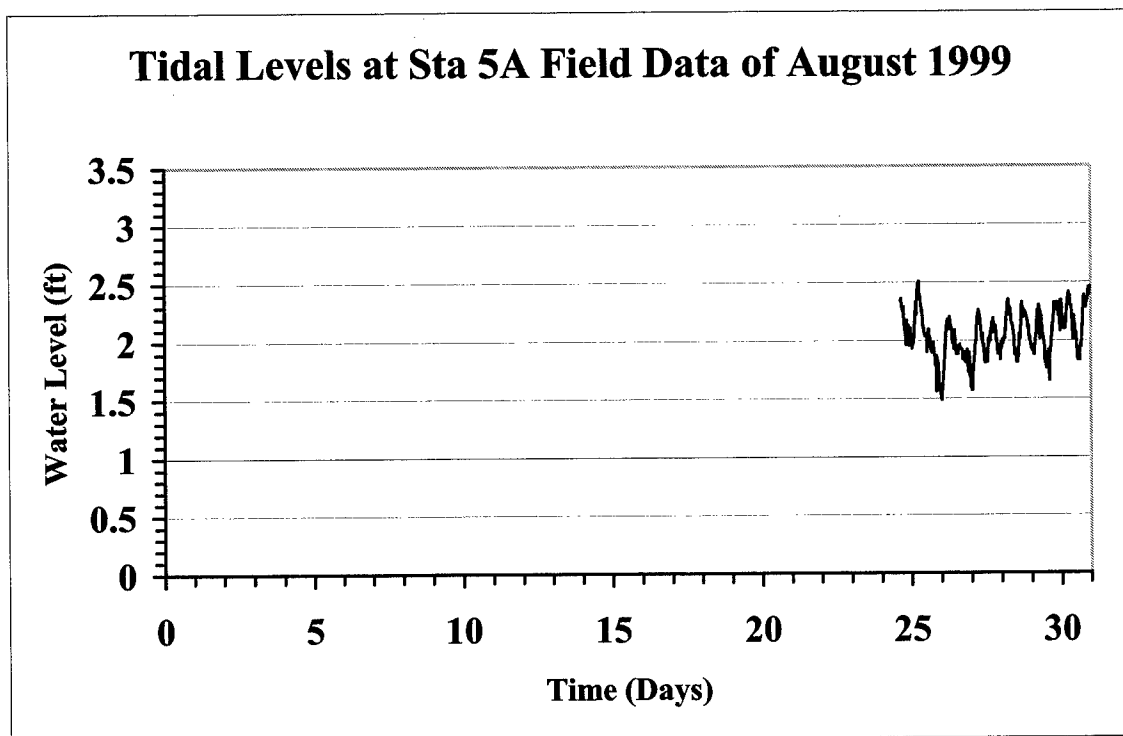
Figure 7.   Tides observed at a) sta 5A and b) sta 6A during August 1999
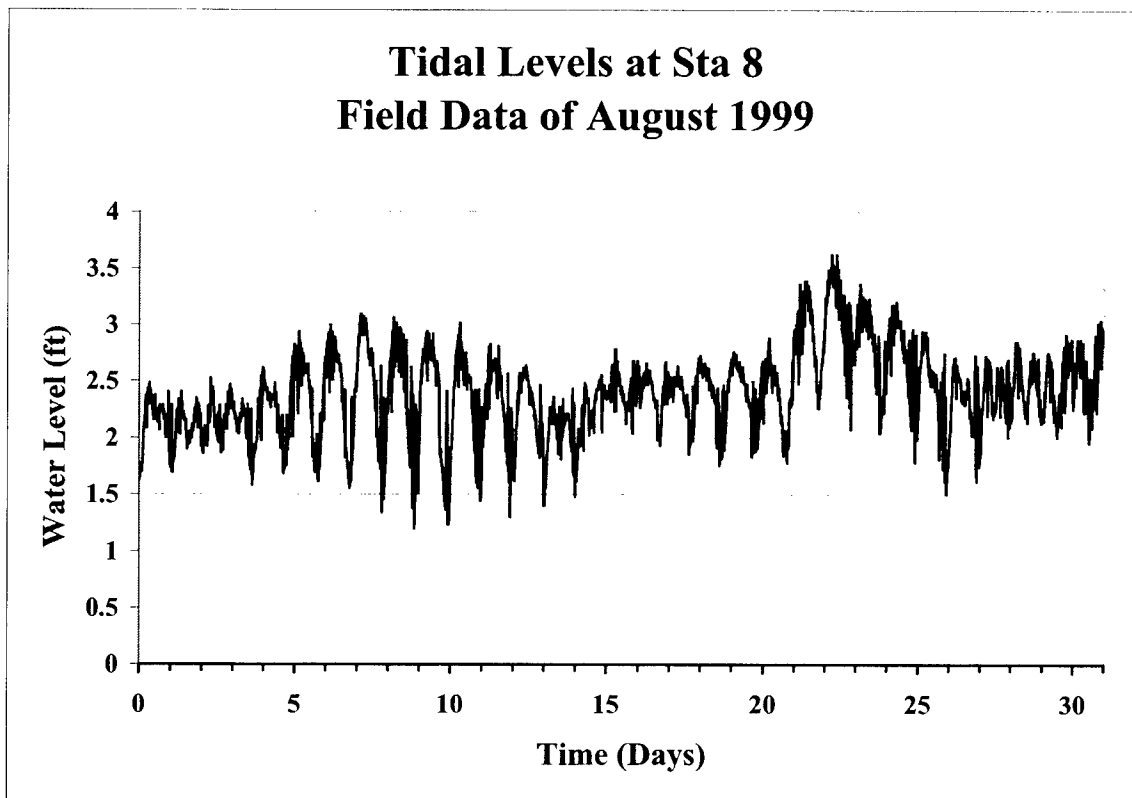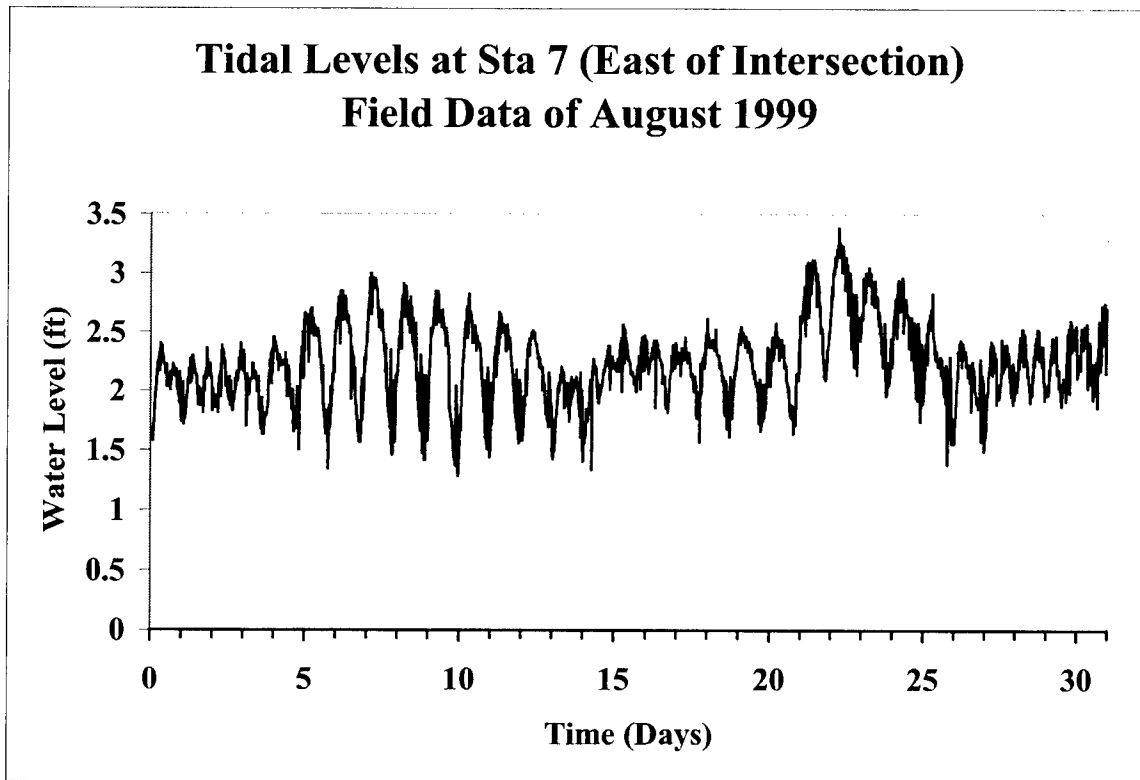
Figure 8.   Tides observed at a) sta 7 and b) 8 during August 1999

Tidal Levels at Sta 10 (Brazos River Intersection)
Field Data of August 1999
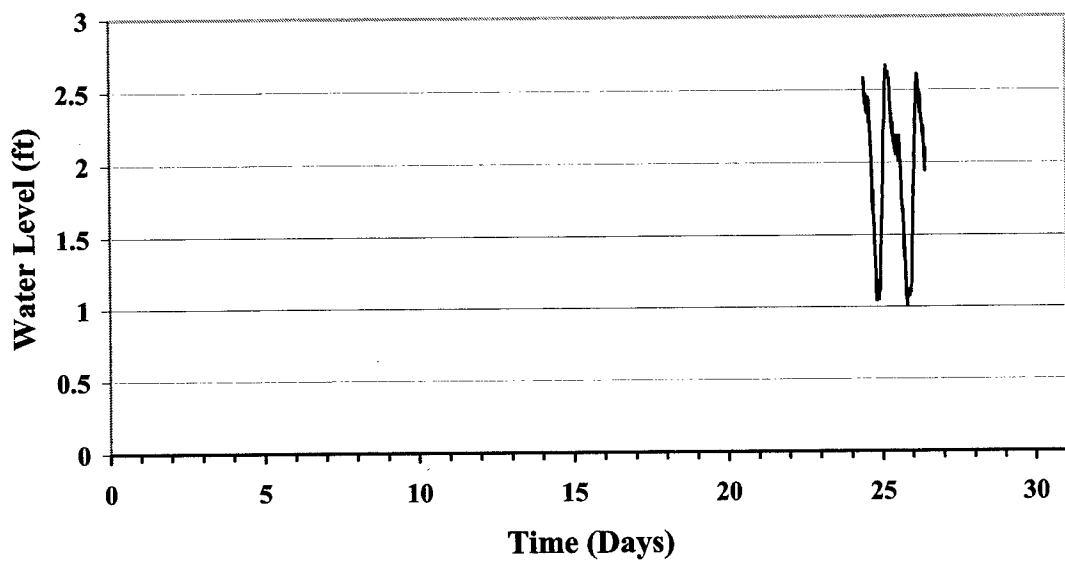
Figure 9.   Tides observed at sta 10 during August 1999
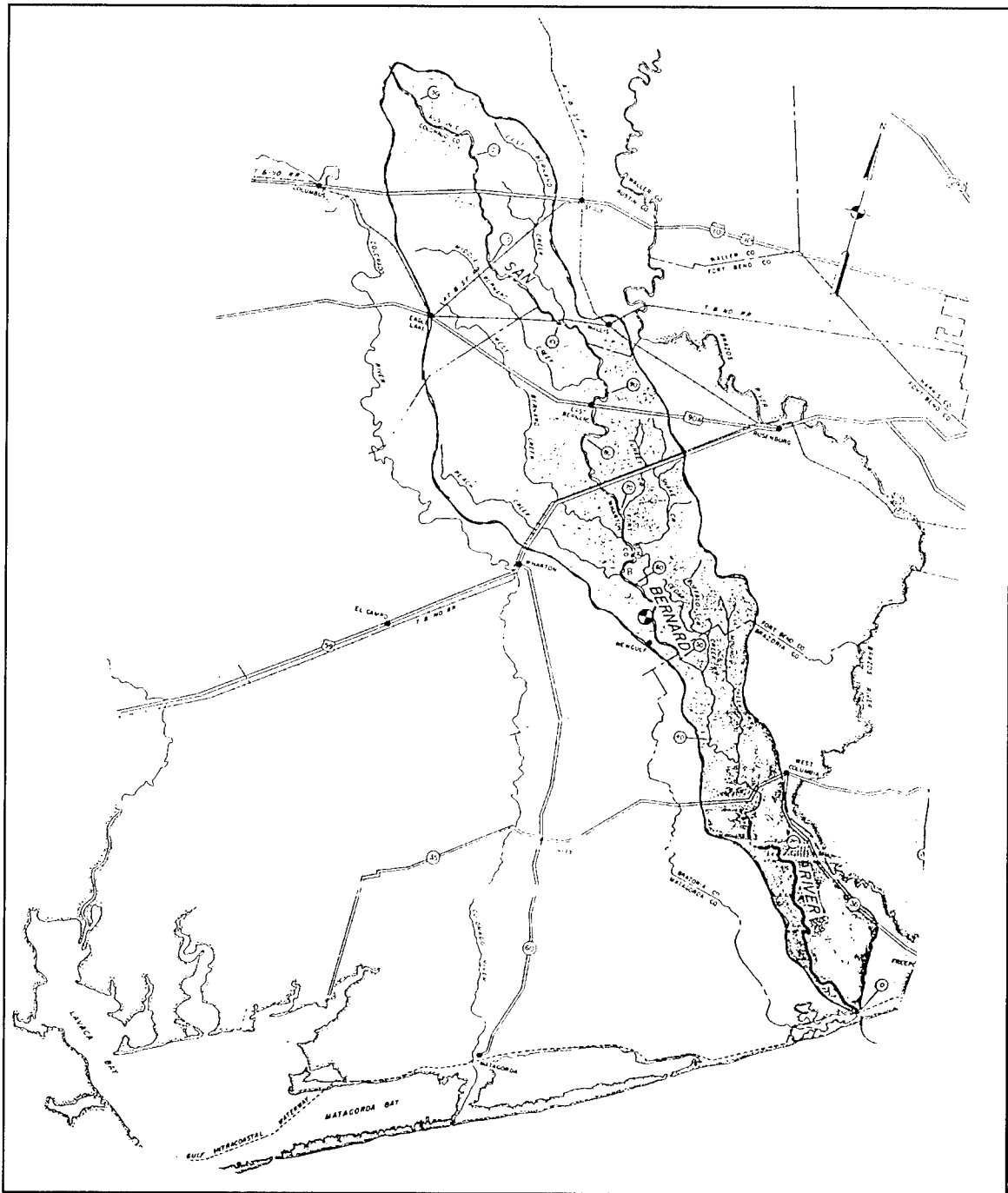
Figure 10. Drainage area boundary of San Bernard River

San Bernard River Discharge: 1990

San Bernard River Discharge: 1991
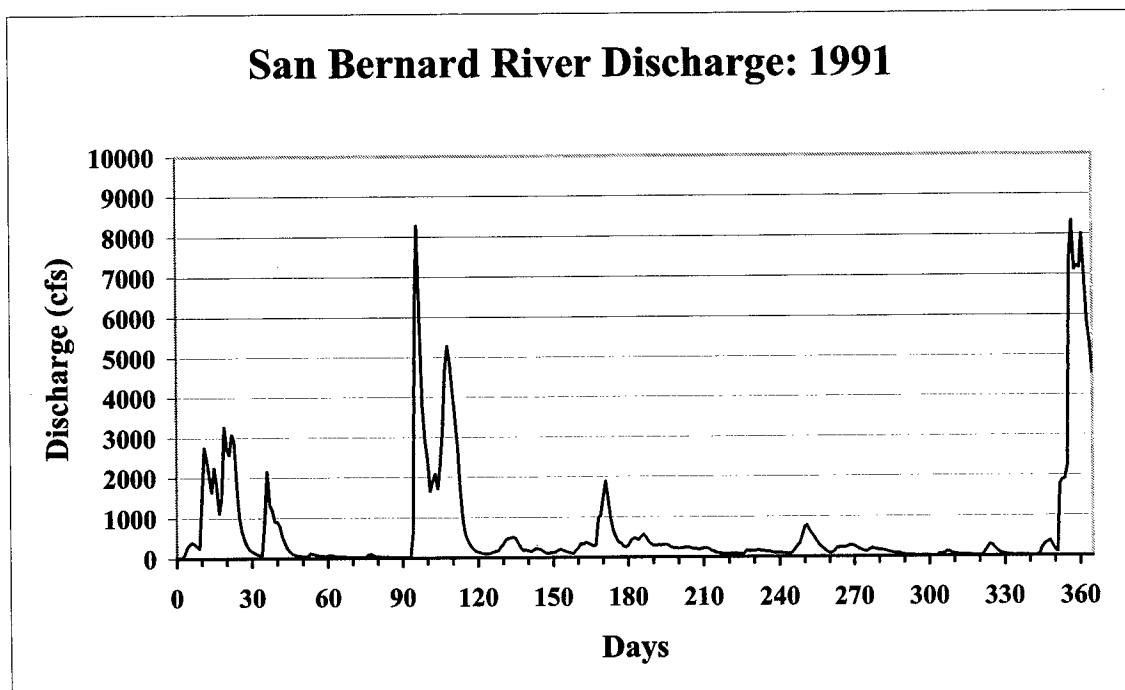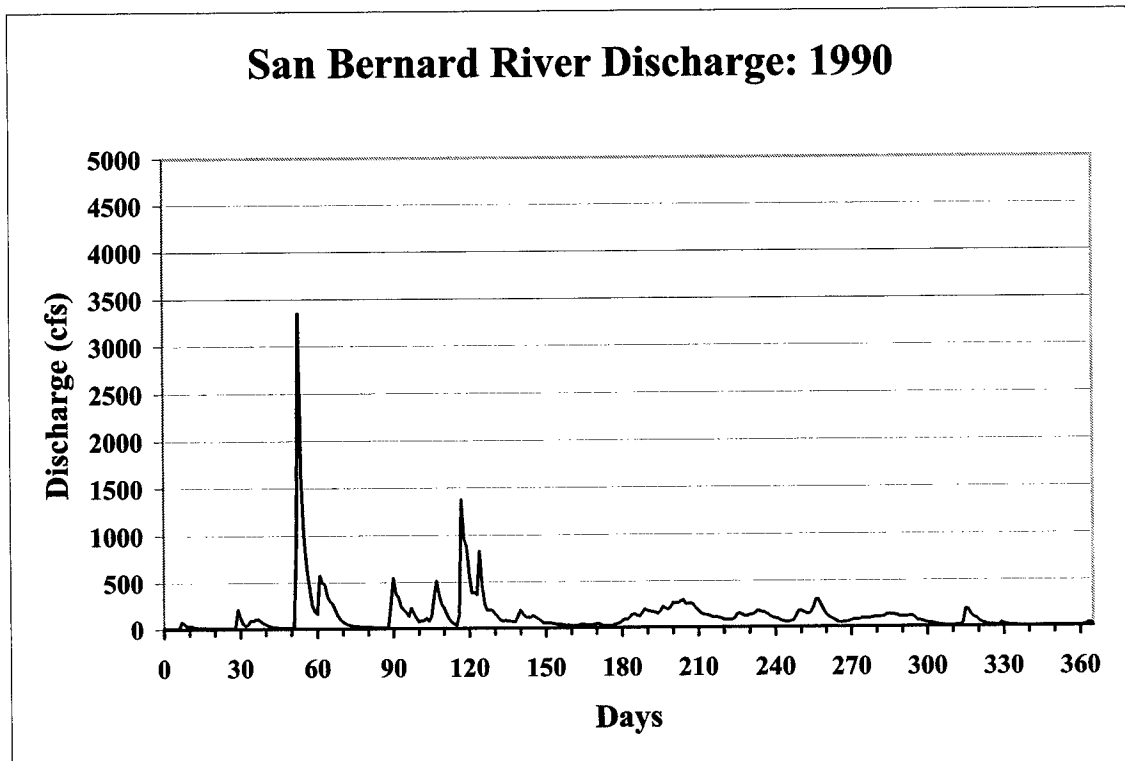
Figure 11. San Bernard River discharge for a) year 1990 and b) year 1991 (Discharge is in cubic feet per second, to convert to cubic meters per second, multiply by 0.02831)
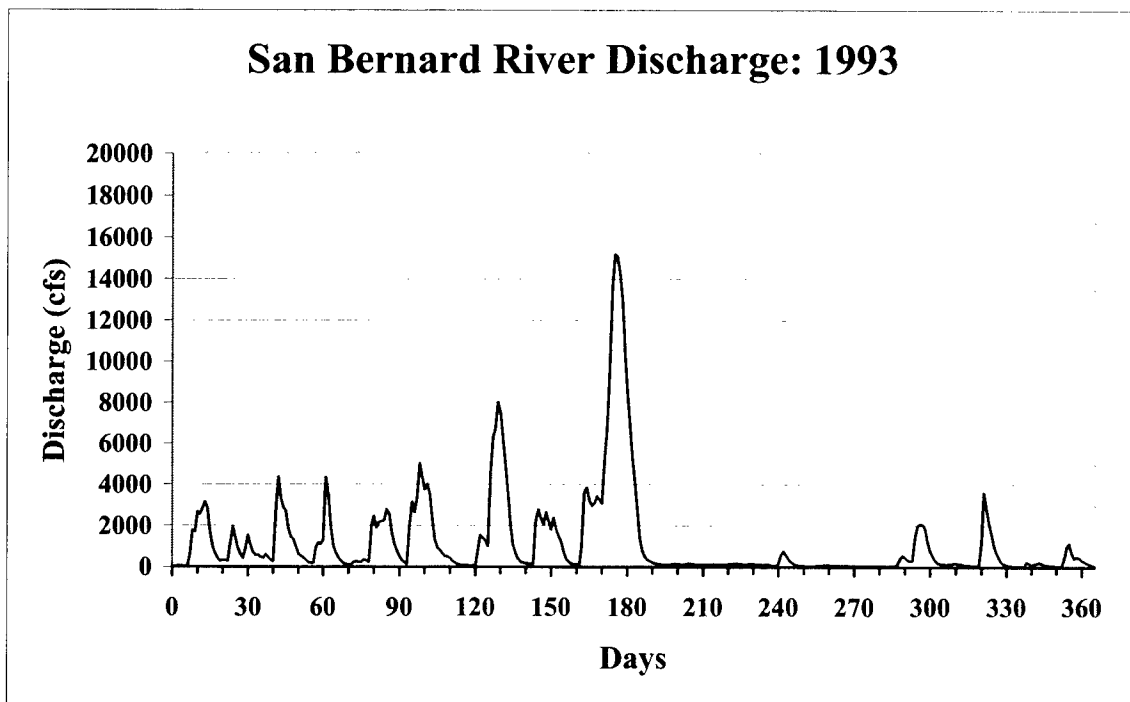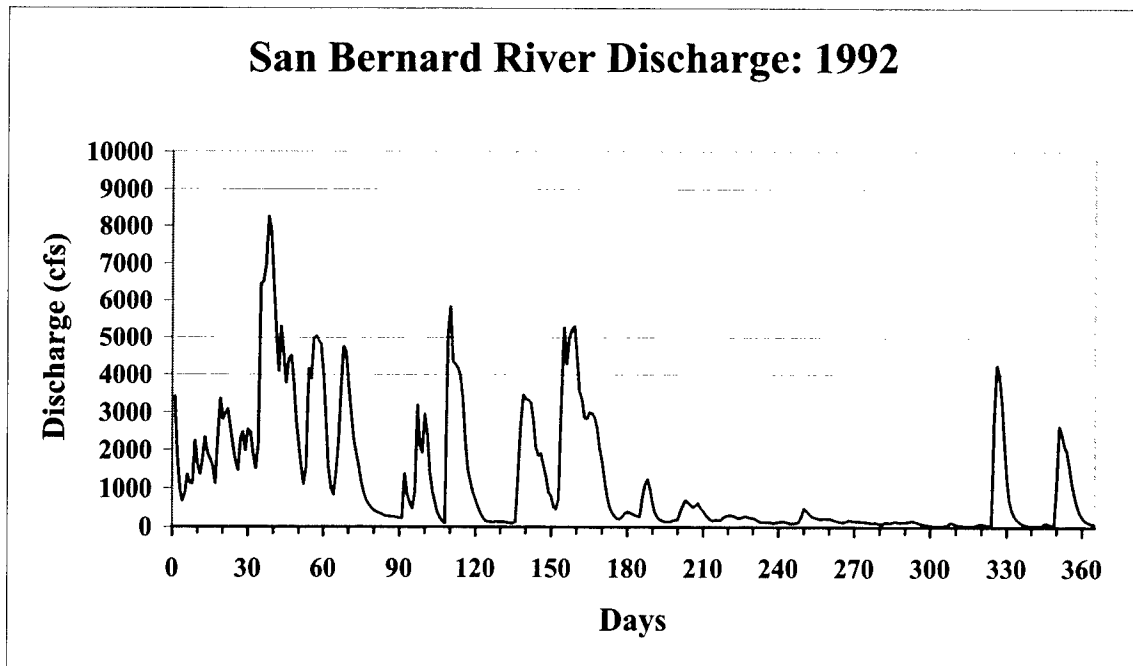
Figure 12. San Bernard River discharge for a) year 1992 and b) year 1993
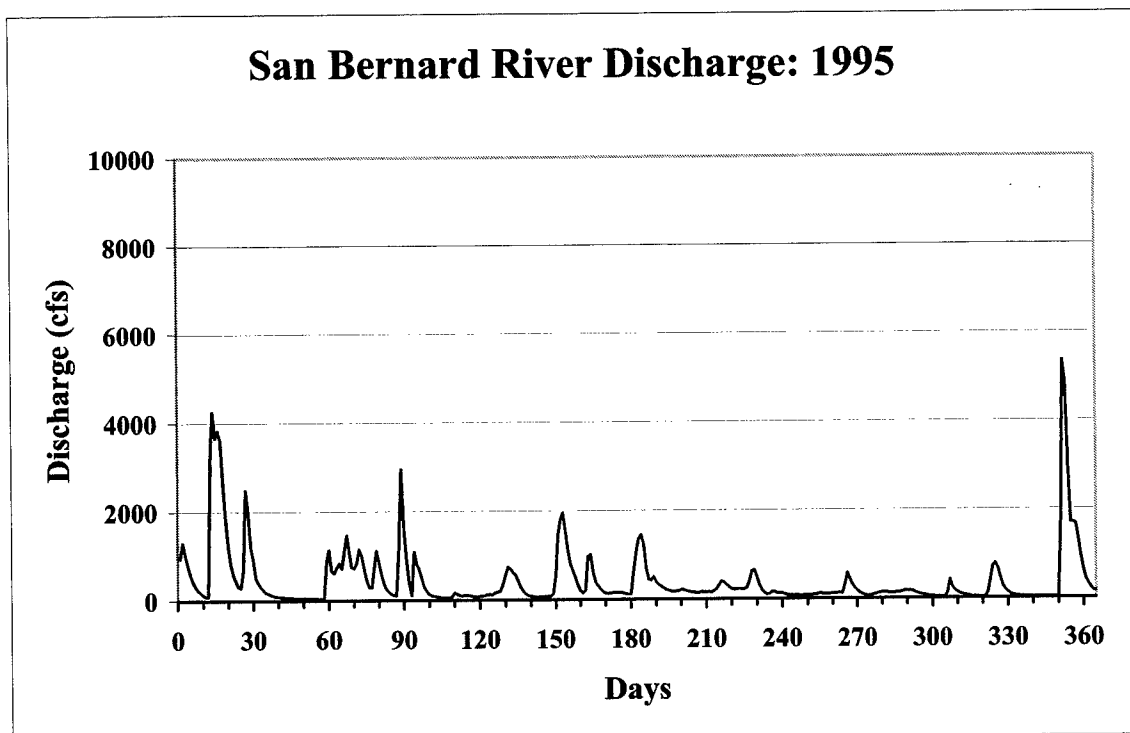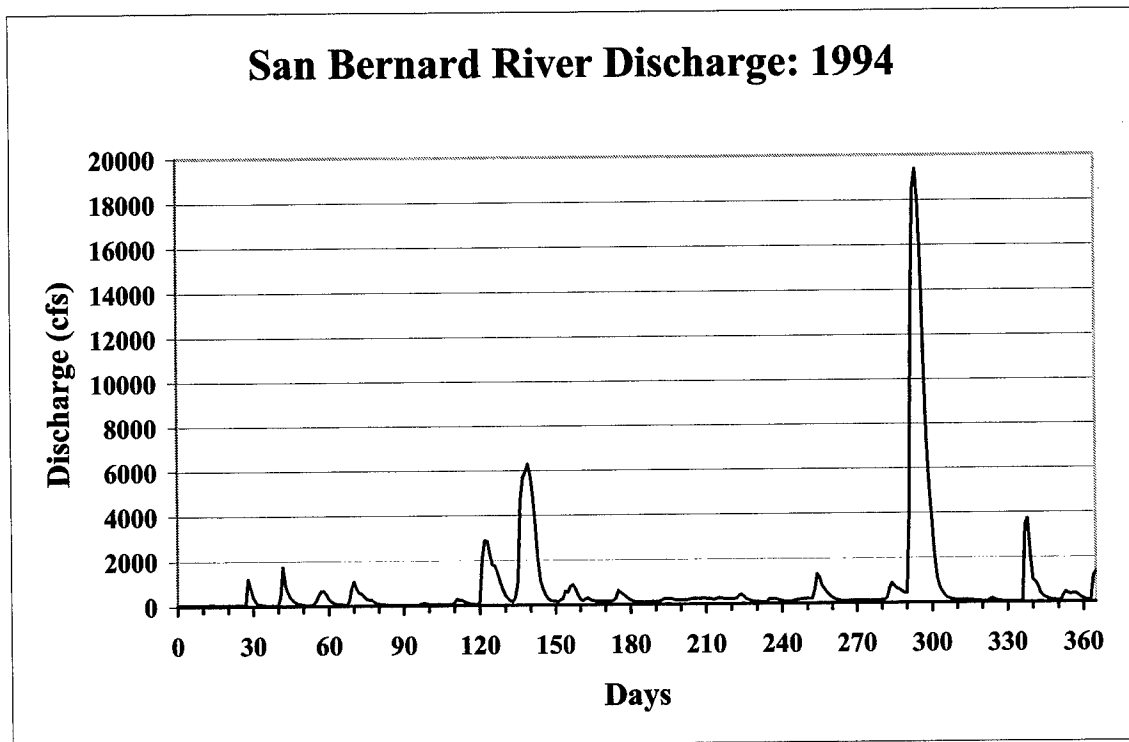
Figure 13.   San Bernard River discharge for a) year 1994 and b) year 1995

San Bernard River Discharge: 1996

San Bernard River Discharge: 1997
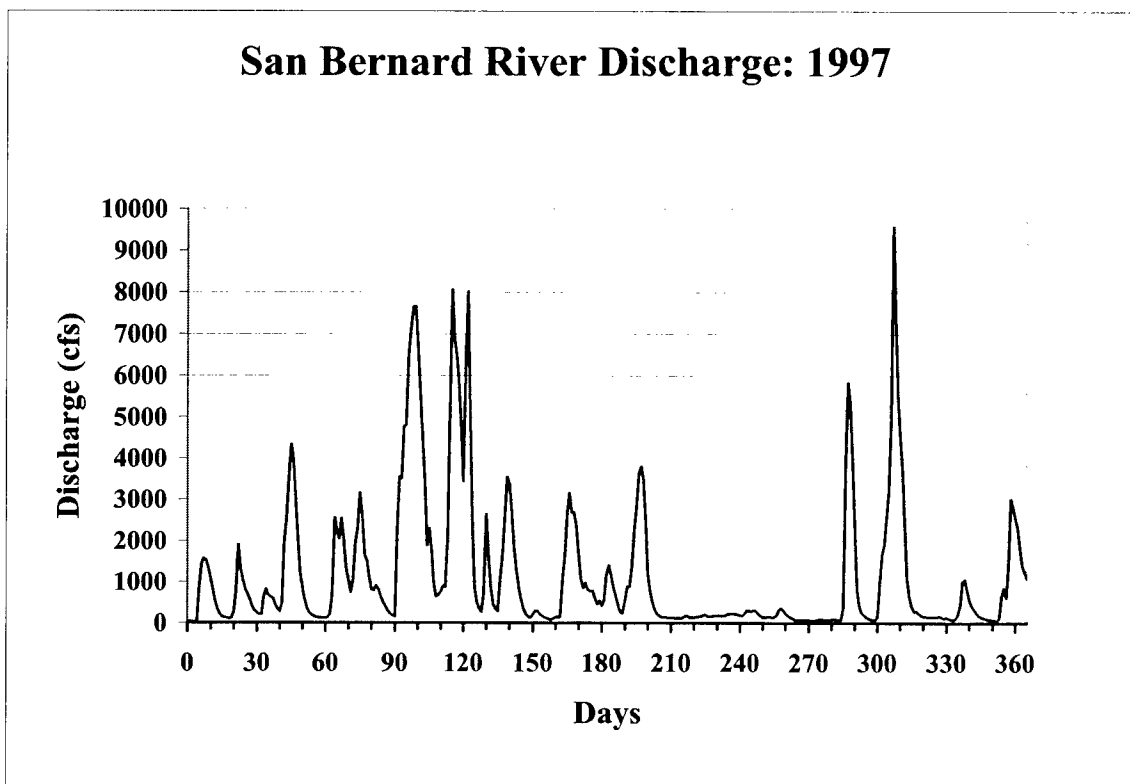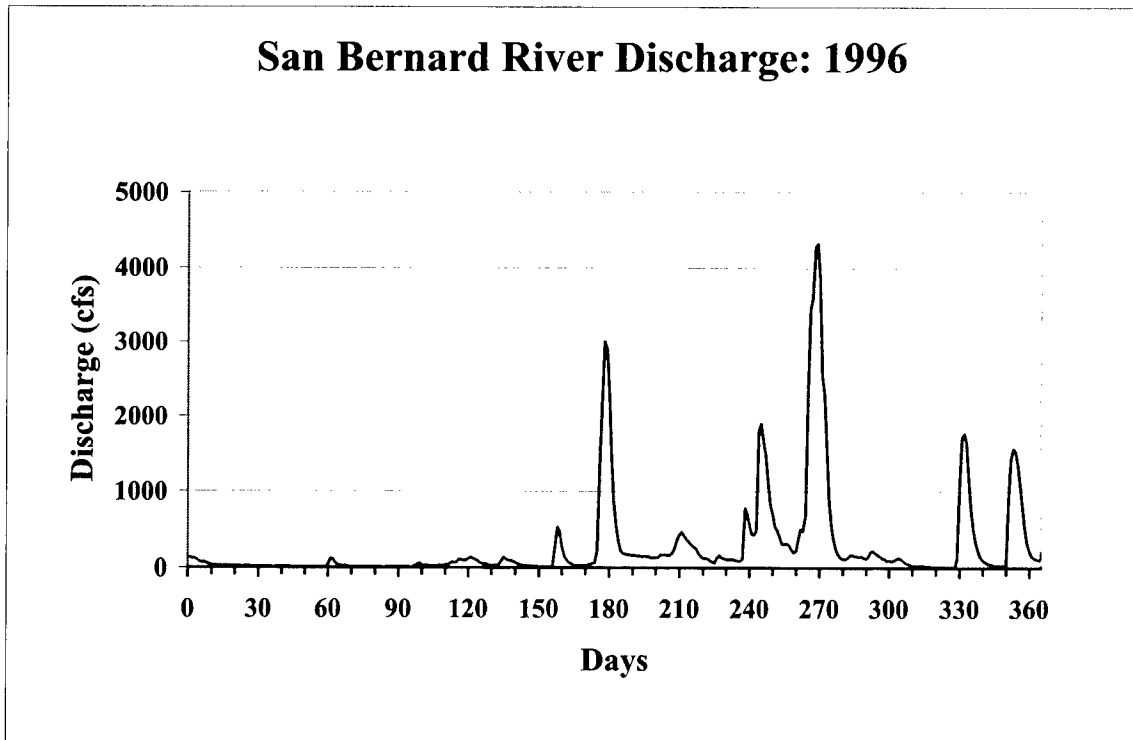
Figure 14.   San Bernard River discharge for a) year 1996 and b) year 1997

San Bernard River Discharge: 1998

Discharge (cfs) vs. Days
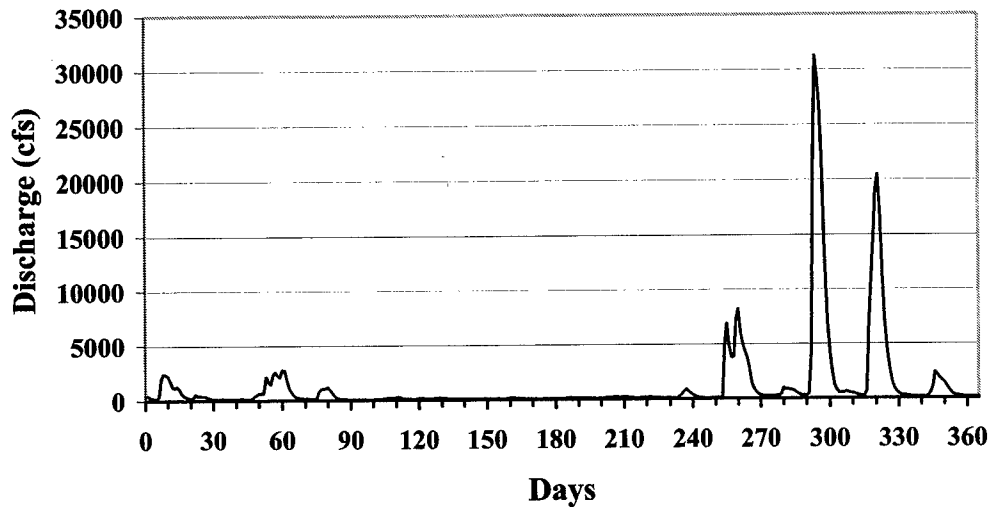
San Bernard River Discharge: 1999

Discharge (cfs) vs. Days
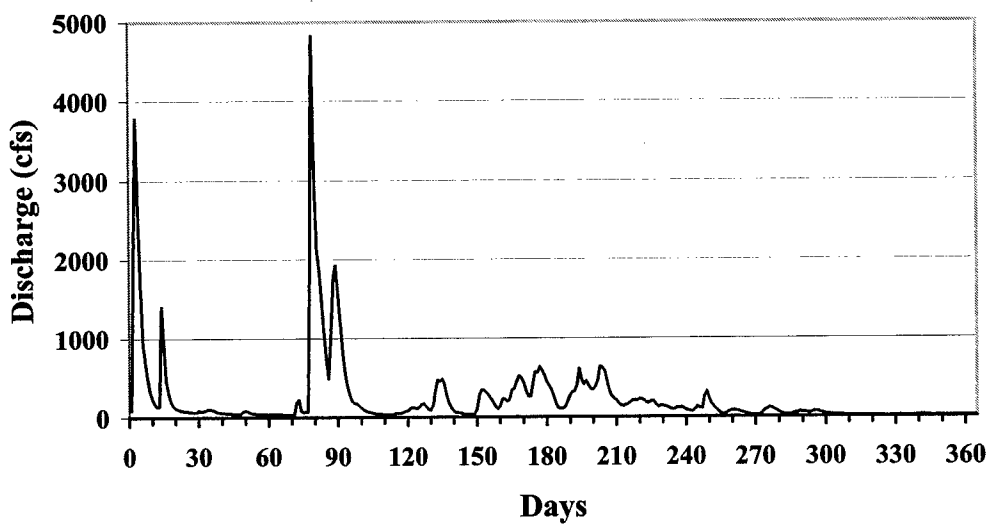
Figure 15.   San Barnard River discharge for a) year 1998 and b) year 1999
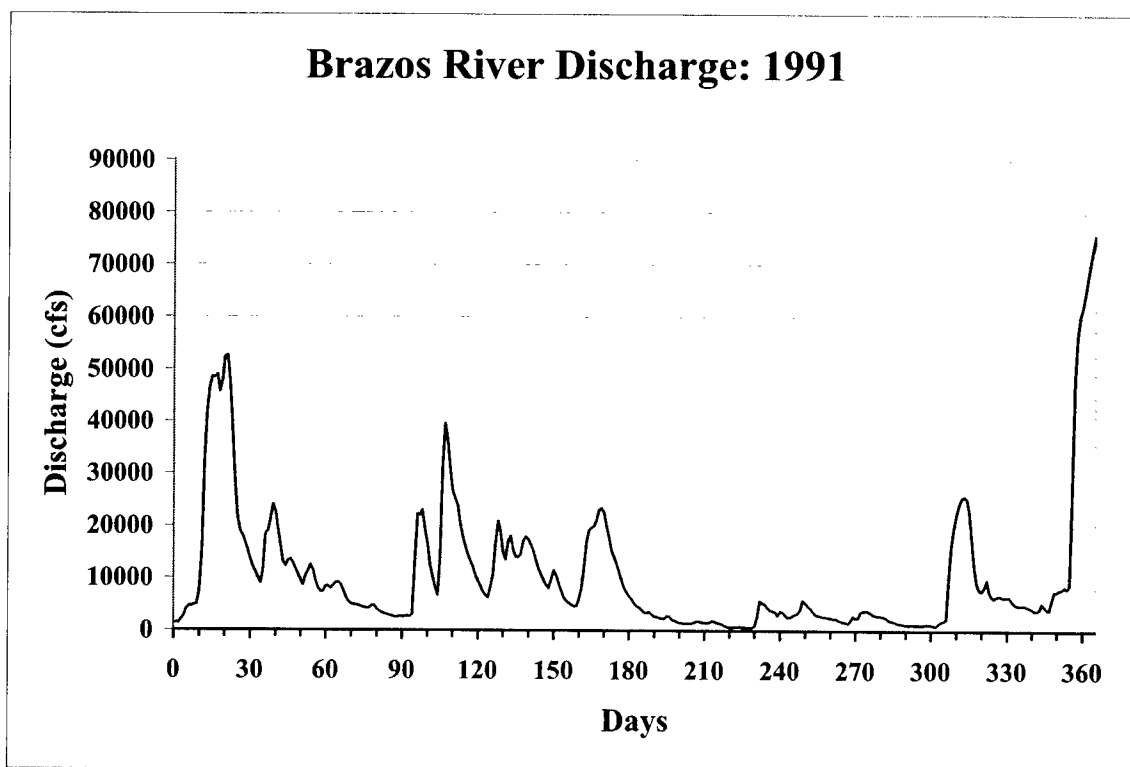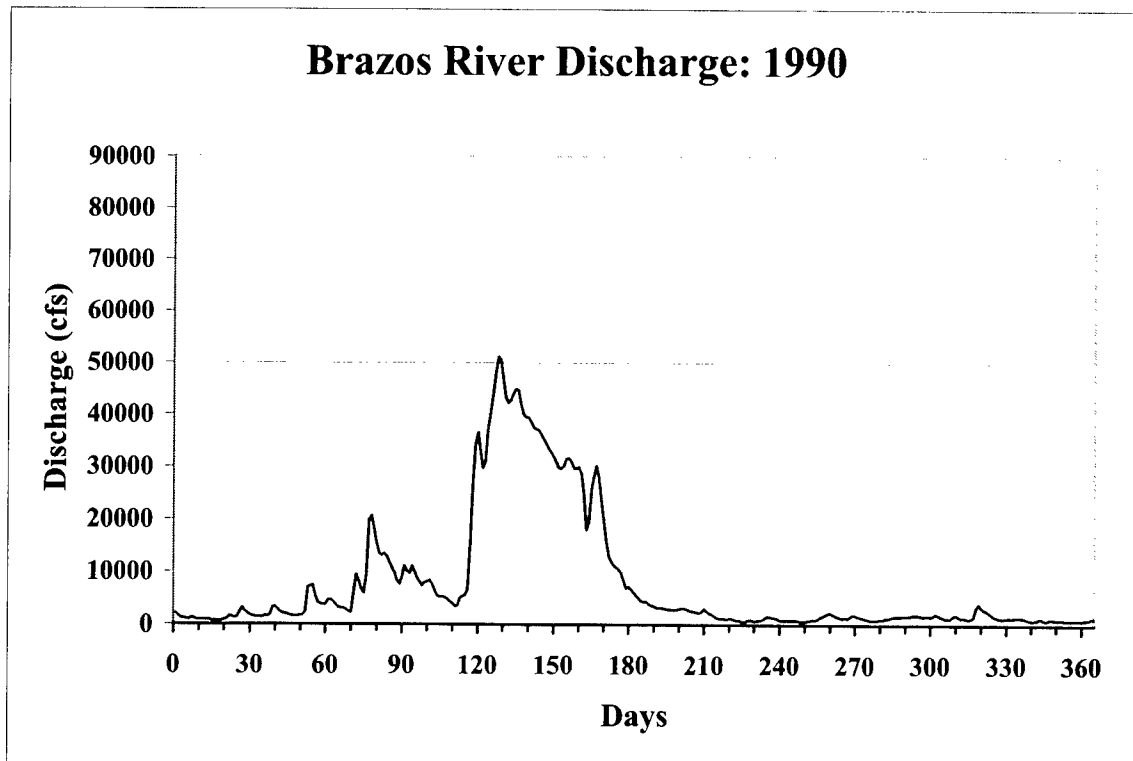
Figure 16. Brazos River discharge for a) year 1990 and b) year 1991
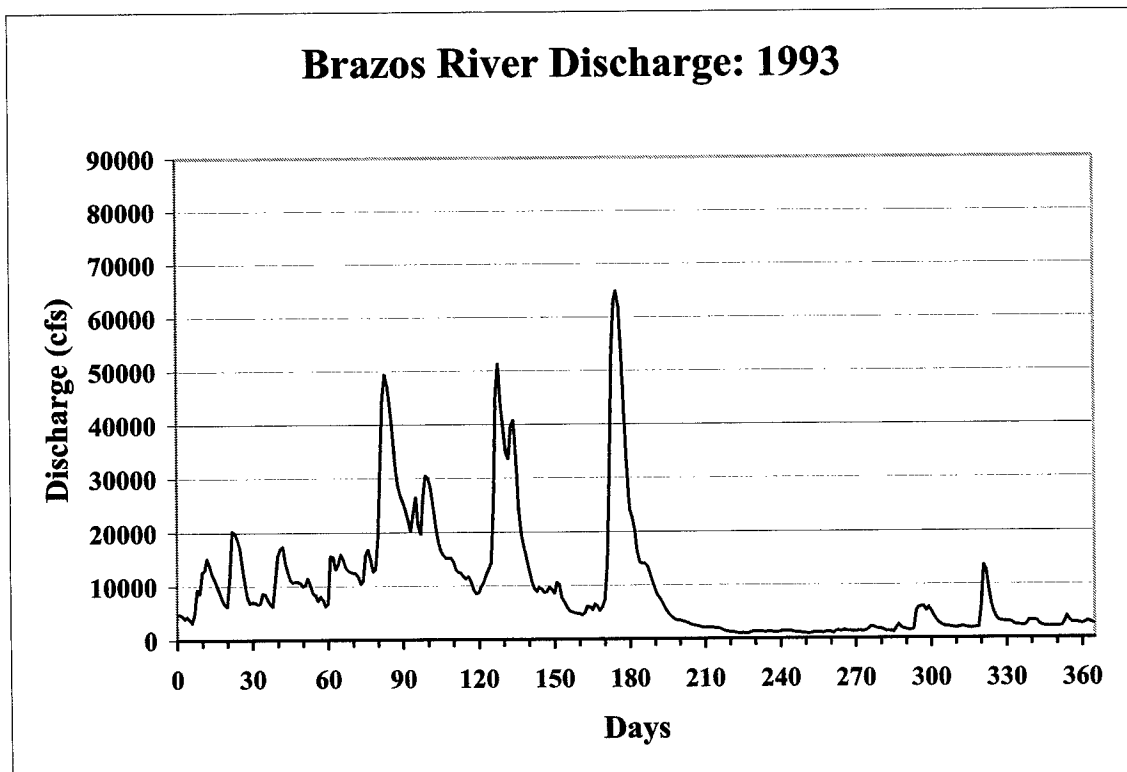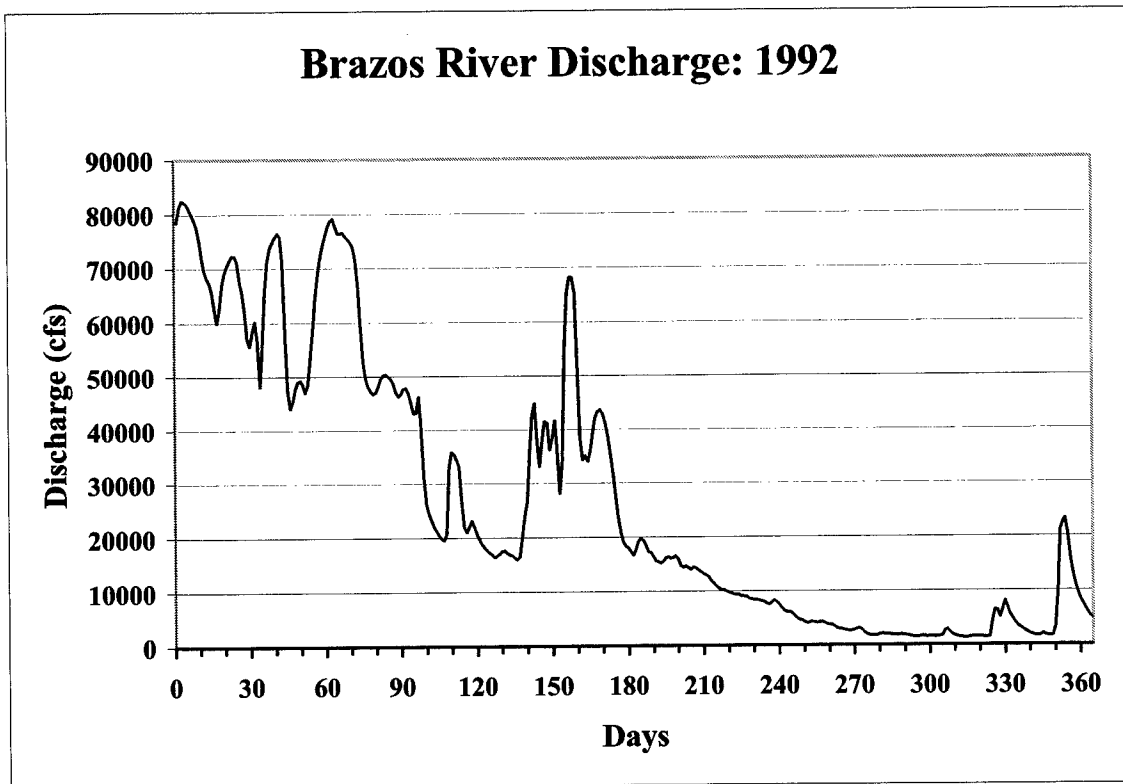
Figure 17. Brazos River discharge for a) year 1992 and b) year 1993
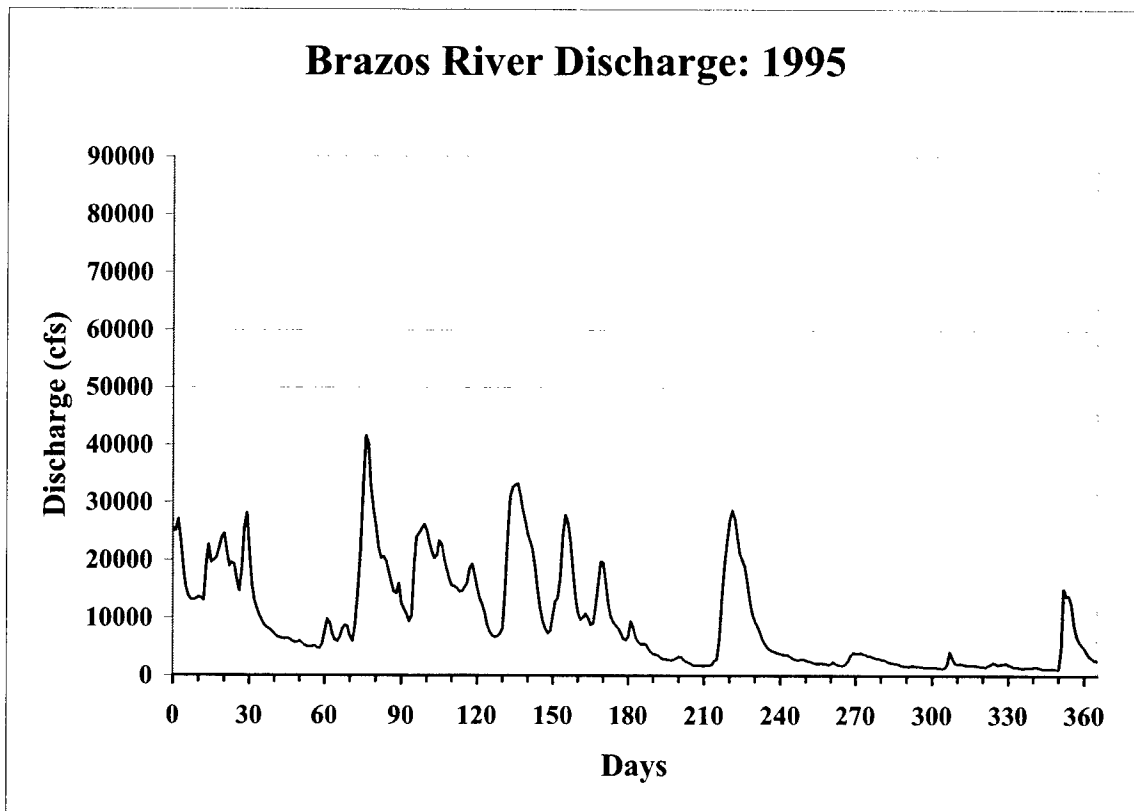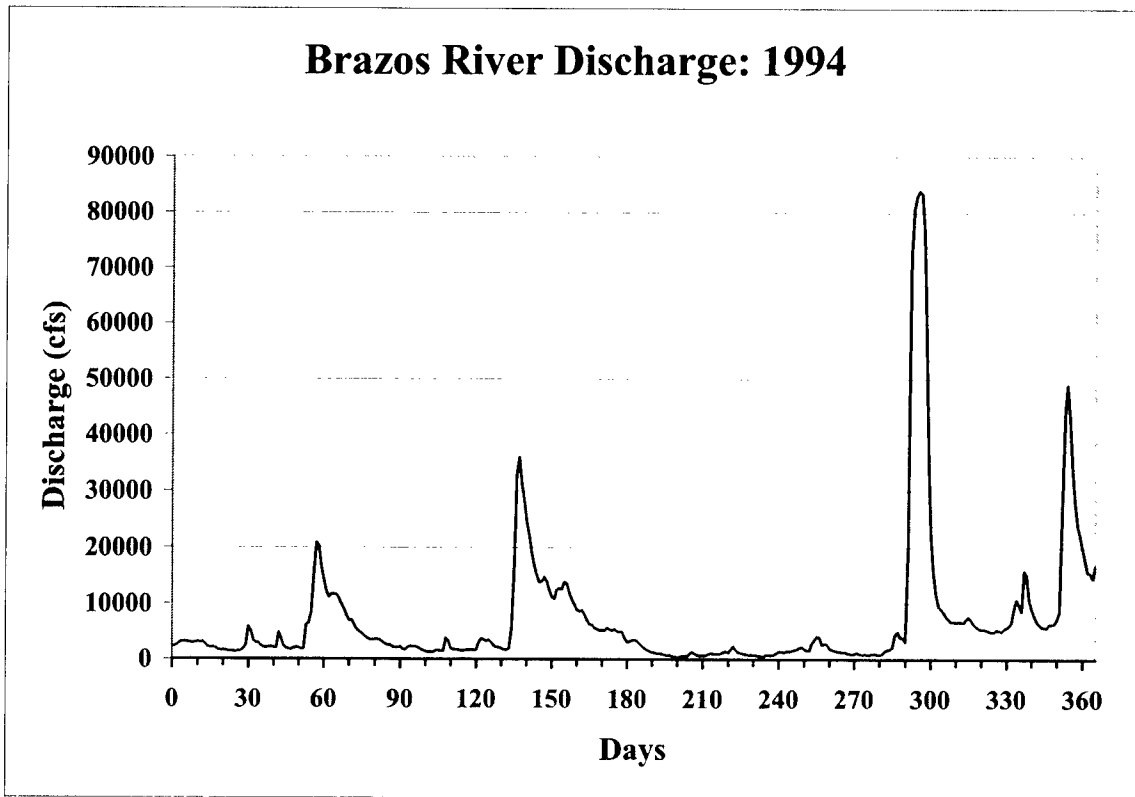
Figure 18.   Brazos River discharge for a) year 1994 and b) year 1995
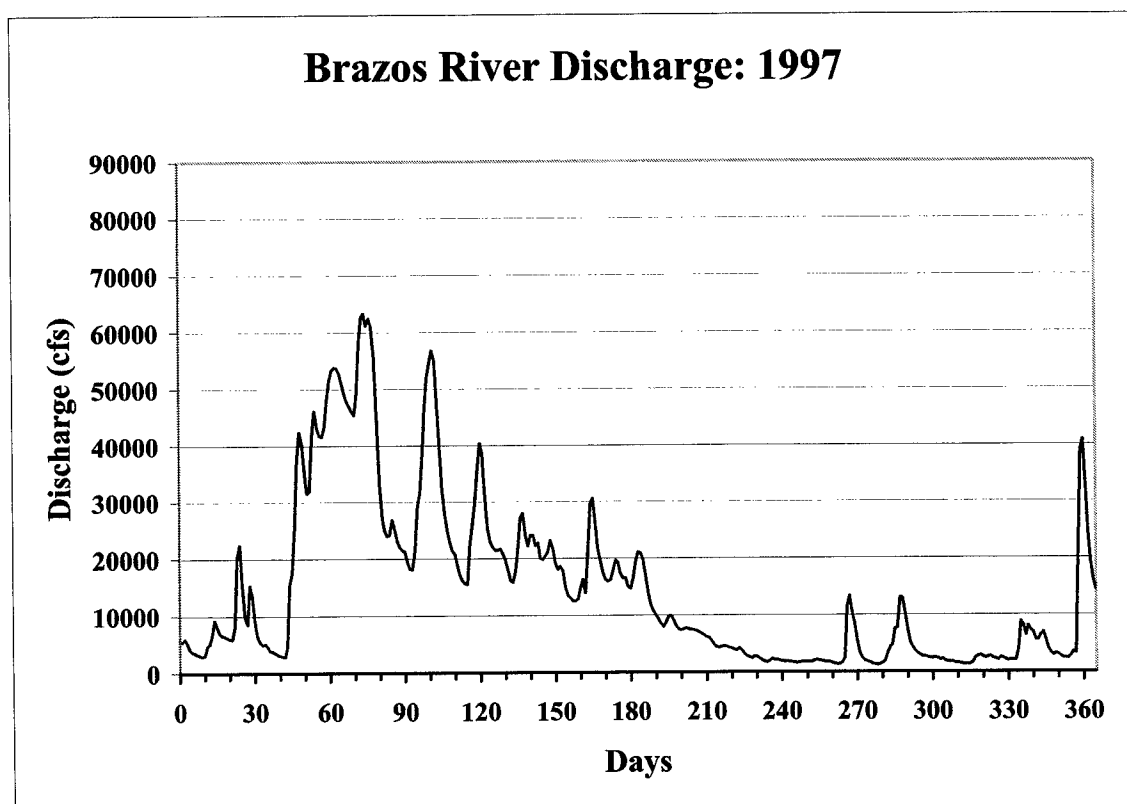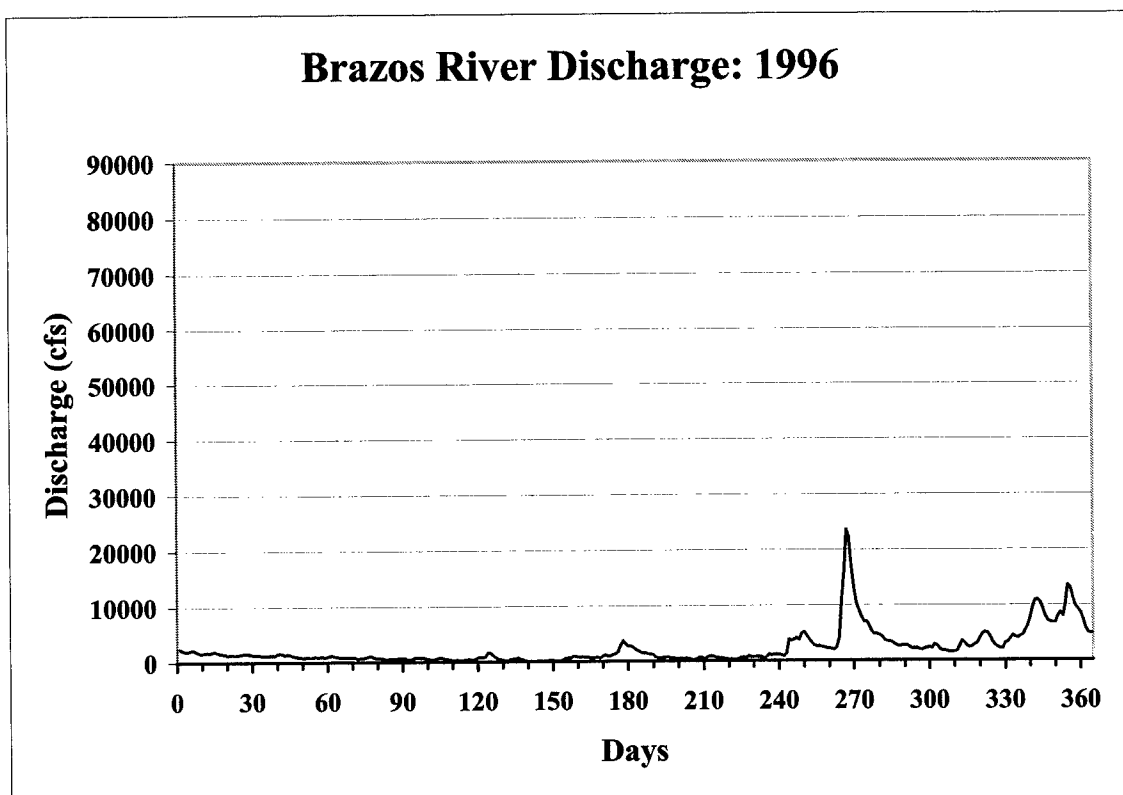
Figure 19.   Brazos River Discharge for a) year 1996 and b) year 1997
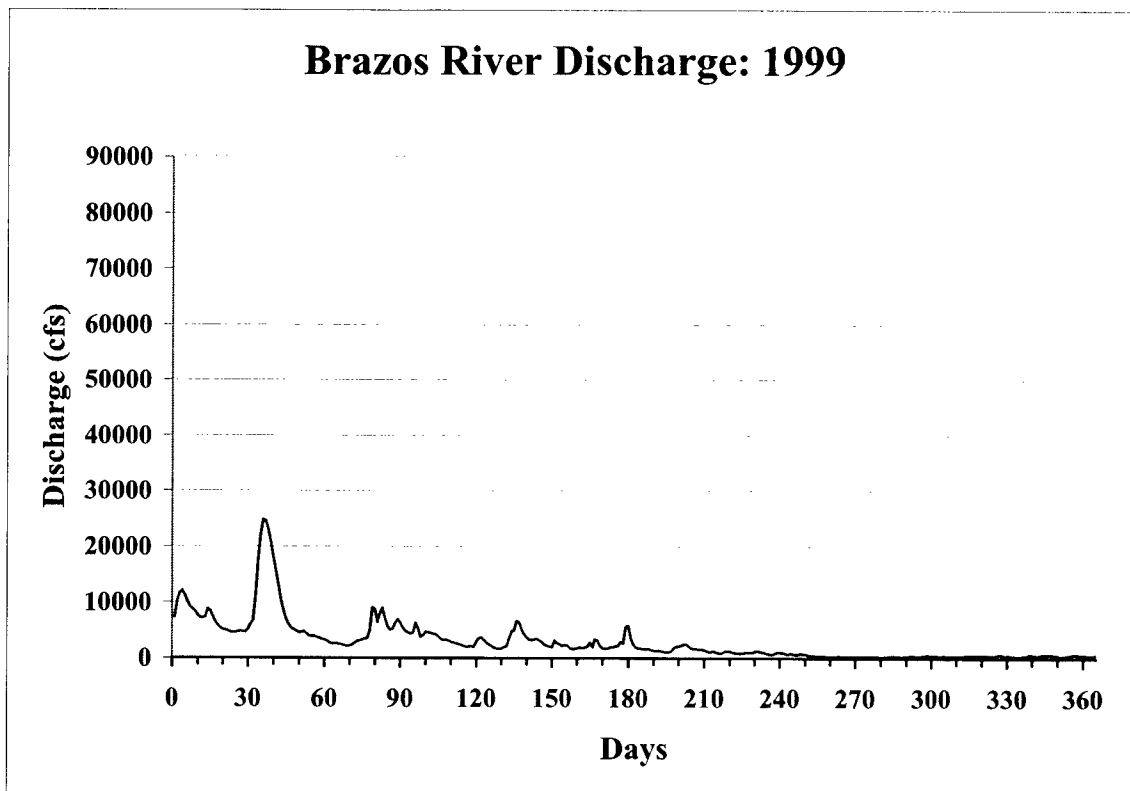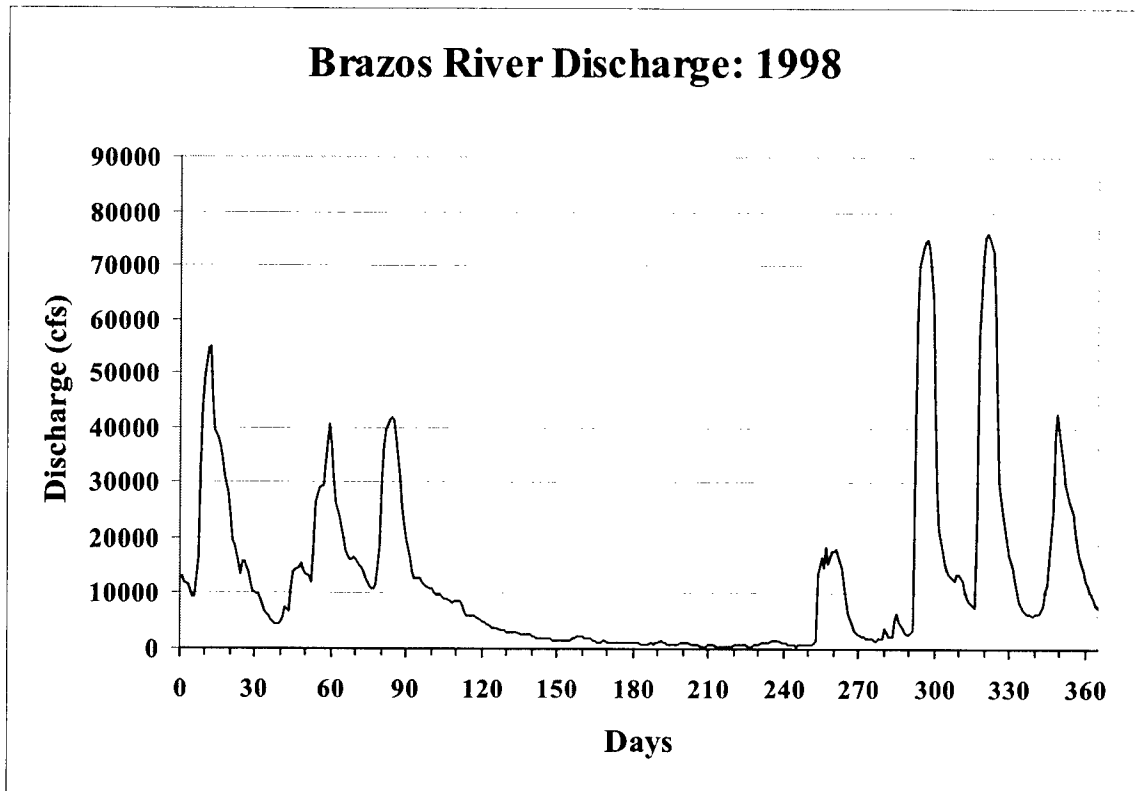
Figure 20. Brazos River discharge for a) year 1998 and b) year 1999
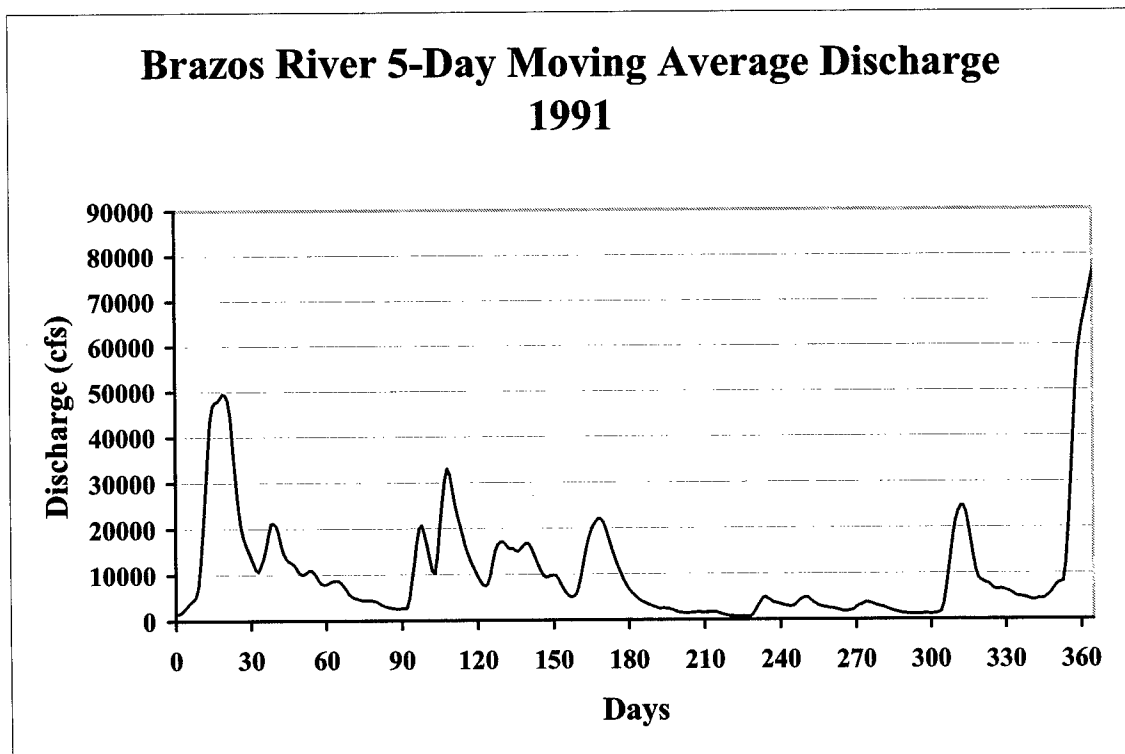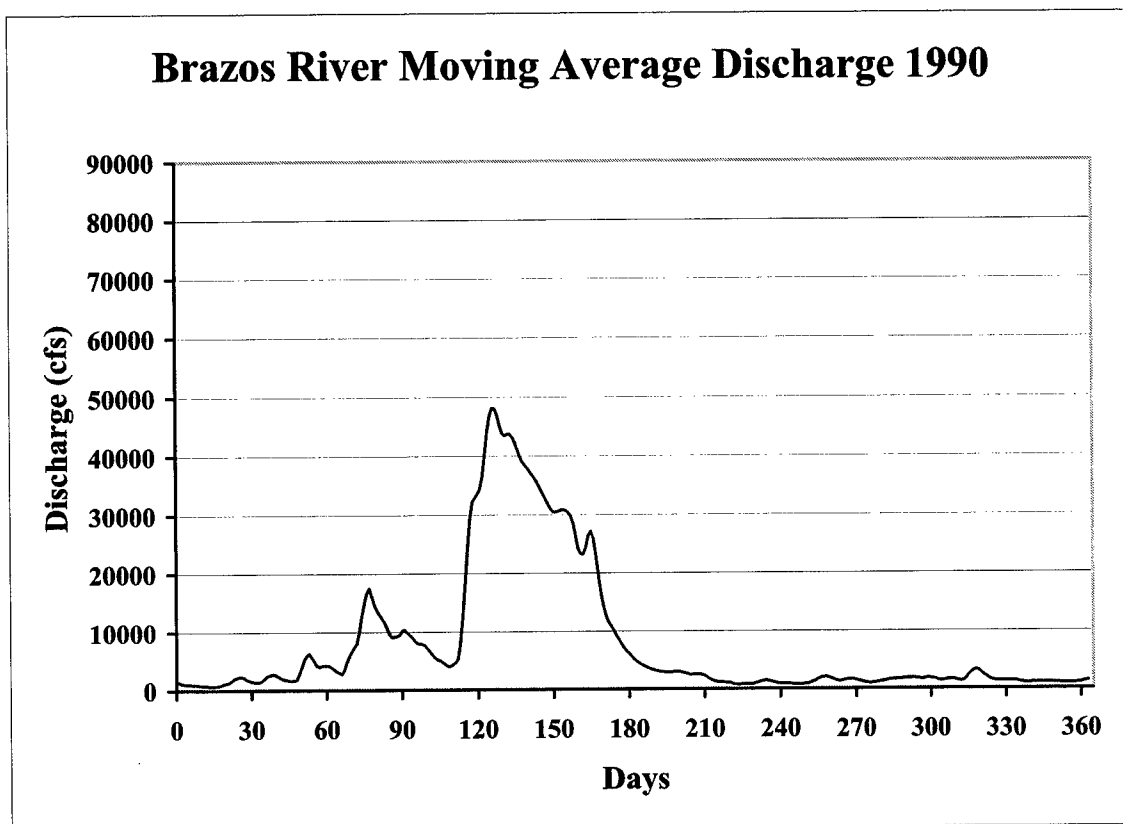
Figure 21. Brazos River 5-day moving average discharge for a) year 1990 and b) year 1991
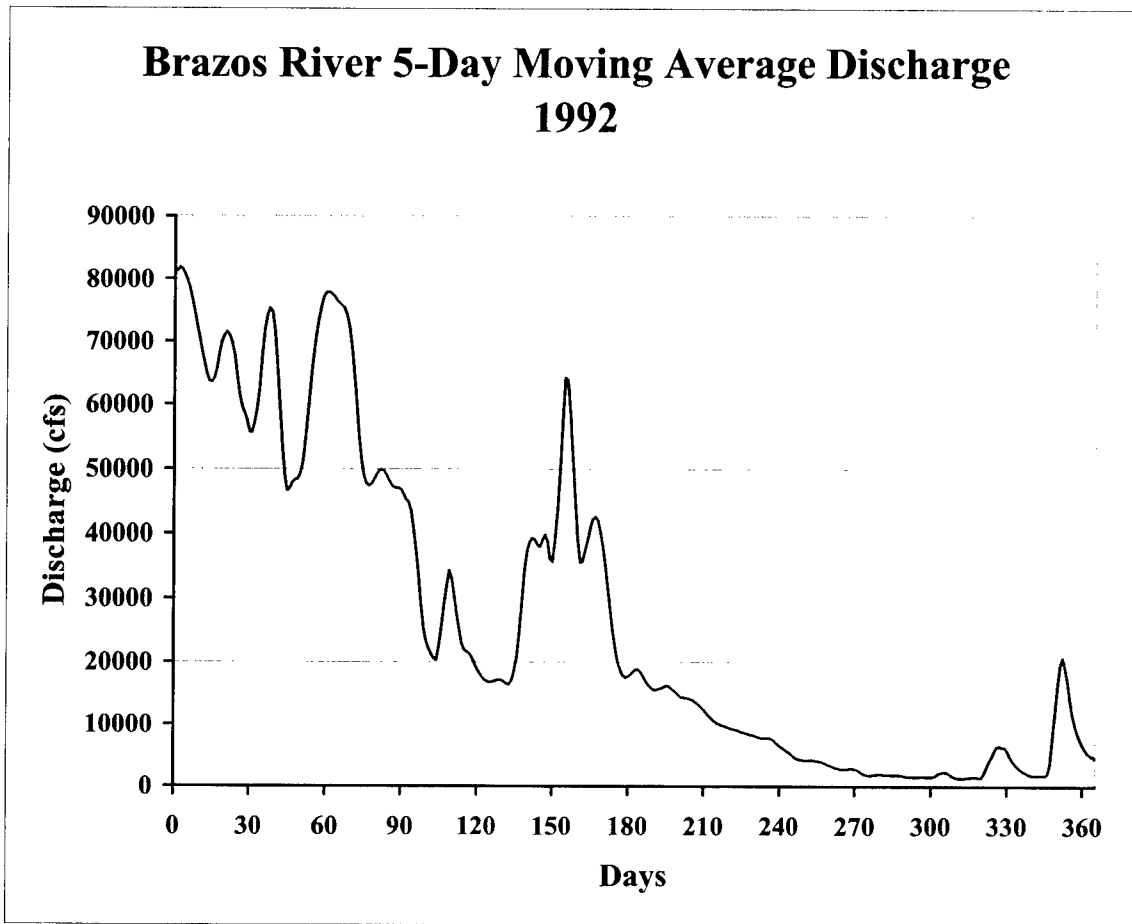
Figure 22. Brazos River 5-day moving average discharge for 1992

Model Simulation of San Bernard River Discharge
Run 1

Discharge (1,000 cfs)

Days

Model Simulation of Brazos River Discharge
Run 1

Discharge (1,000 cfs)

Days
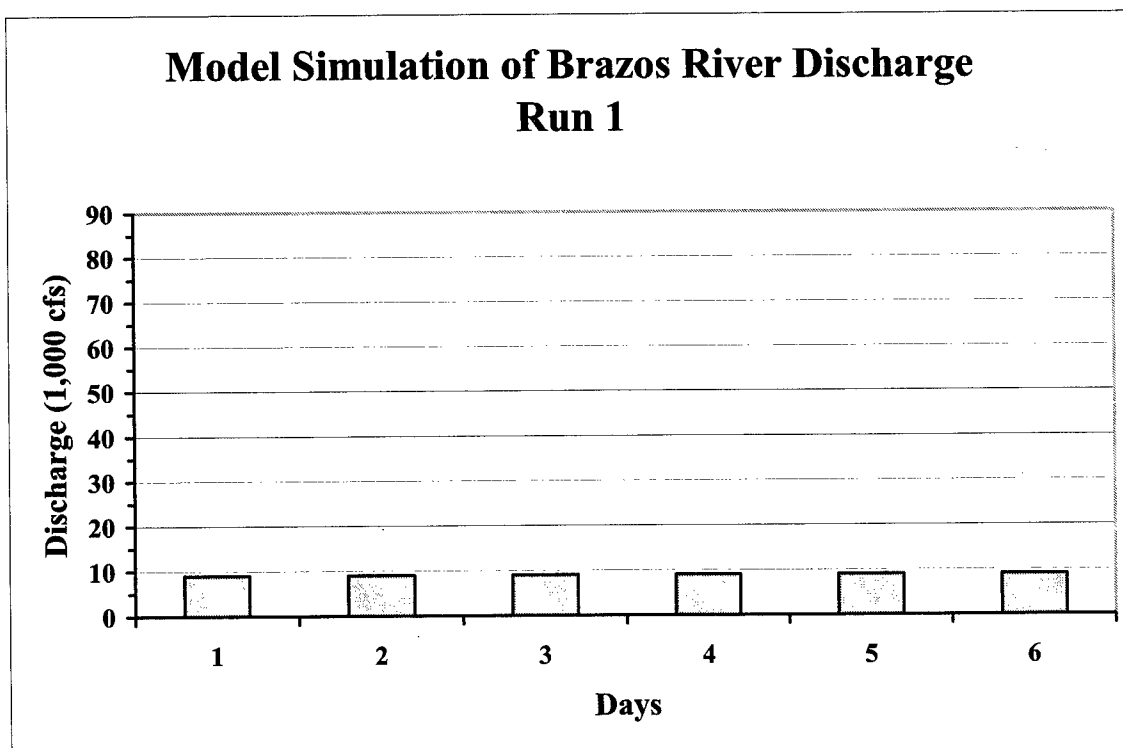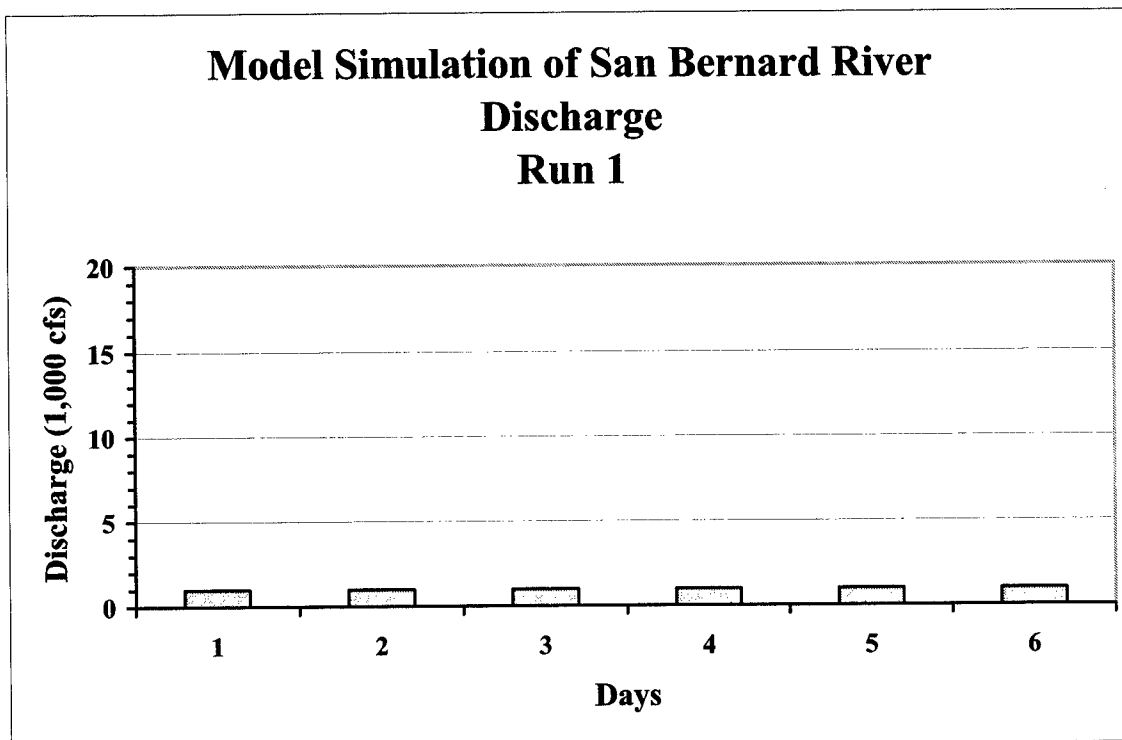
Figure 23.   Model simulation of San Bernard and Brazos River discharges used for Run 1
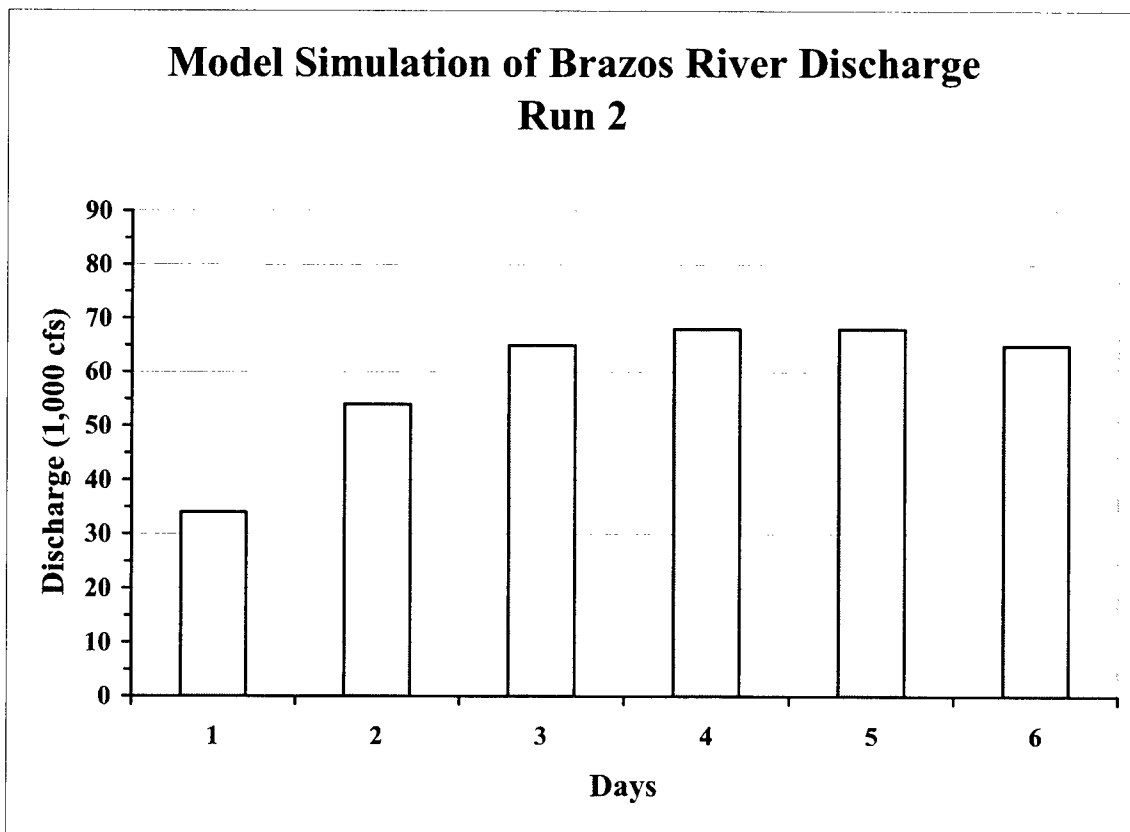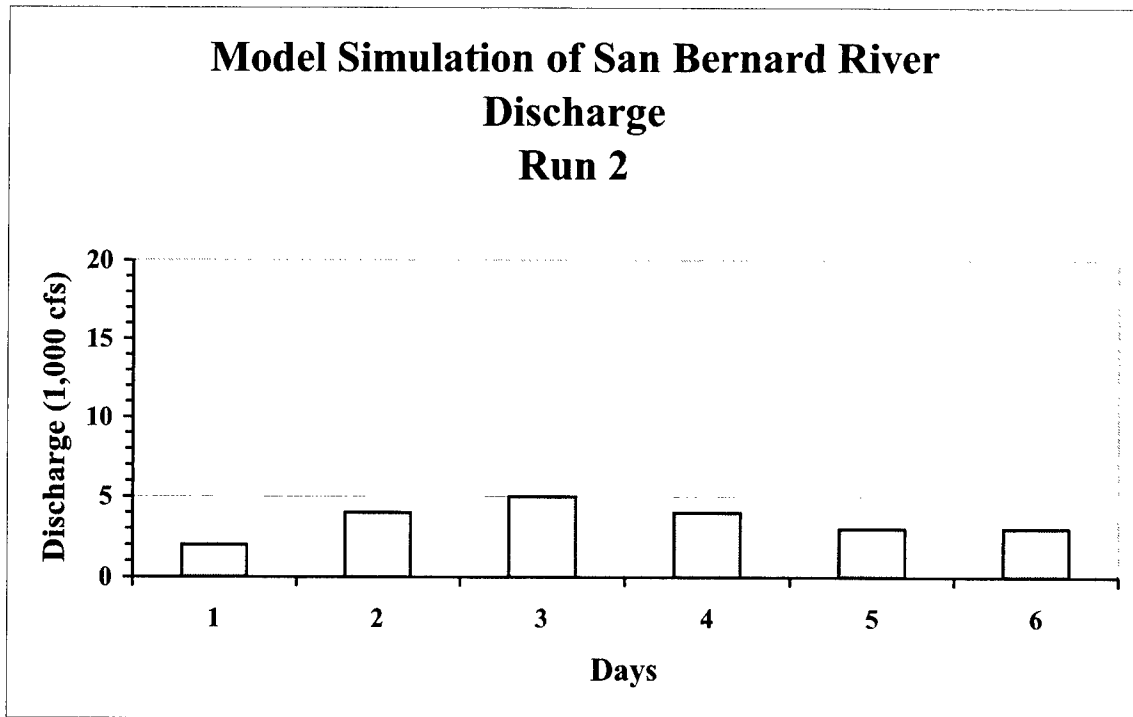
Figure 24. Model simulation of San Bernard and Brazos River discharges used for Run 2
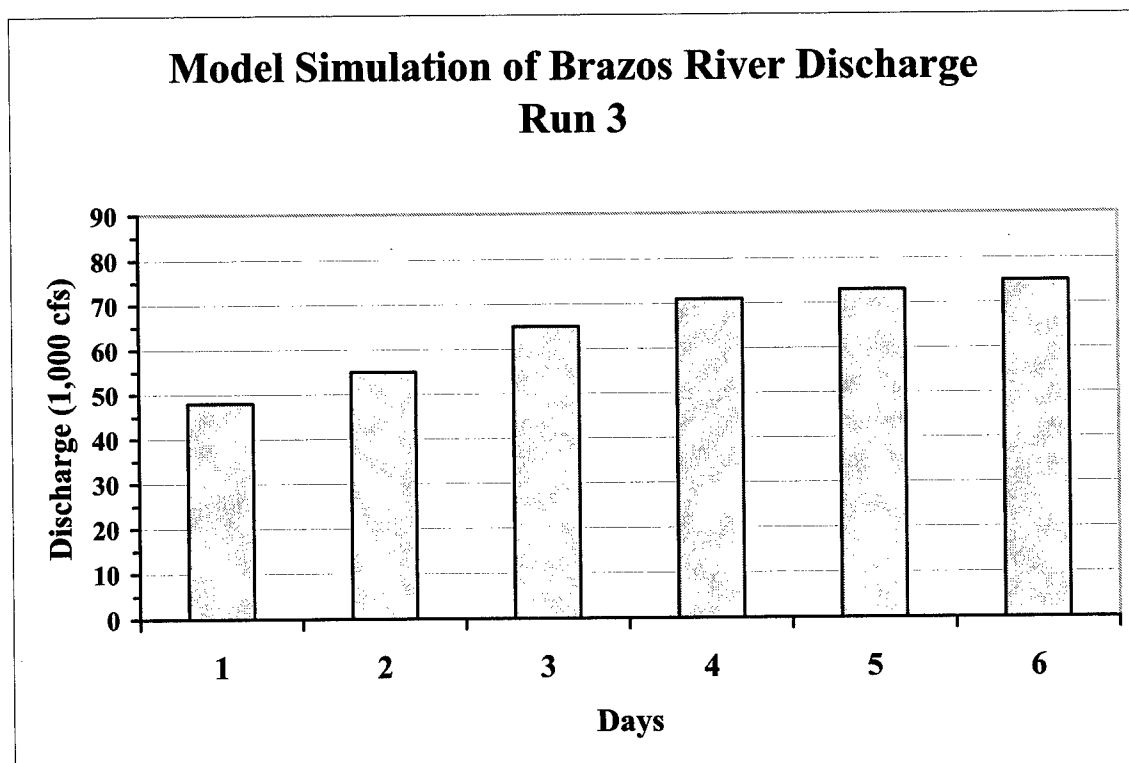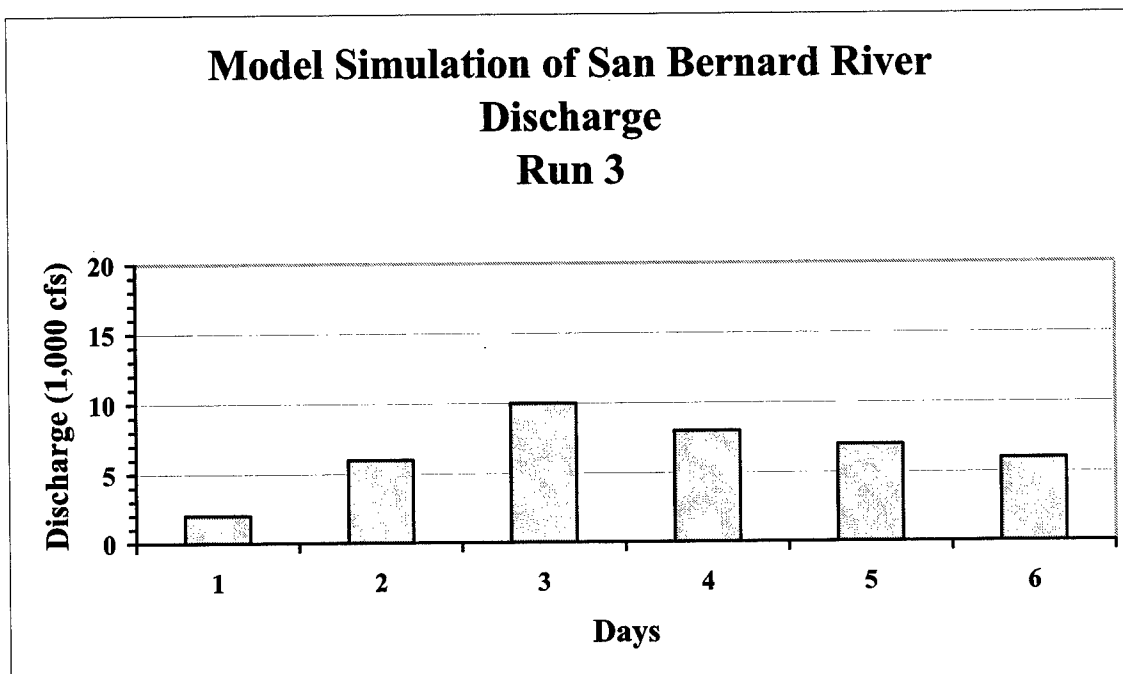
Figure 25.   Model simulation of San Bernard and Brazos River discharges used for Run 3
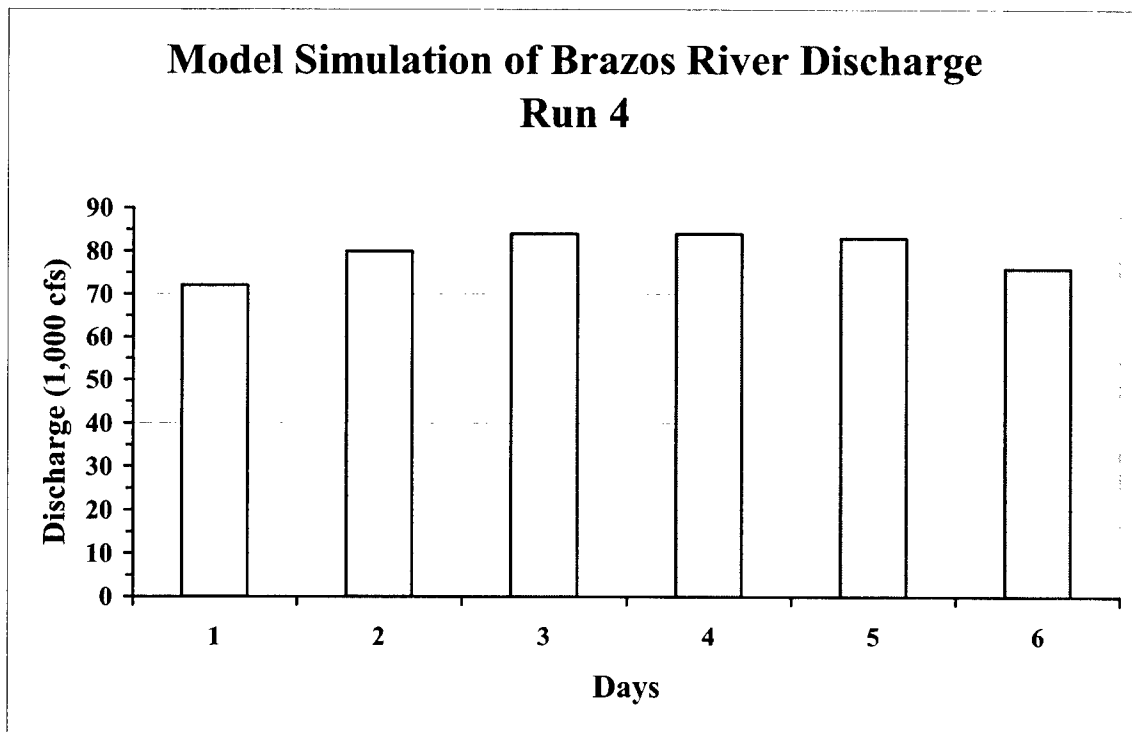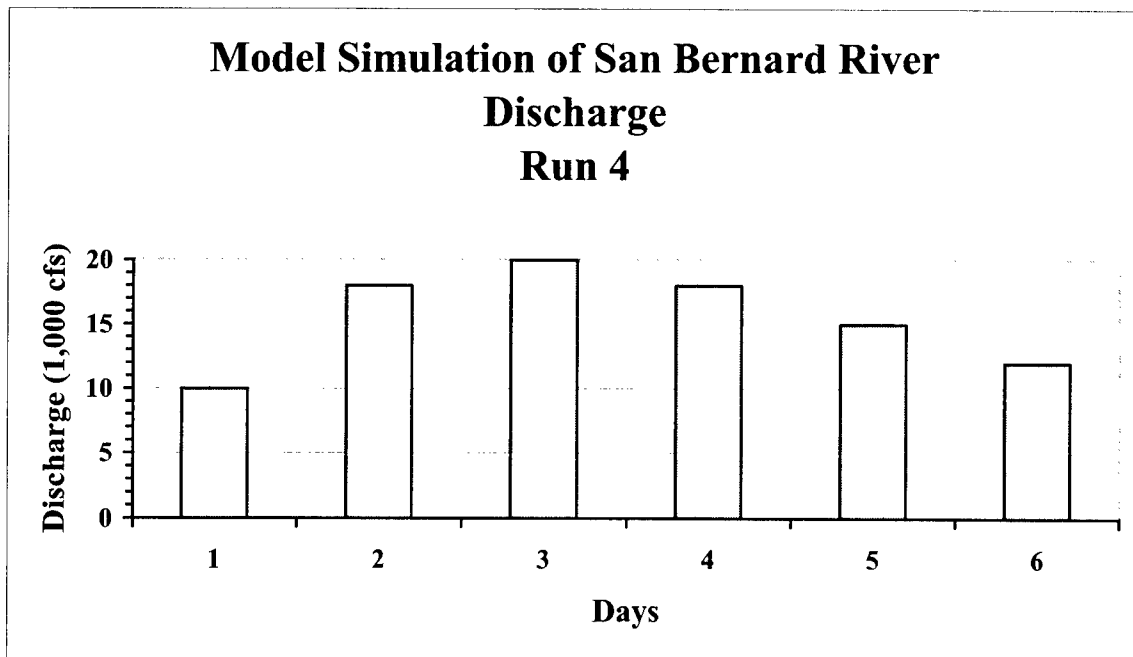
Figure 26. Model simulation of San Bernard and Brazos River discharges used for Run 4

Figure 27.   San Bernard Inlet in year 1971

Figure 28. Aerial photo of San Bernard River (circa 1971)
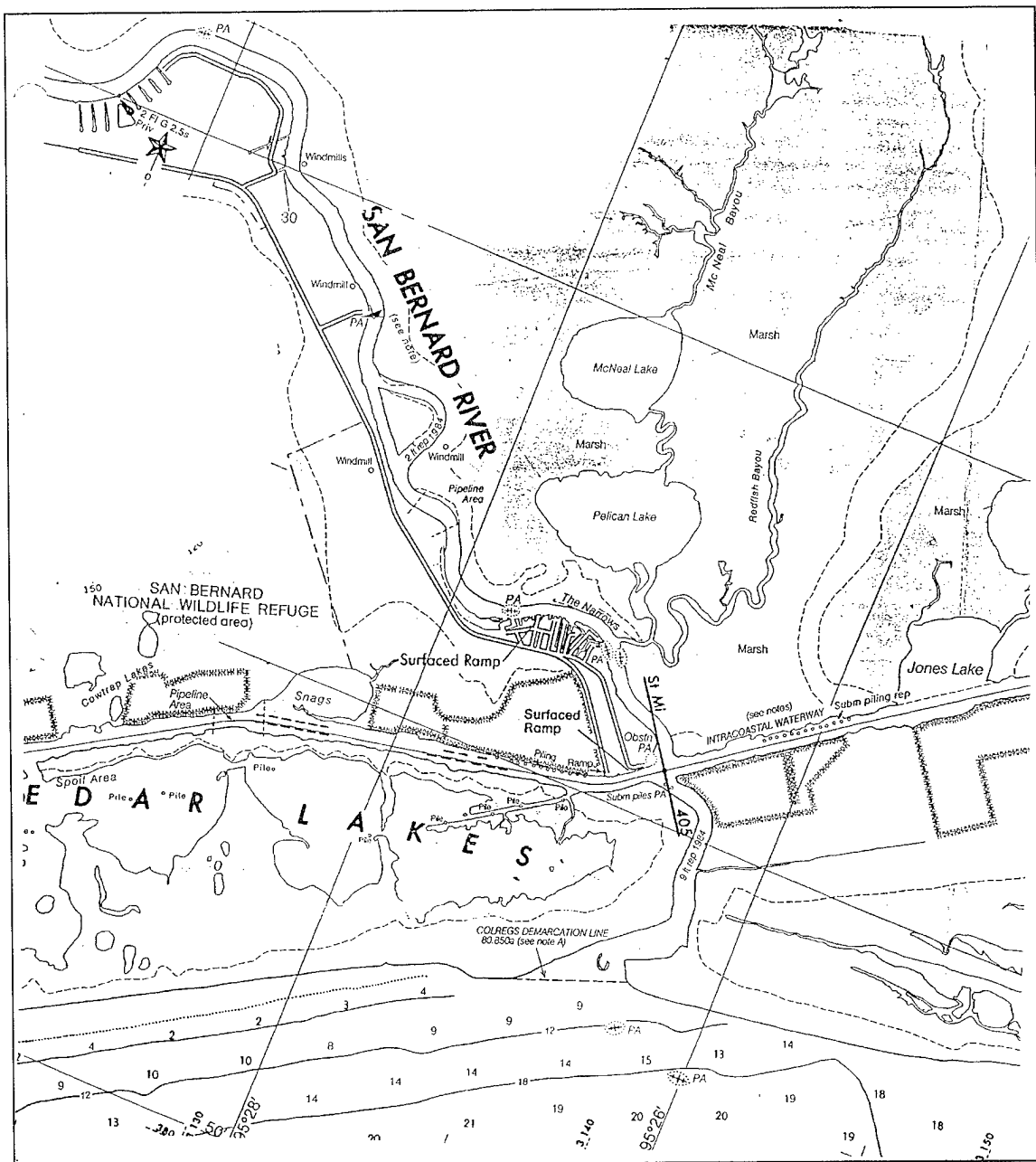
Figure 29.   San Bernard Inlet in year 1984

Figure 30. Aerial photo of San Bernard river (circa 1998)
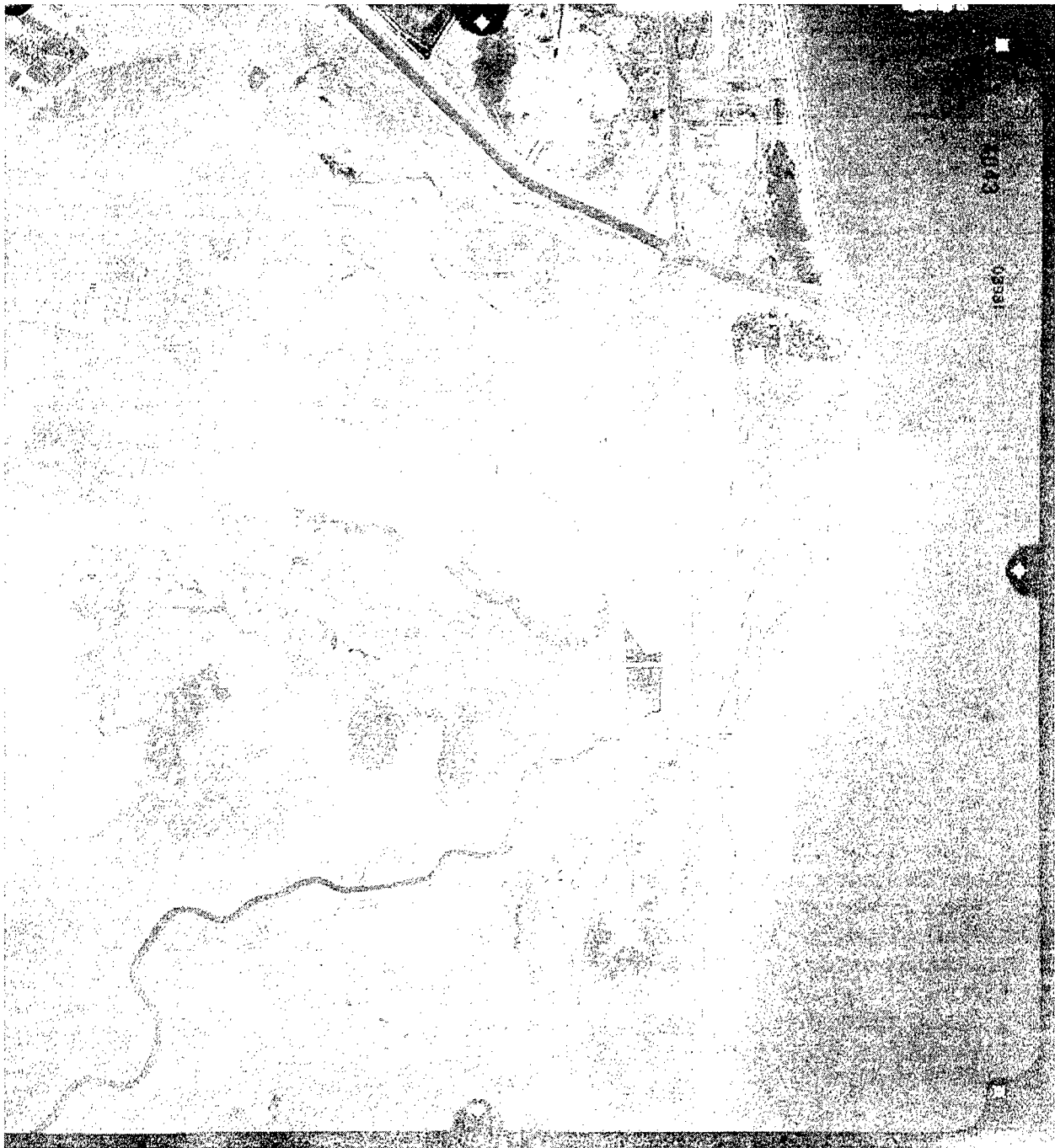
Figure 31. Aerial photo of San Bernard River and Brazos River (circa 1998)
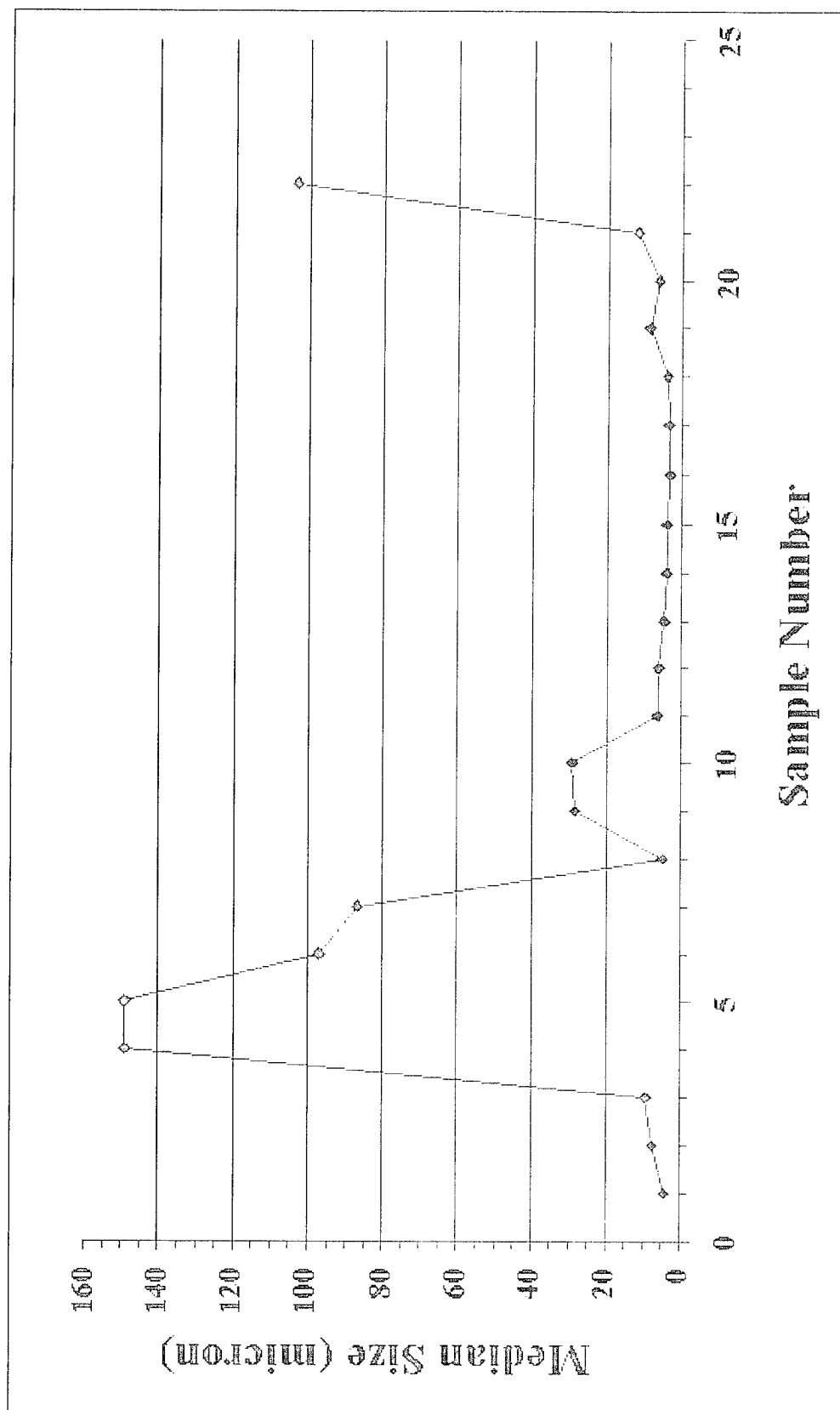
Figure 32. Median diameter of bed sediment
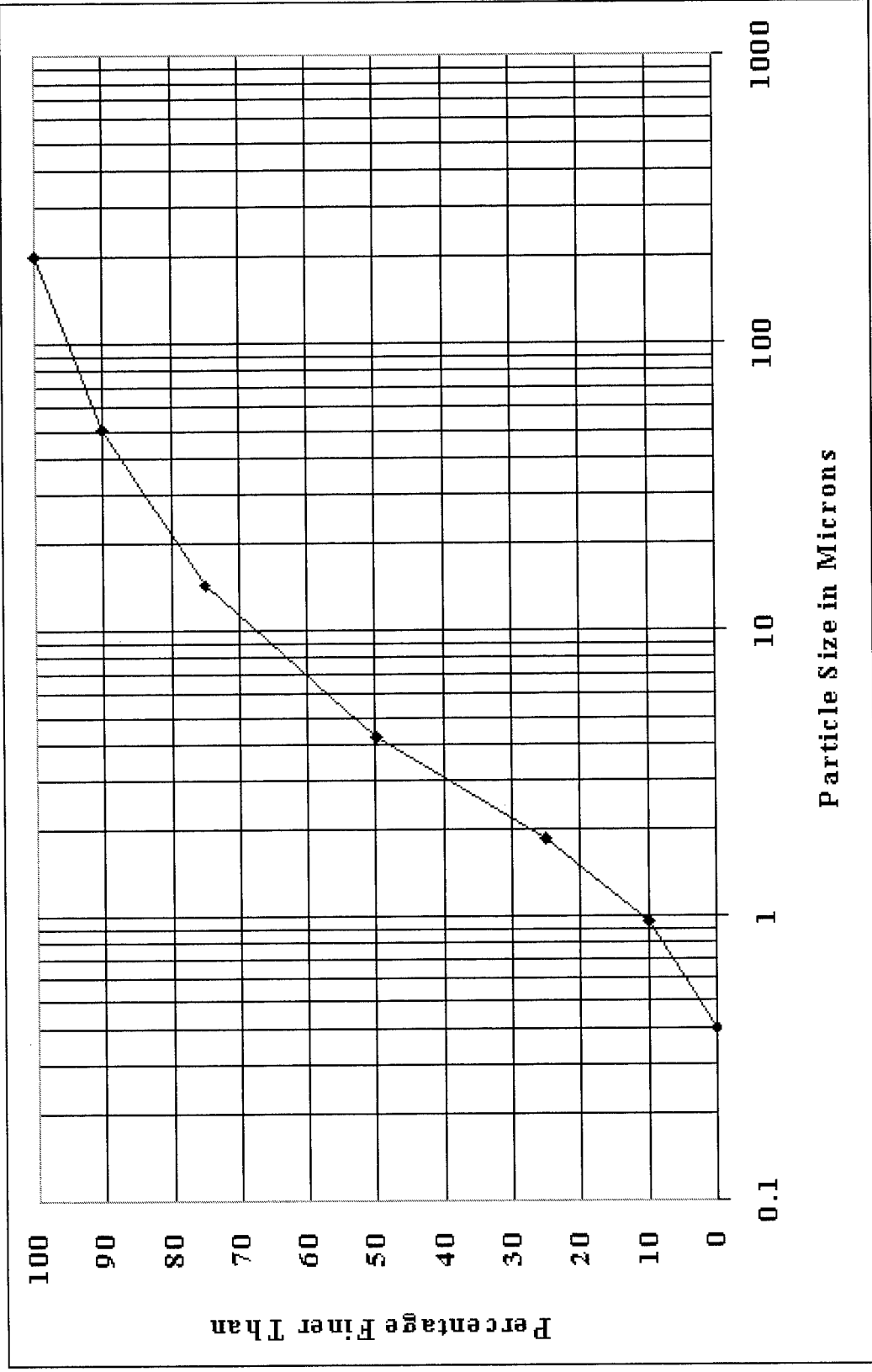
Figure 33. Particle size distribution curve for bed material at sta 1
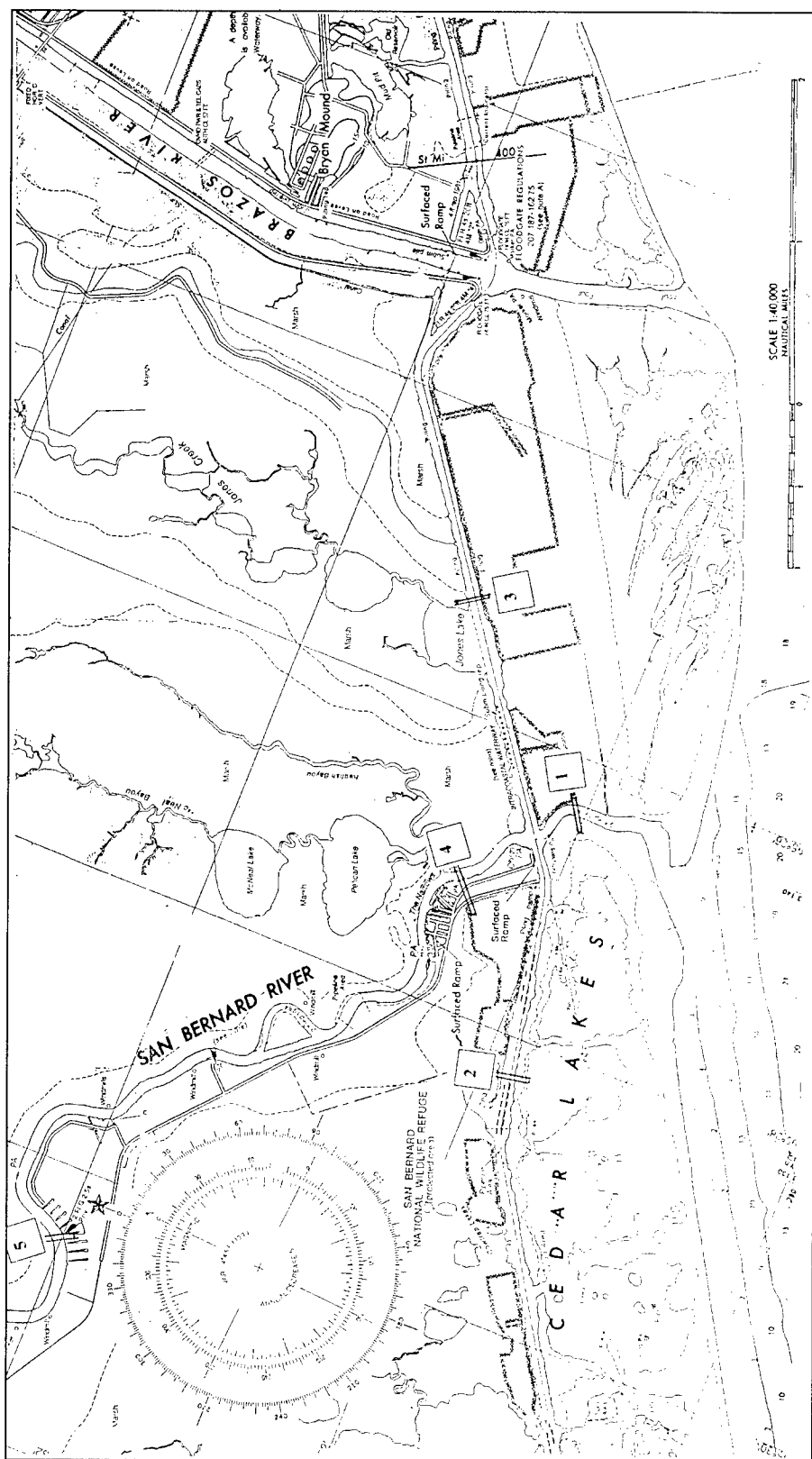
Figure 34.   Locations of transects for water sample collection
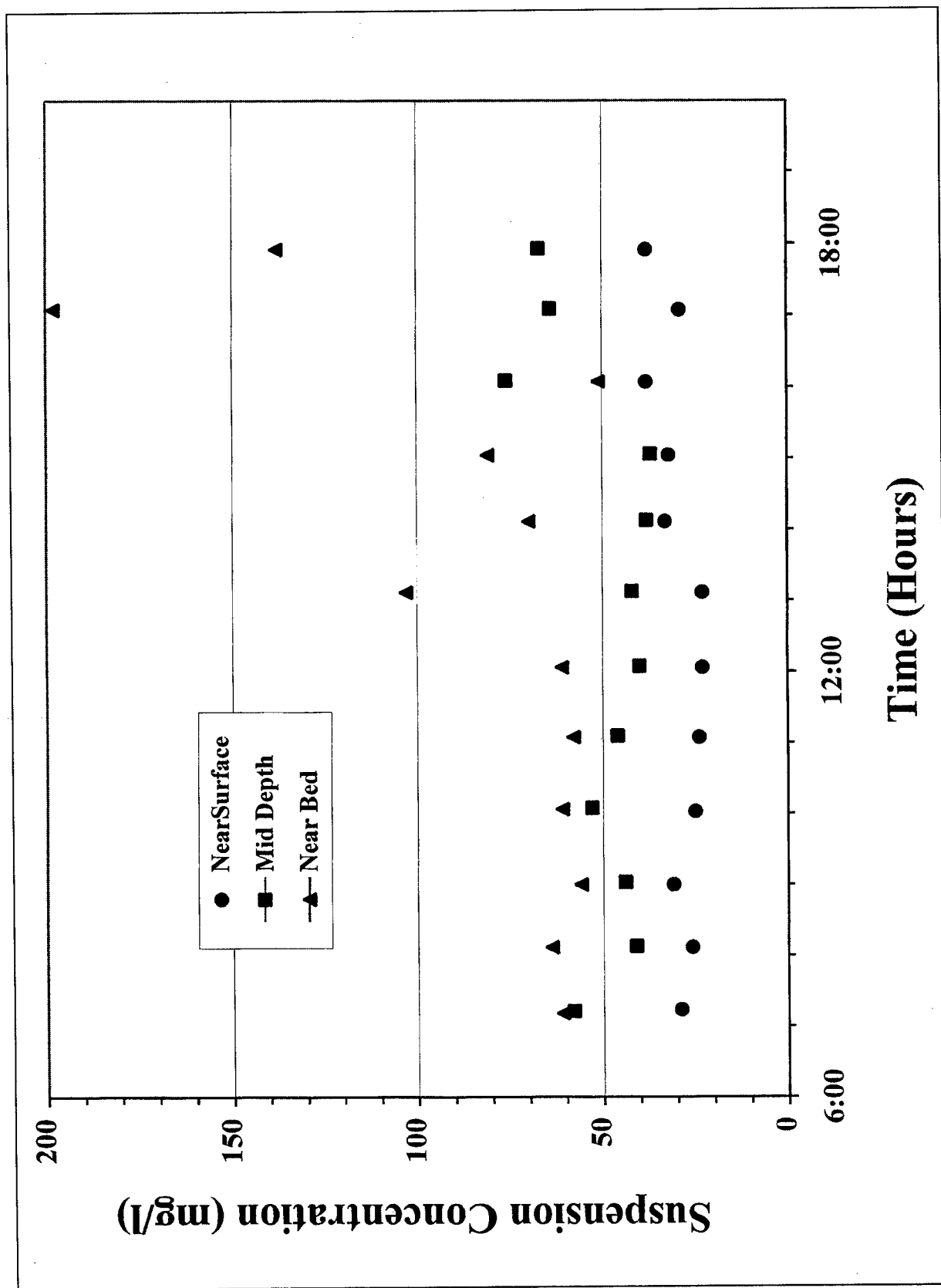
Figure 35.   Suspended sediment concentration at transect R1 on 26 August 1999
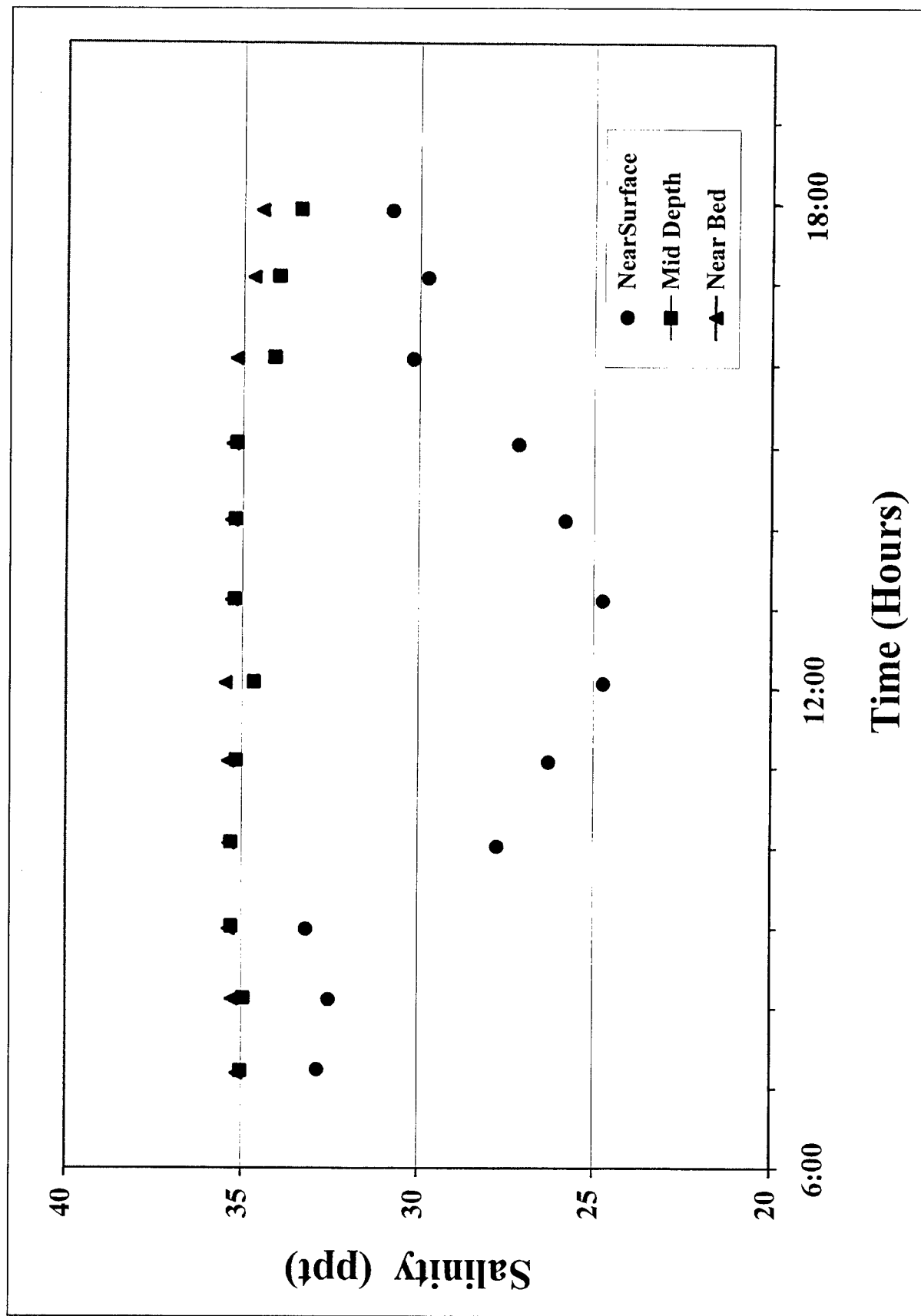
Figure 36. Salinity variation at transect R1 on 26 August 1999
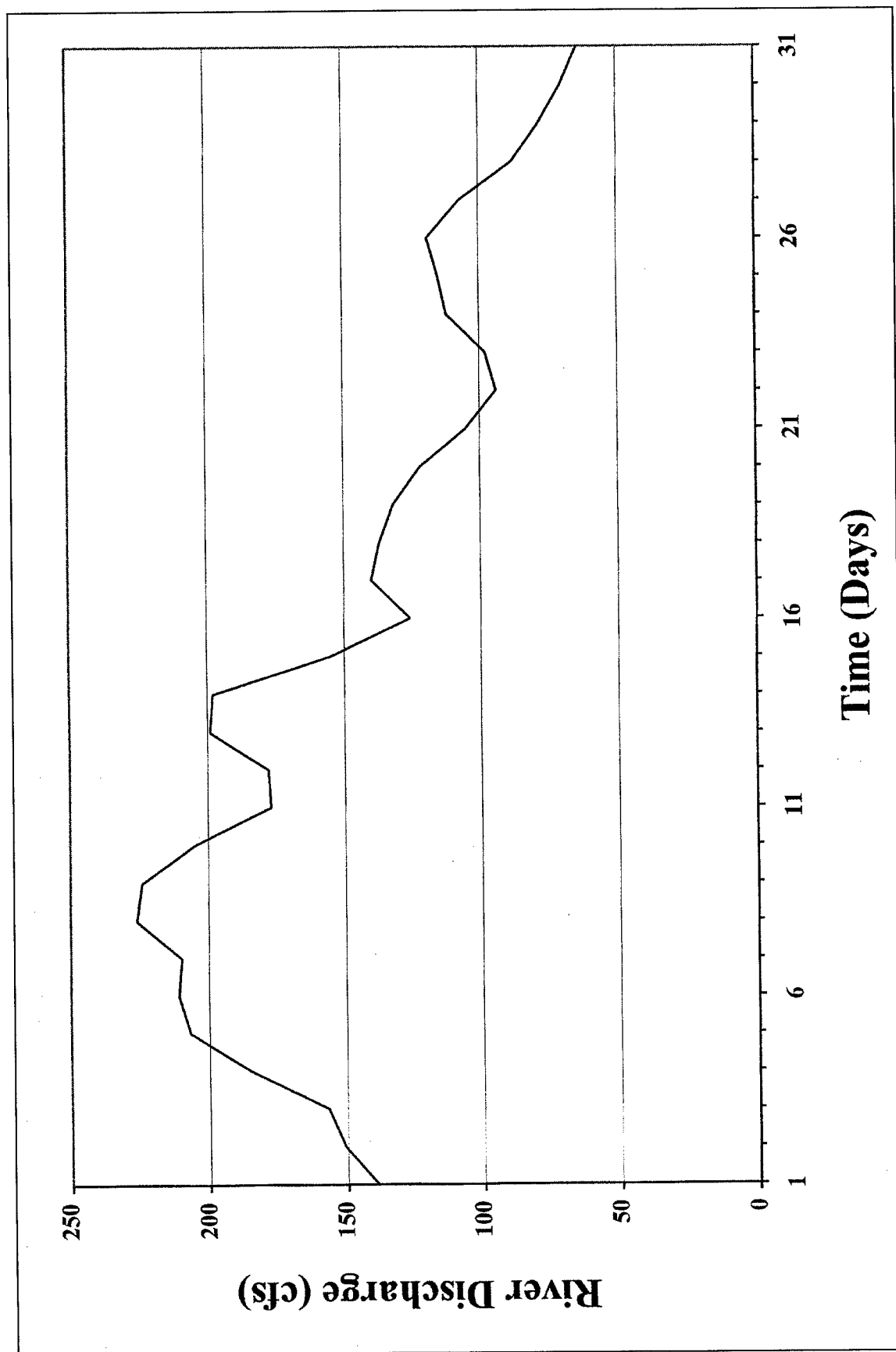
Figure 37. San Bernard River discharge in August 1999 (Discharge is in cubic feet per second, to convert to cubic meters per second, multiply by 0.02831)
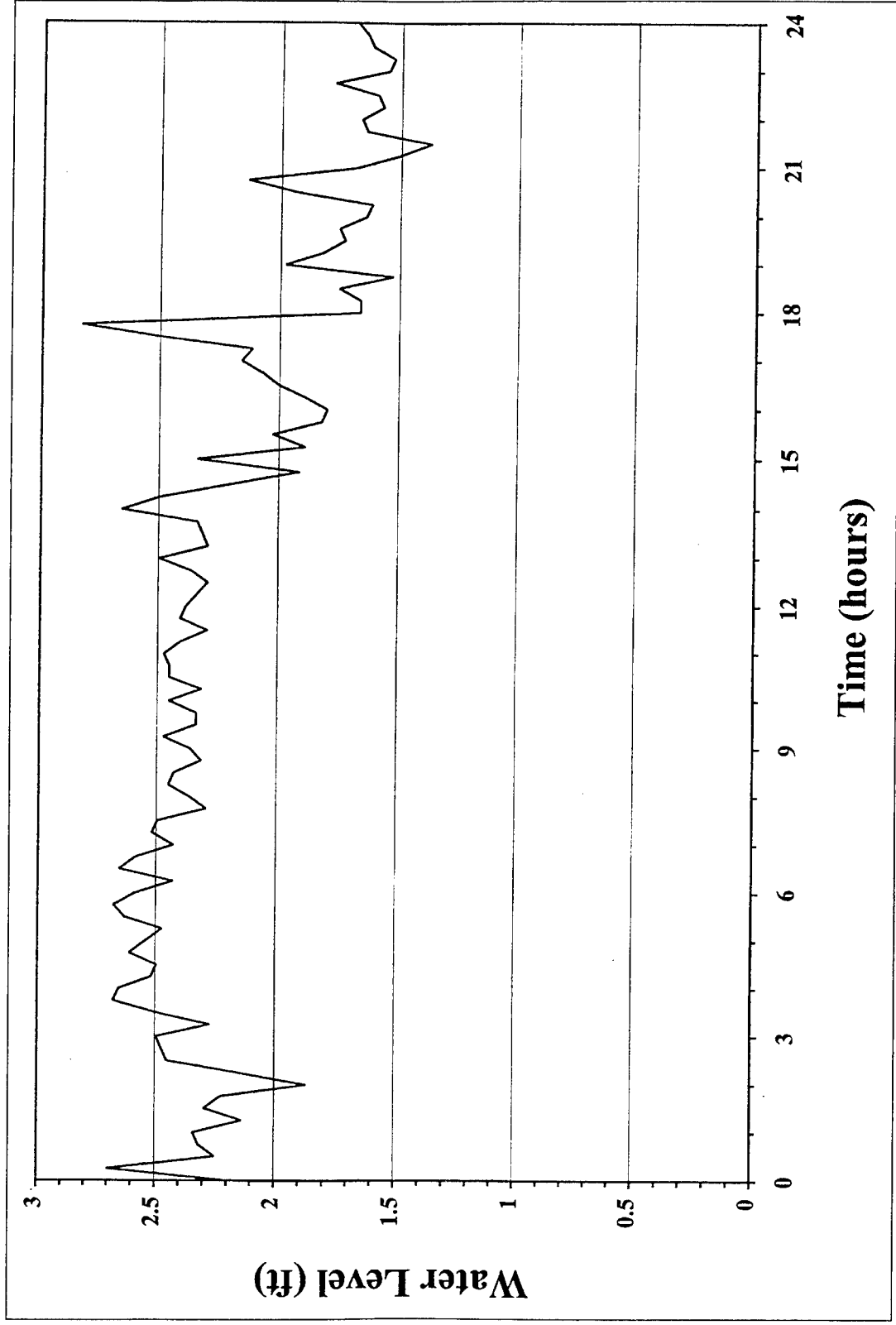
Figure 38. Tidal levels at TG1 on August 26, 1999 (Water level is in feet, to convert feet to meters, multiply by 0.3048)
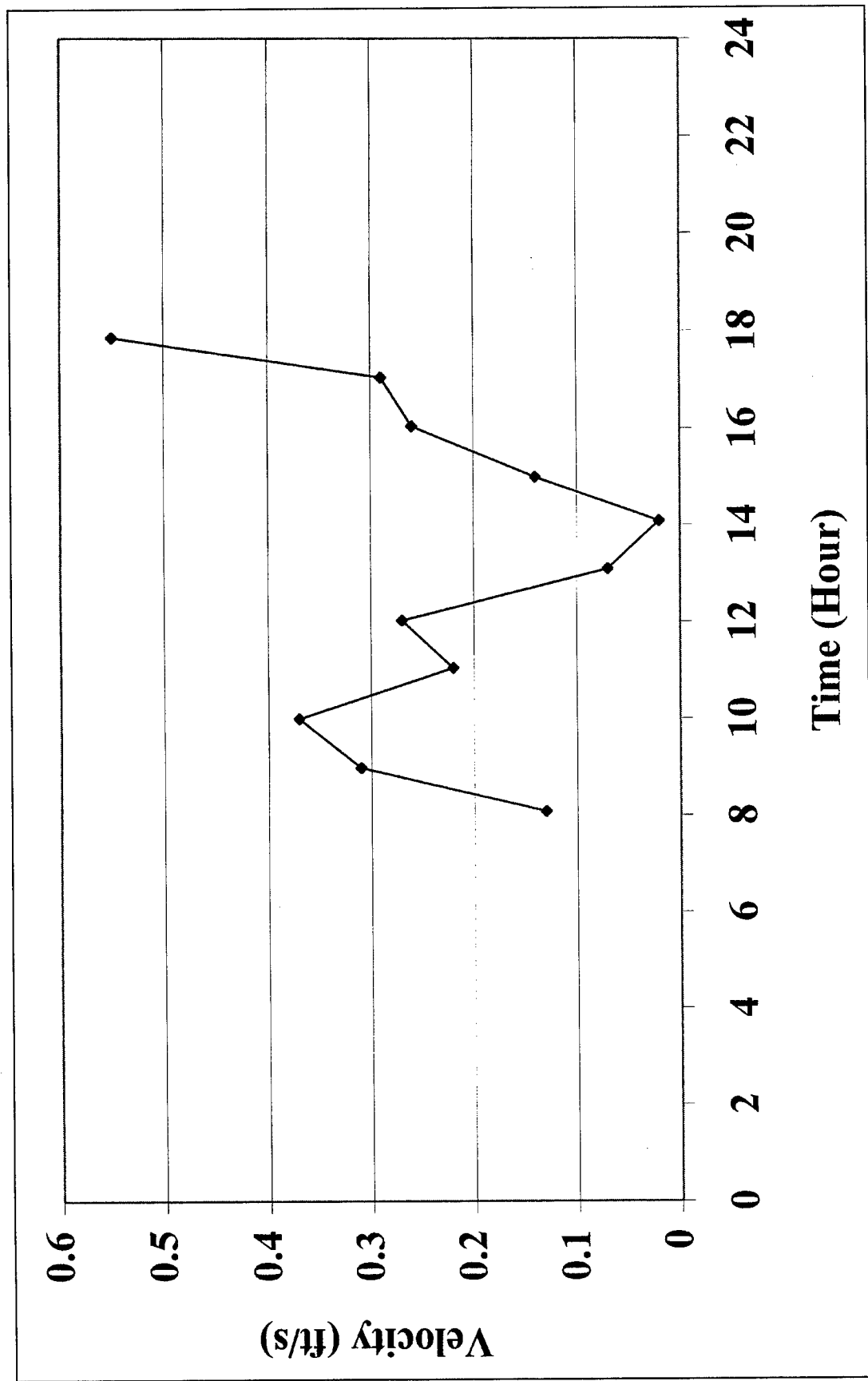
Figure 39. Average velocity at transect 1 on 26 August 1999 (Velocity is in feet per second, to convert to meters per second, multiply by 0.3048)
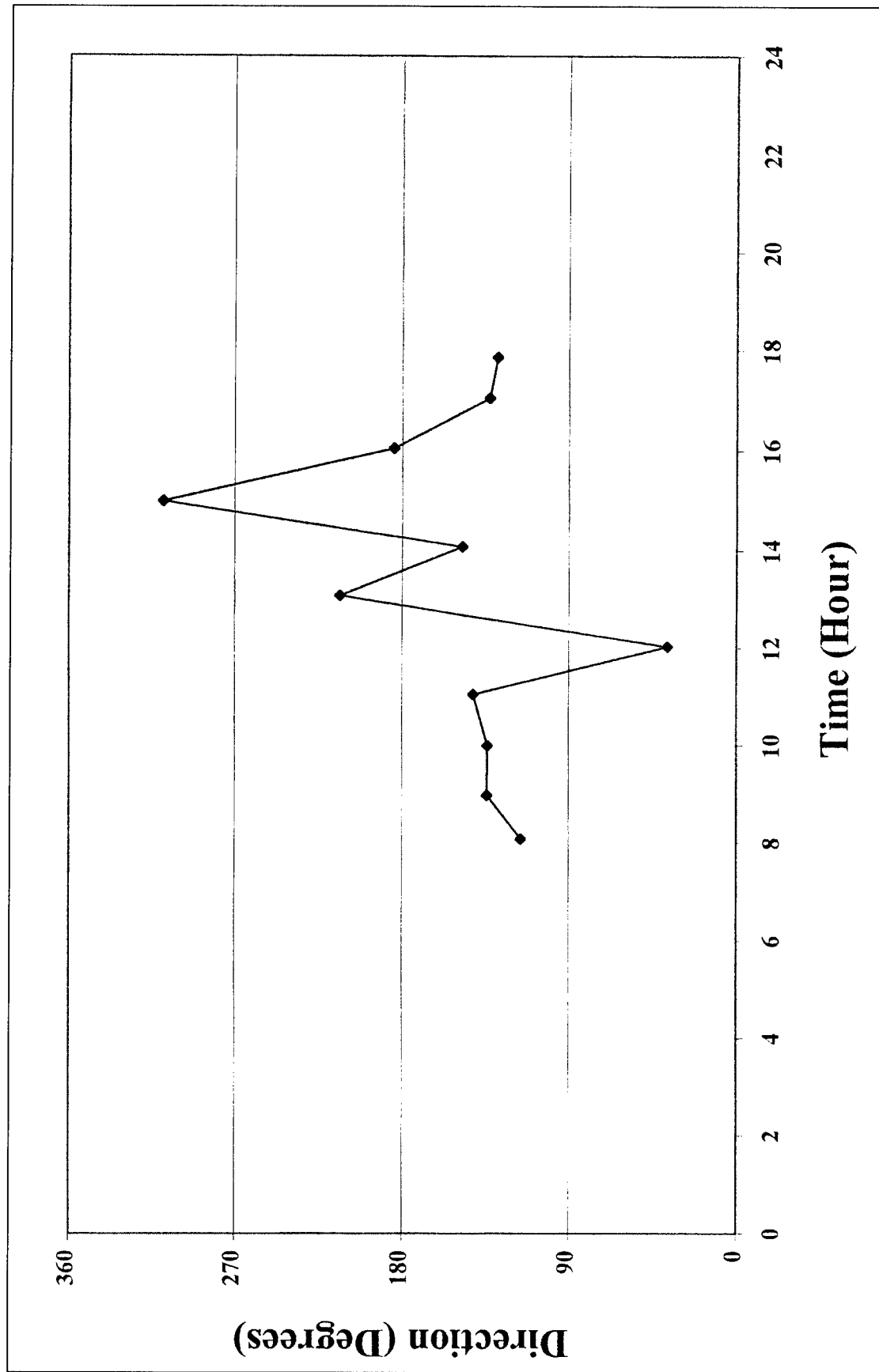
Figure 40. Current direction at transect 1 on 26 August 1999
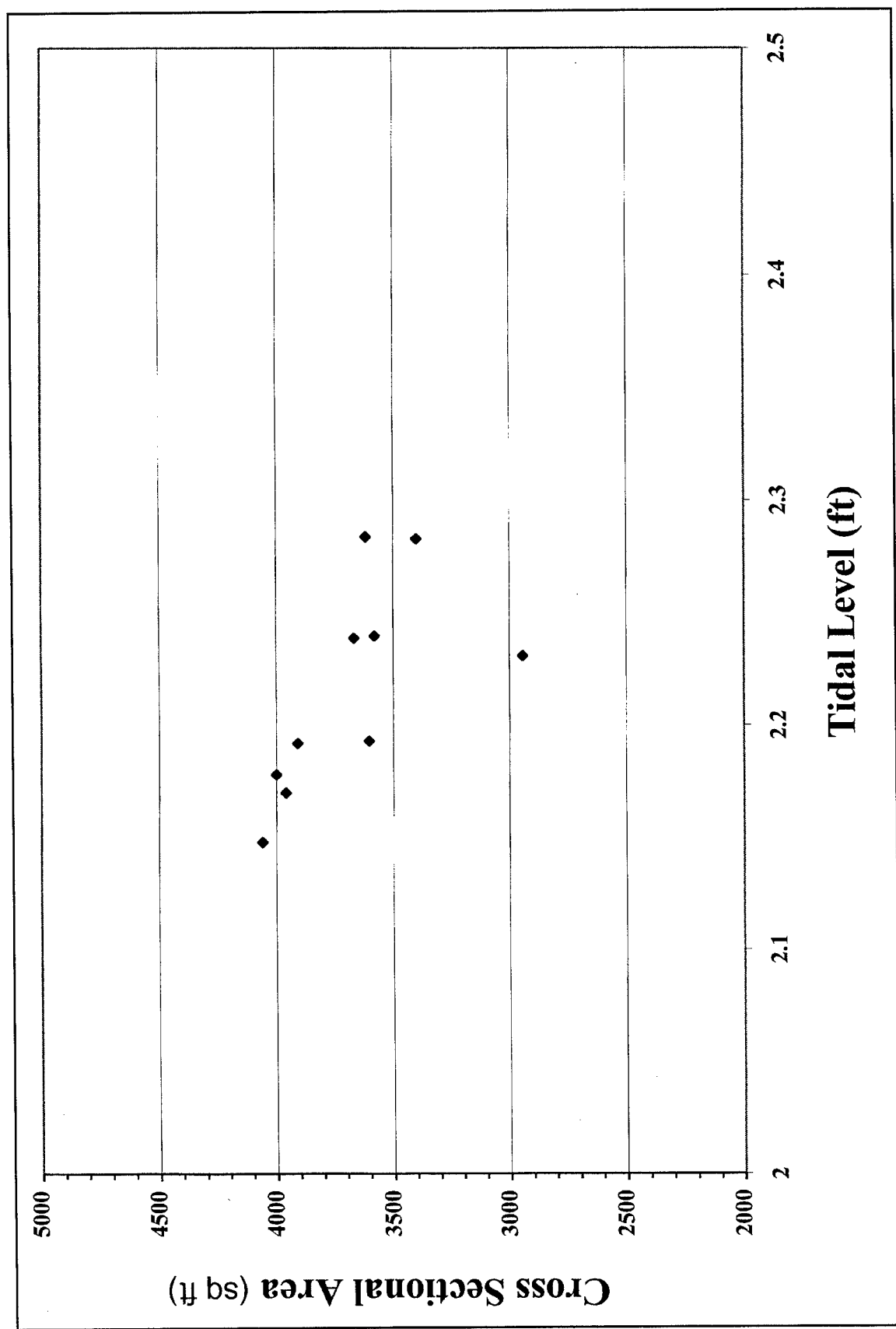
Figure 41. Inlet cross-sectional area as a function of tidal level (Area is in square feet, to convert to square meters, multiply by 0.092290304)
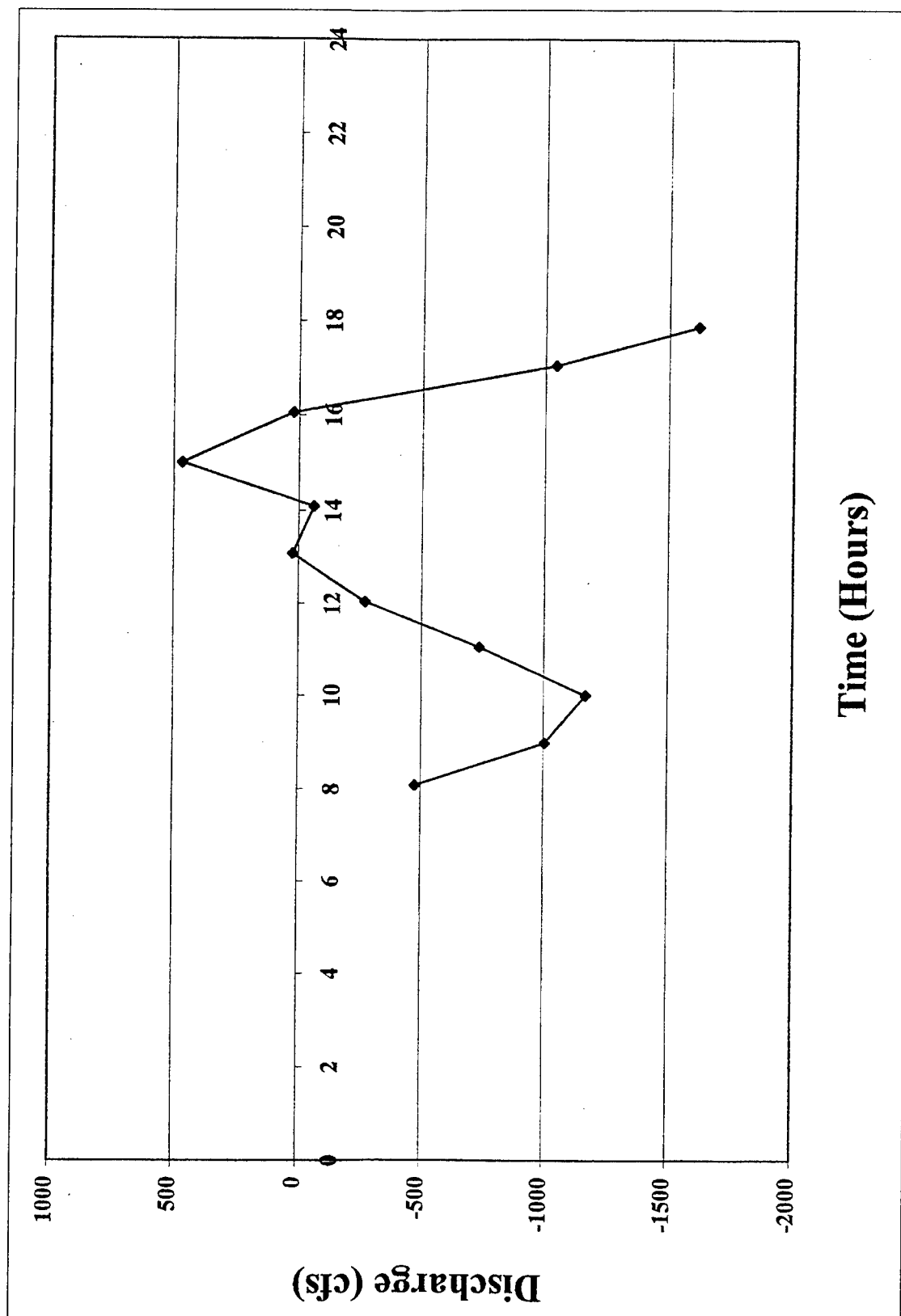
Figure 42.   Tidal discharge at transect 1 on August 26, 1999 (Discharge is in cubic feet per second, to convert to cubic meters per second, multiply by 0.02831)
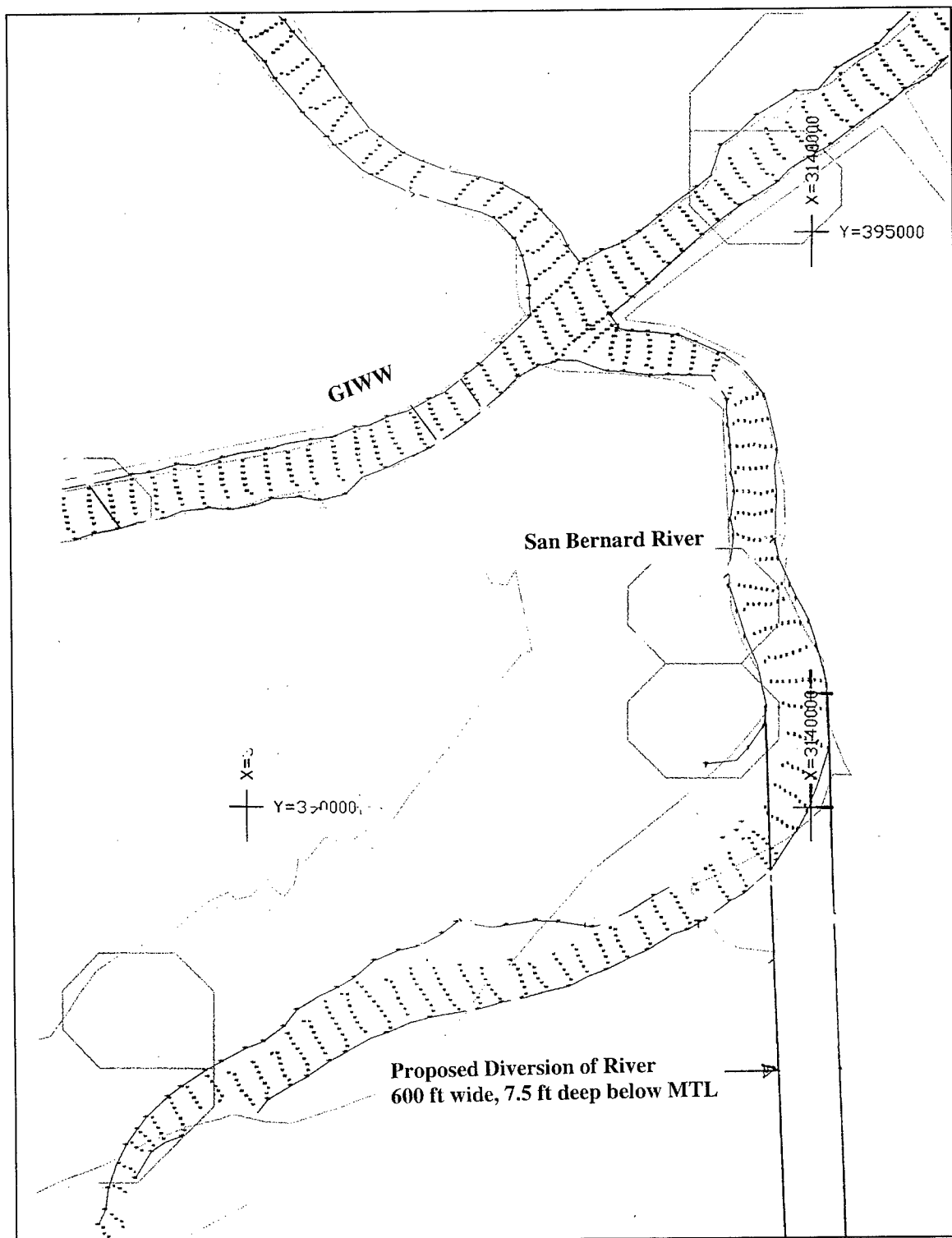
Figure 43. New inlet geometry examined on numerical model (To convert feet to meters, multiply by 0.3048)
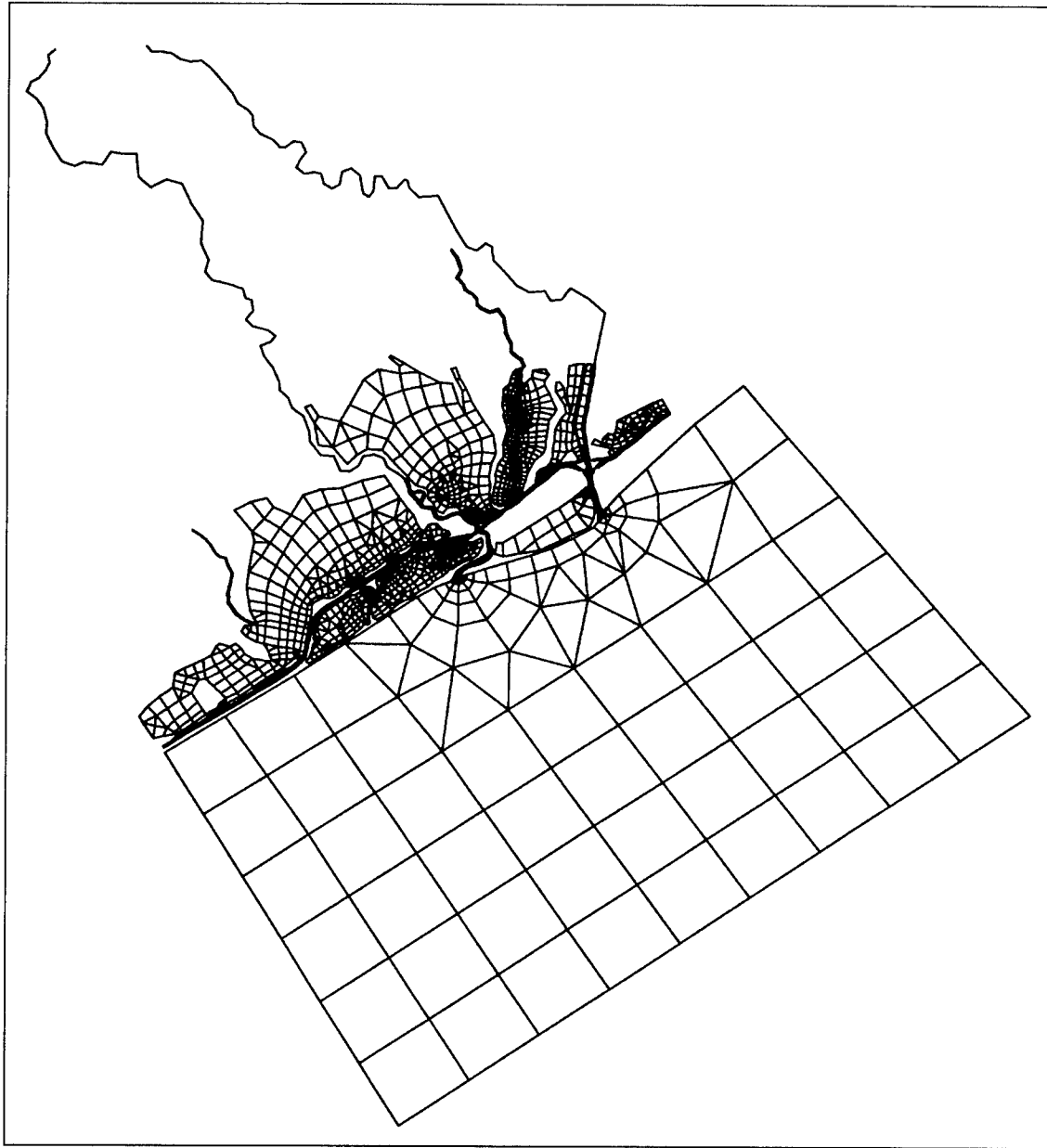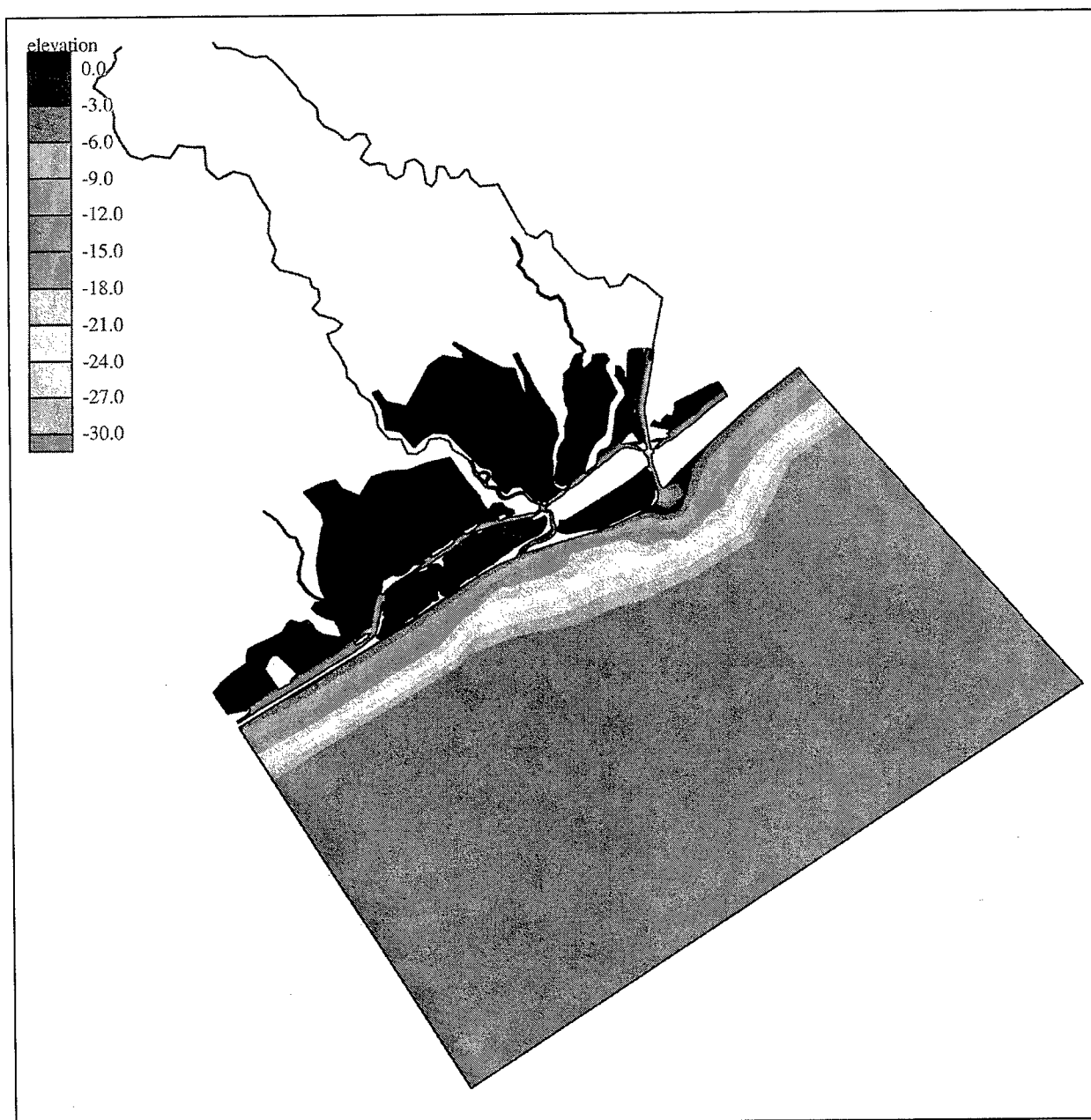
Figure 44.   Numerical mesh

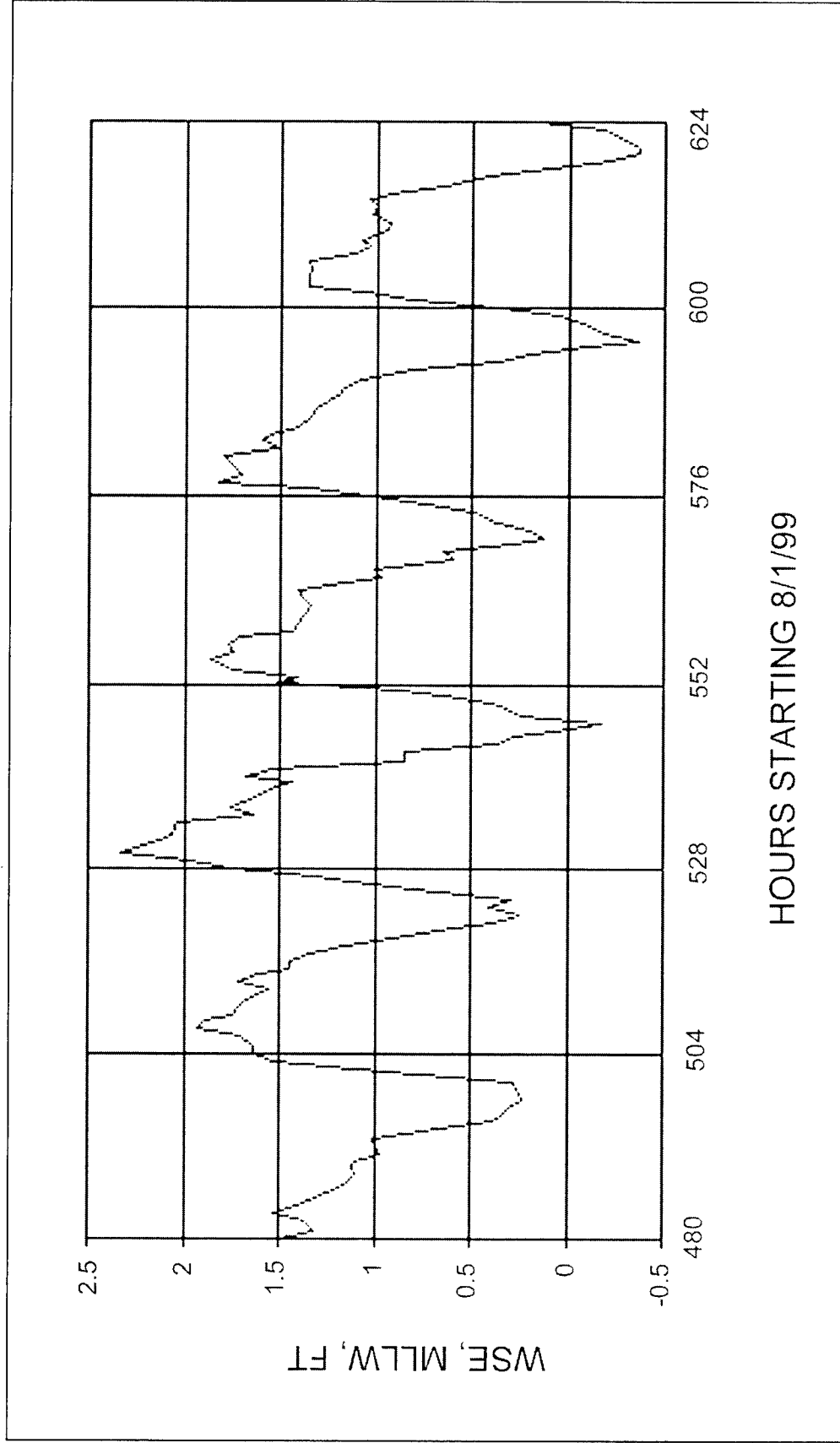Figure 45.   Elevation contour map

Figure 46. Tide at Freeport, TX (To convert feet to meters, multiply by 0.3048)
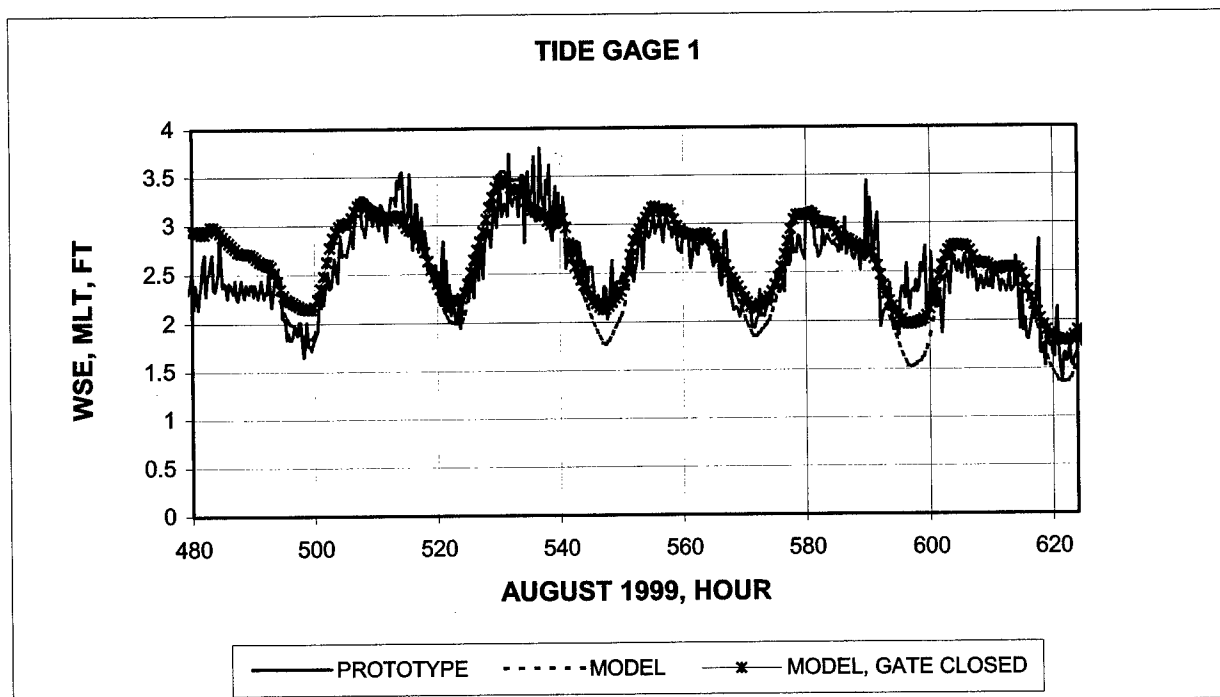
Figure 47.   Prototype and model water-surface elevation at Gage 1 (Mean low tide is in feet, to convert feet to meters, multiply by 0.3048)
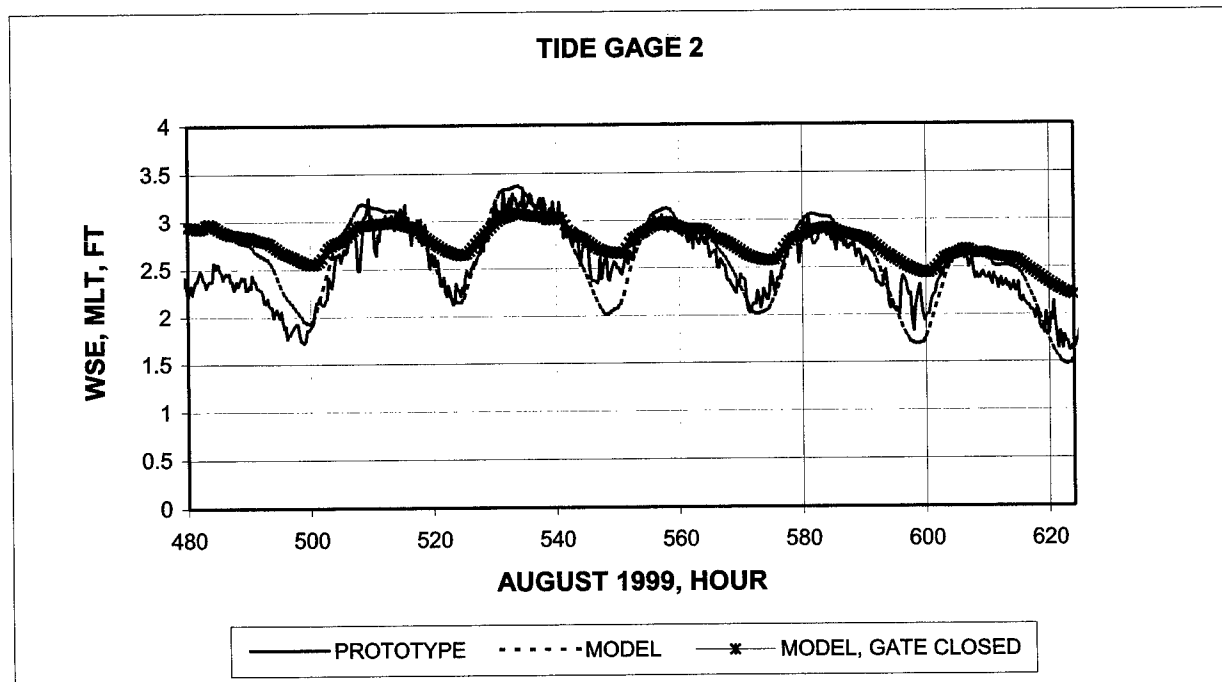

Figure 48.   Prototype and model water-surface elevation at Gage 2 (Mean low tide is in feet, to convert feet to meters, multiply by 0.3048)

Figure 49.   Prototype and model water-surface elevation at Gage 3 (Mean low tide is in feet, to convert feet to meters, multiply by 0.3048)

Figure 50.   Prototype and model water-surface elevation at Gage 5A (Mean low tide is in feet, to convert feet to meters, multiply by 0.3048)

Figure 51.   Prototype and model water-surface elevation at Gage 6A (Mean low tide is in feet, to convert feet to meters, multiply by 0.3048)

Figure 52.   Prototype and model water-surface elevation at Gage 7 (Mean low tide is in feet, to convert feet to meters, multiply by 0.3048)
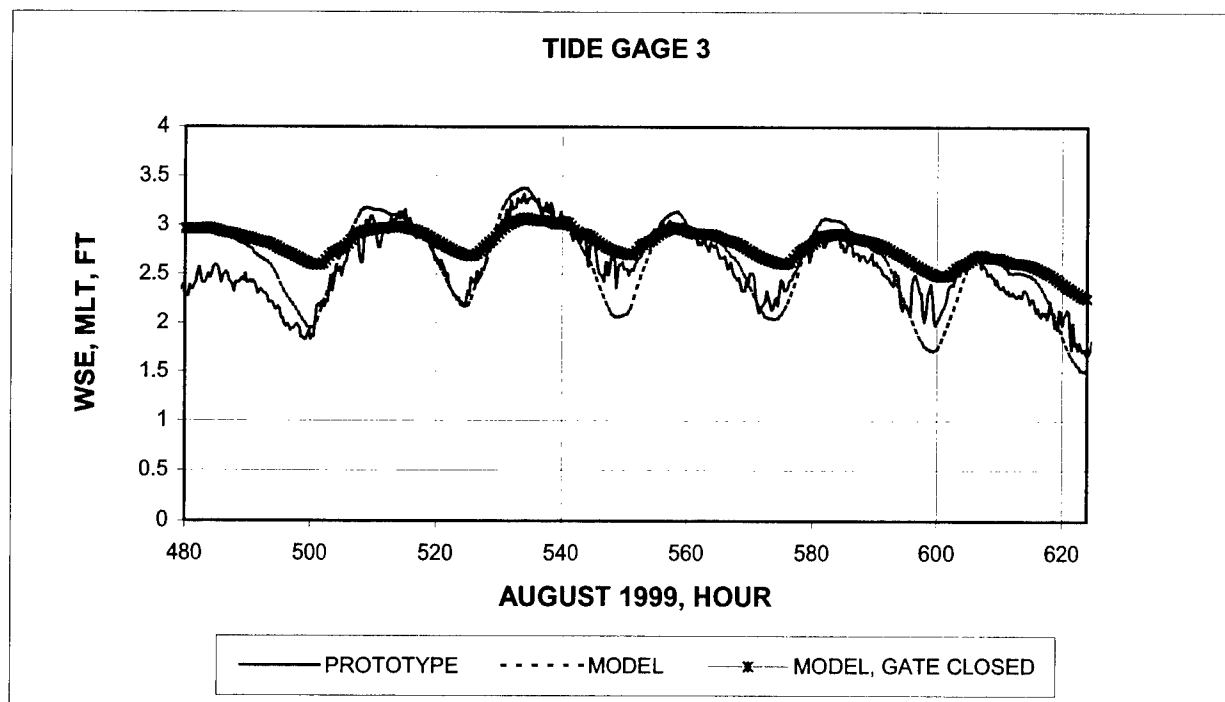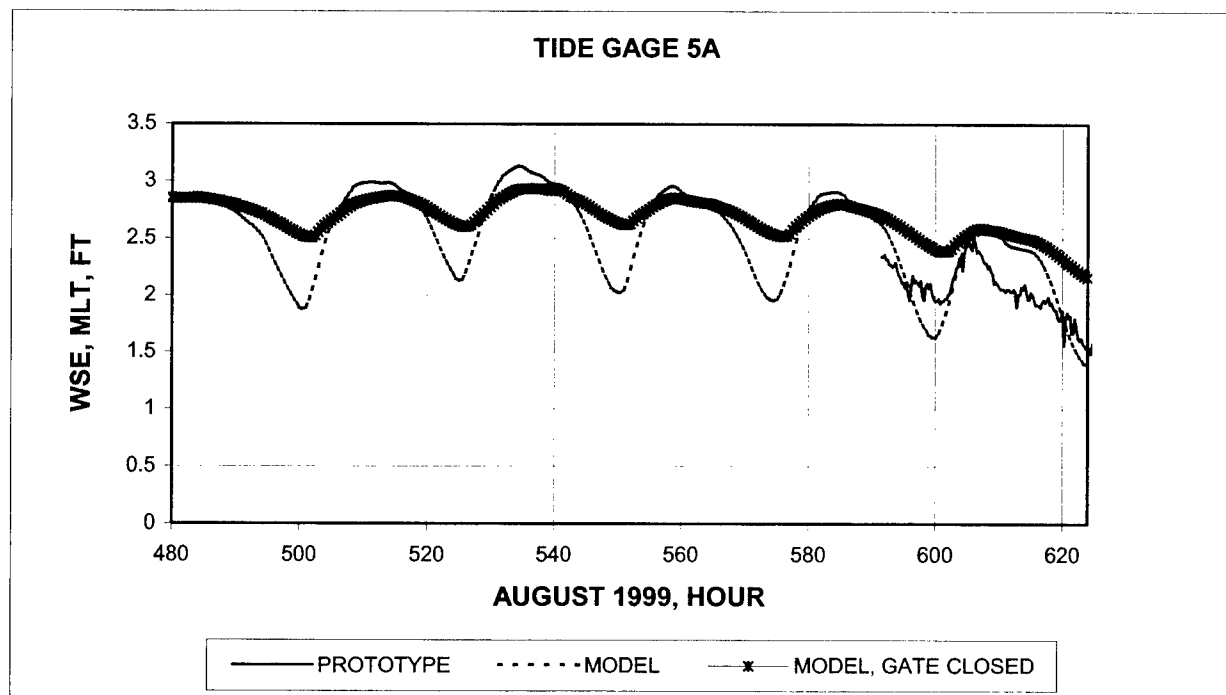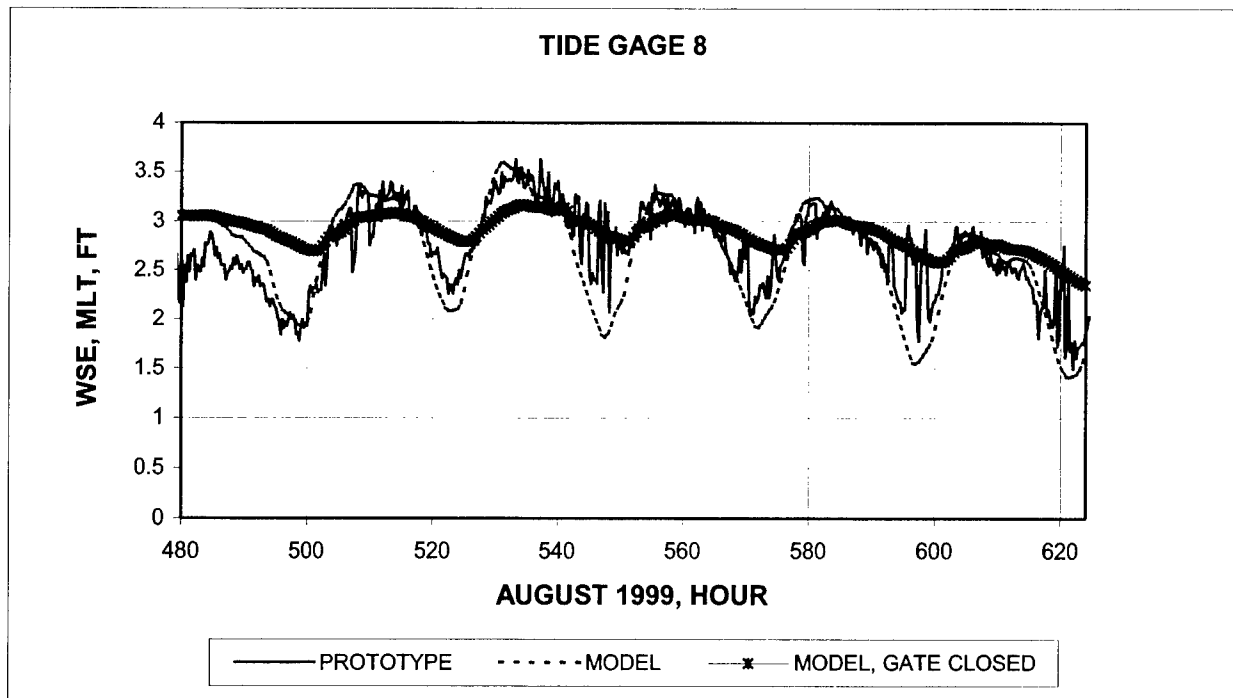
Figure 53.   Prototype and model water-surface elevation at Gage 8 (Mean low tide is in feet, to convert feet to meters, multiply by 0.3048)
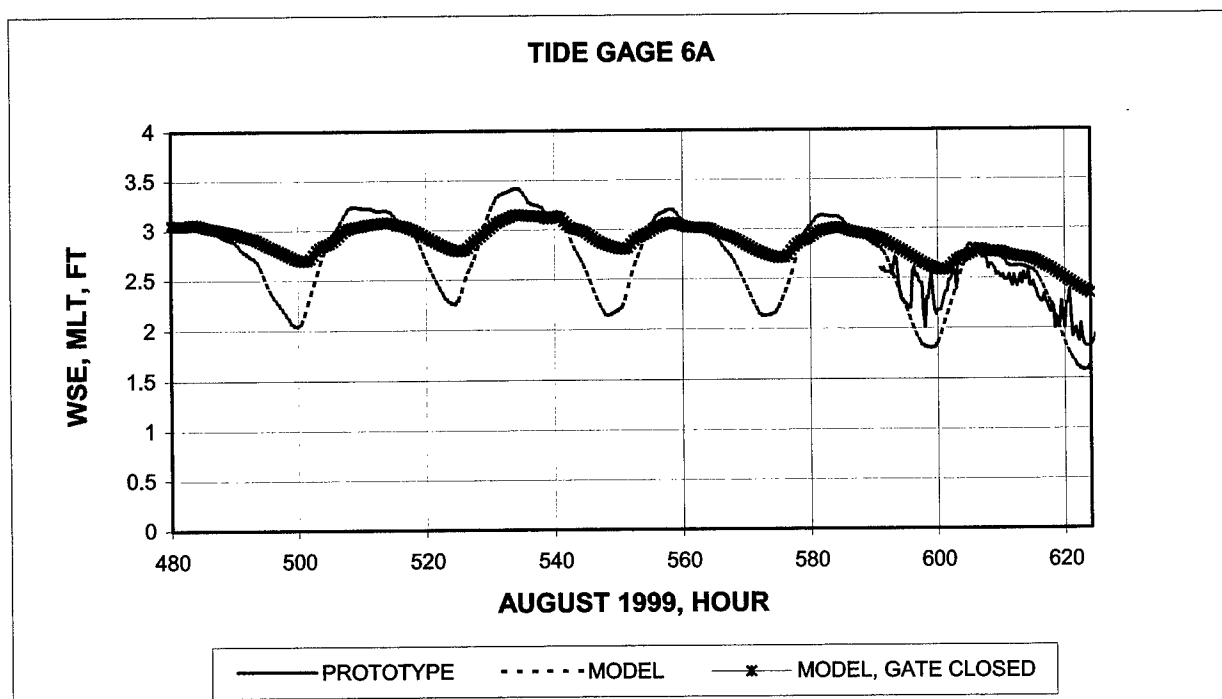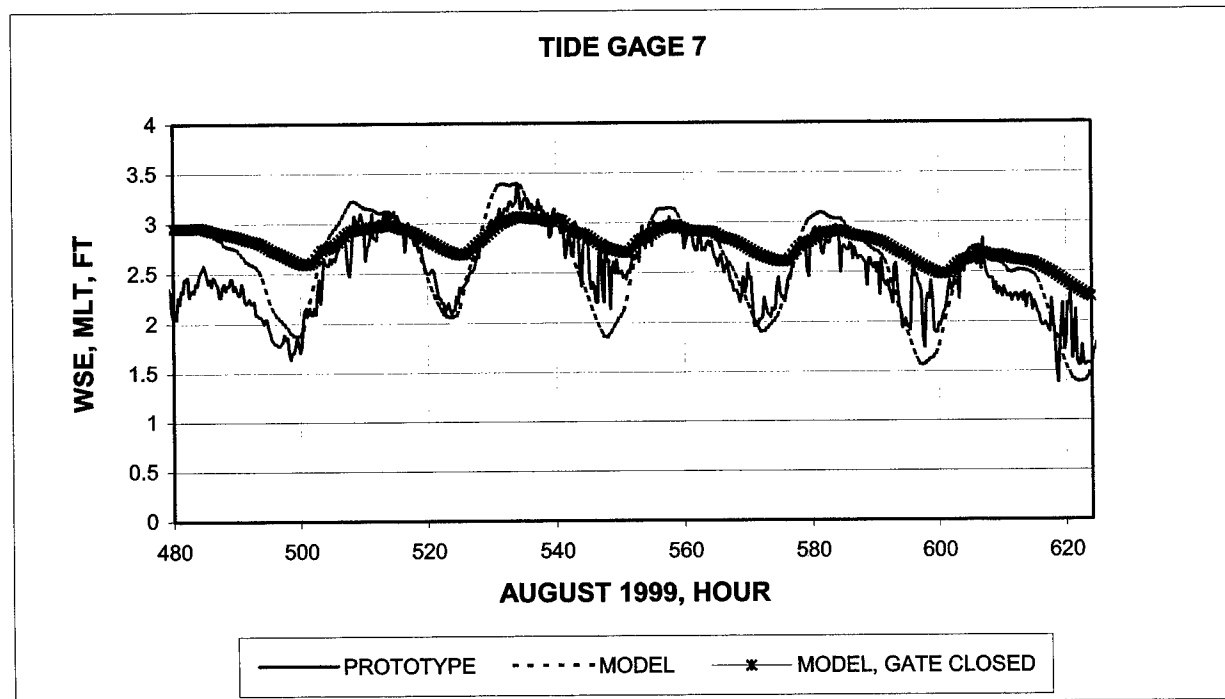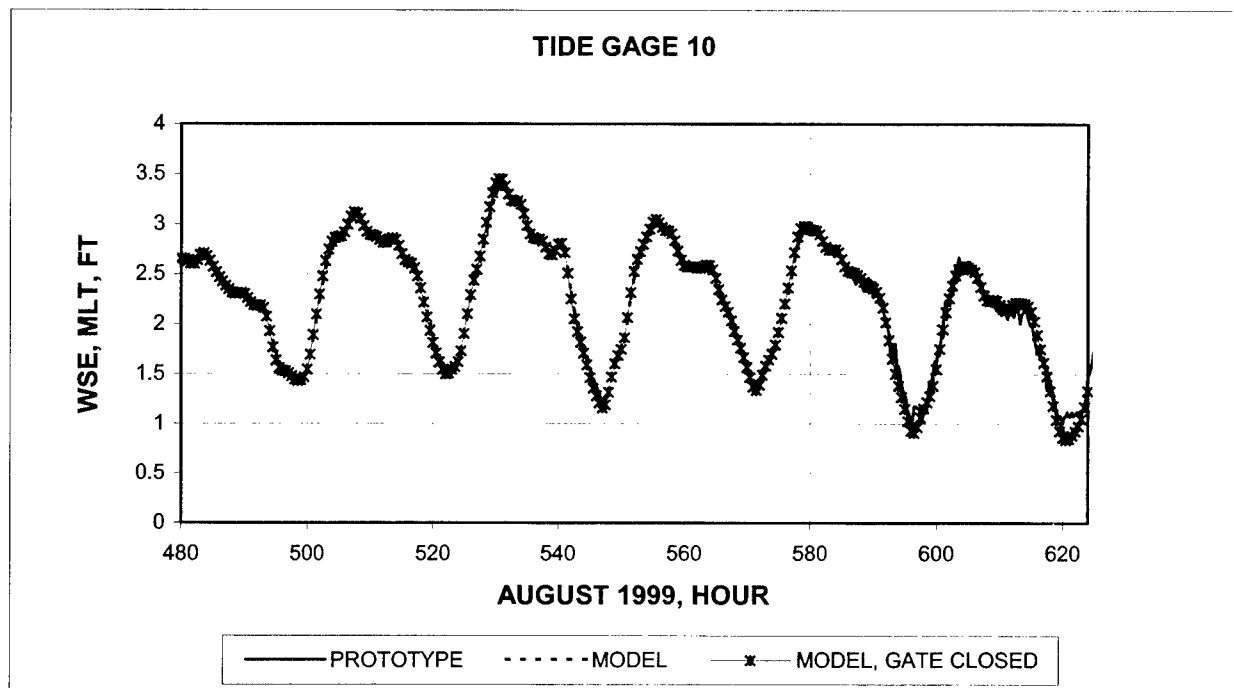

Figure 54.   Prototype and model water-surface elevation at Gage 10 (Mean low tide is in feet, to convert feet to meters, multiply by 0.3048)

Figure 55. Prototype and model discharge at Range 1 (Discharge is in cubic feet per second, to convert to cubic meters per second, multiply by 0.02831)

Figure 56. Prototype and model discharge at Range 2 (Discharge is in cubic feet per second, to convert to cubic meters per second, multiply by 0.02831)
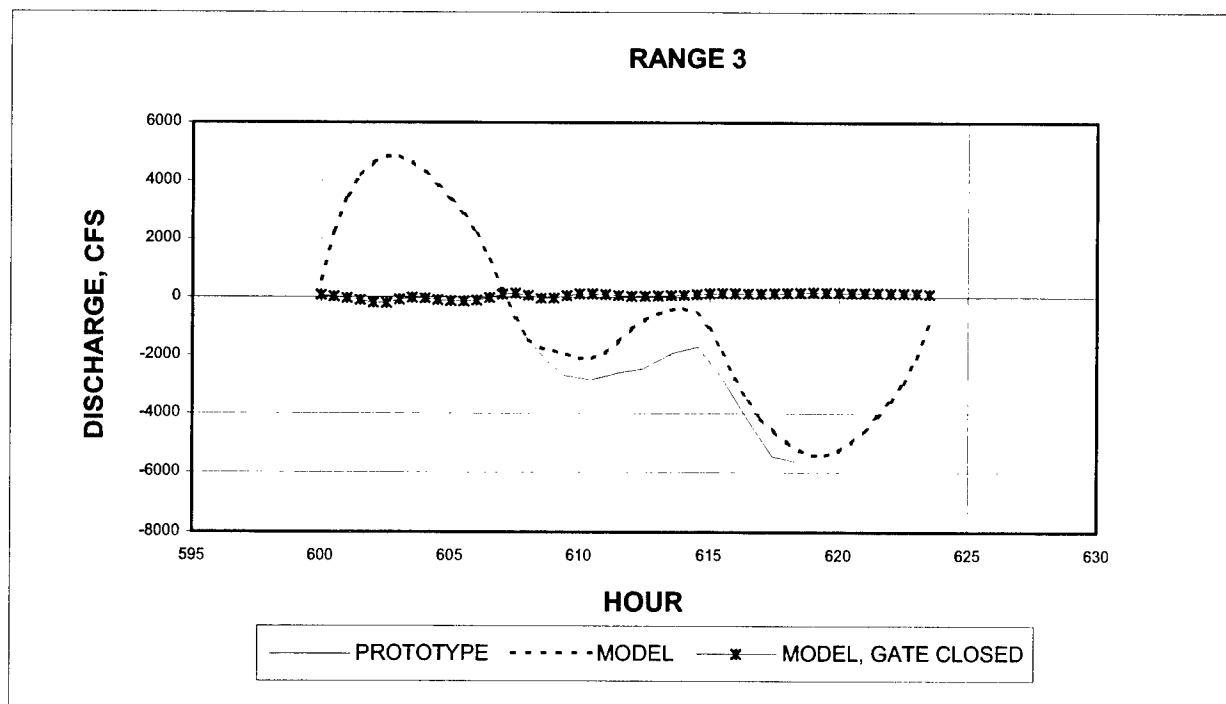
Figure 57.   Prototype and model discharge at Range 3 (Discharge is in cubic feet per second, to convert to cubic meters per second, multiply by 0.02831)
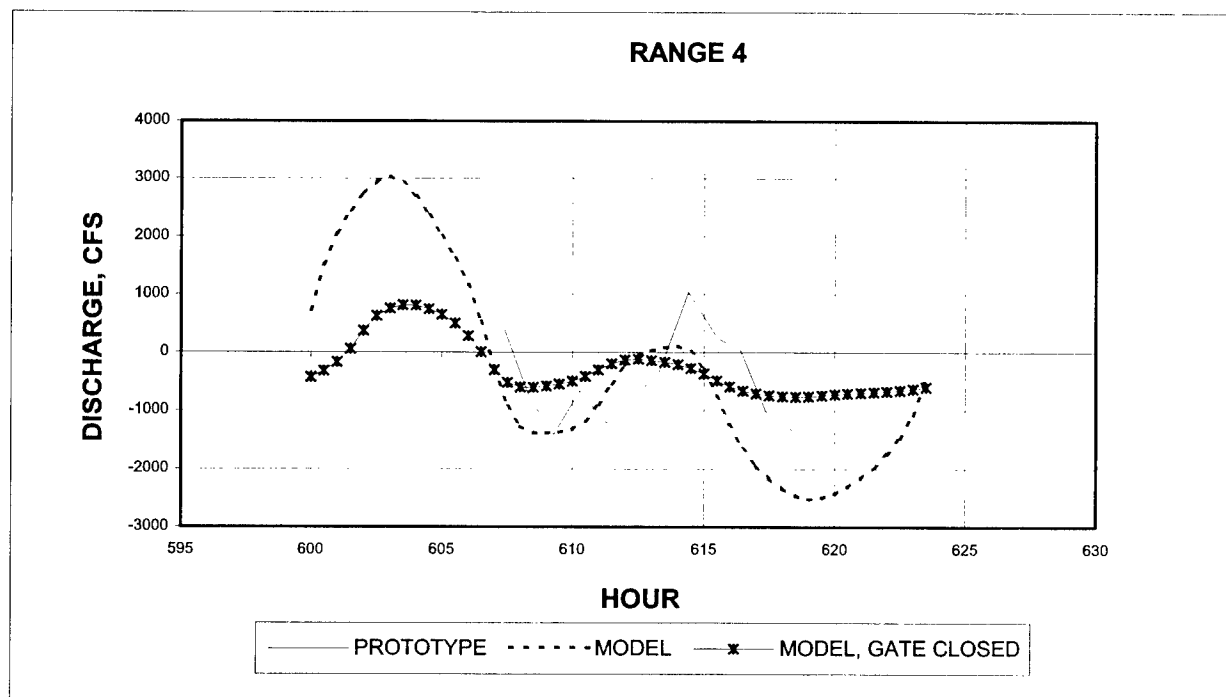
Figure 58.   Prototype and model discharge at Range 4 (Discharge is in cubic feet per second, to convert to cubic meters per second, multiply by 0.02831)

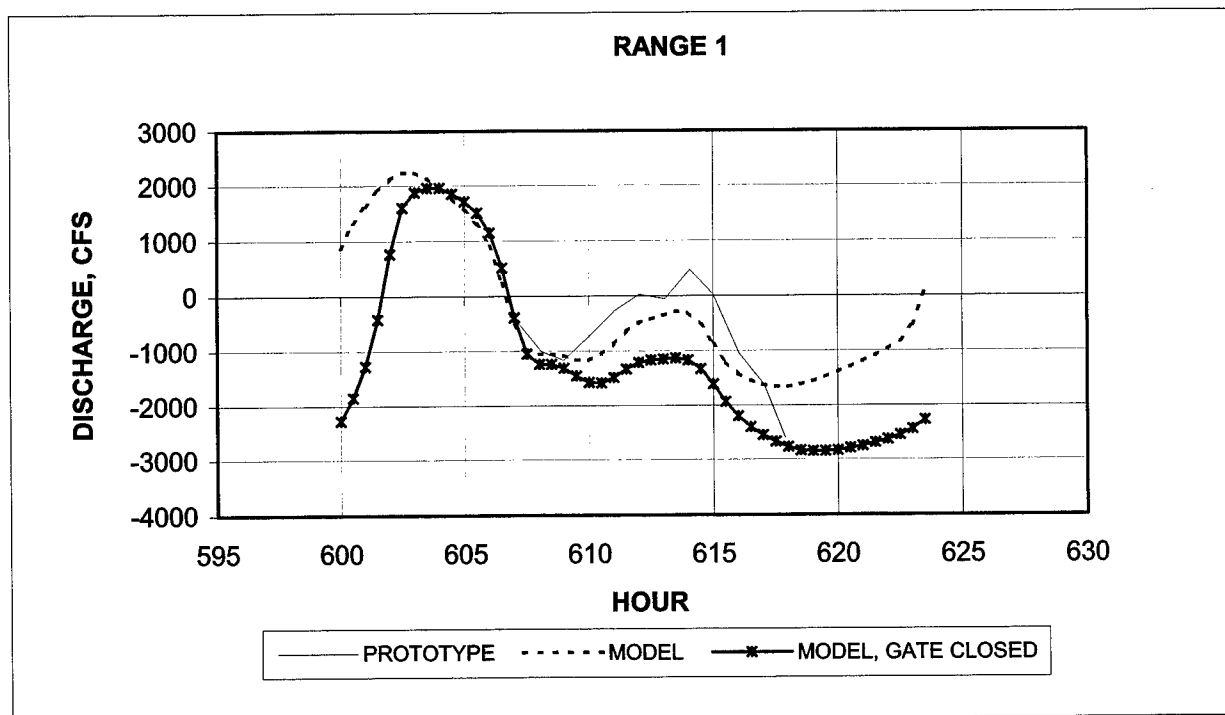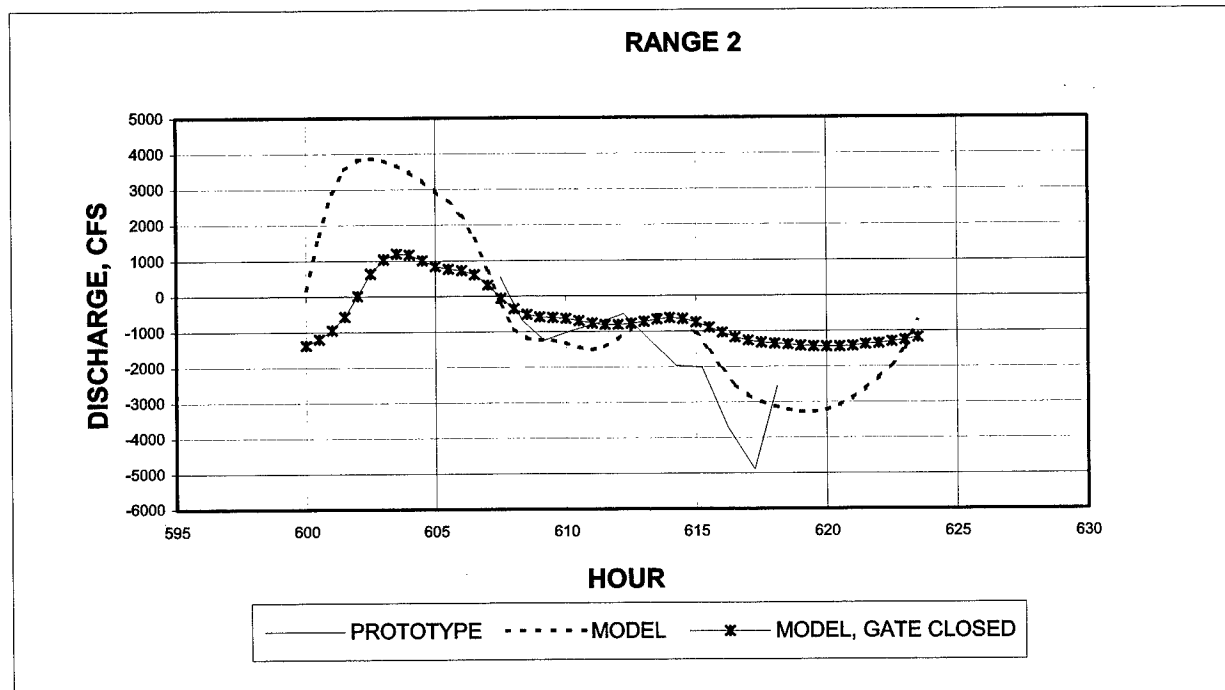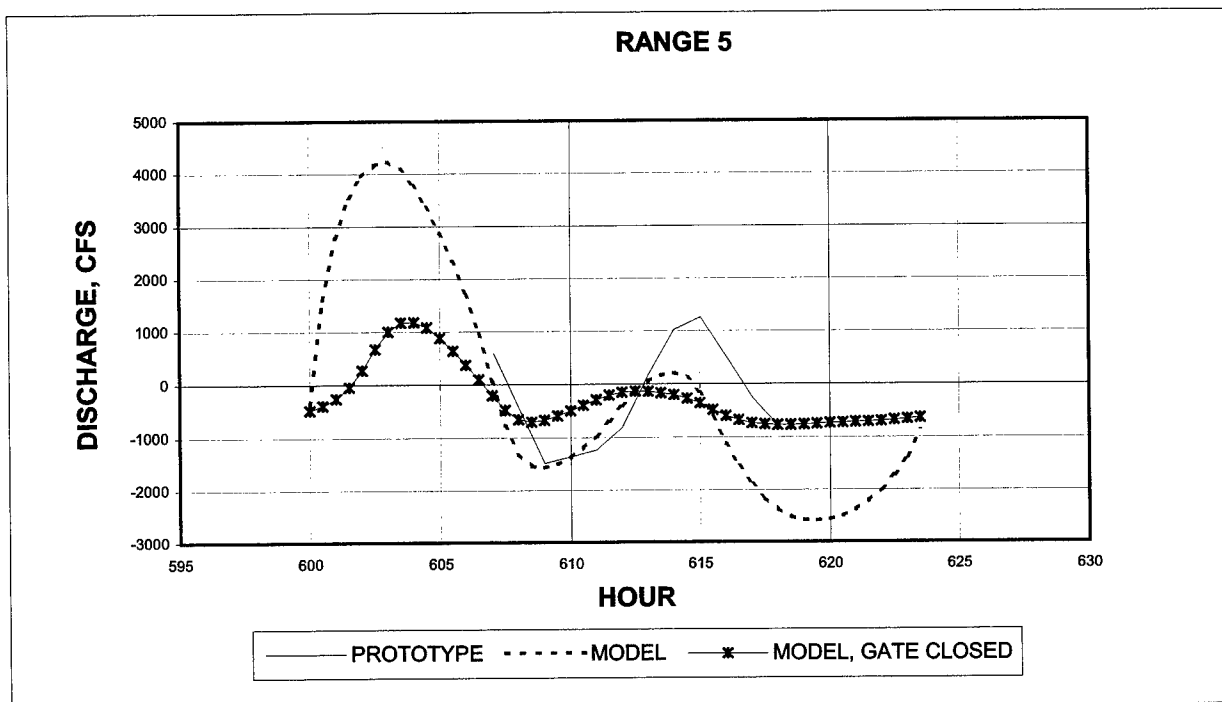Figure 59.   Prototype and model discharge at Range 5 (Discharge is in cubic feet per second, to convert to cubic meters per second, multiply by 0.02831)
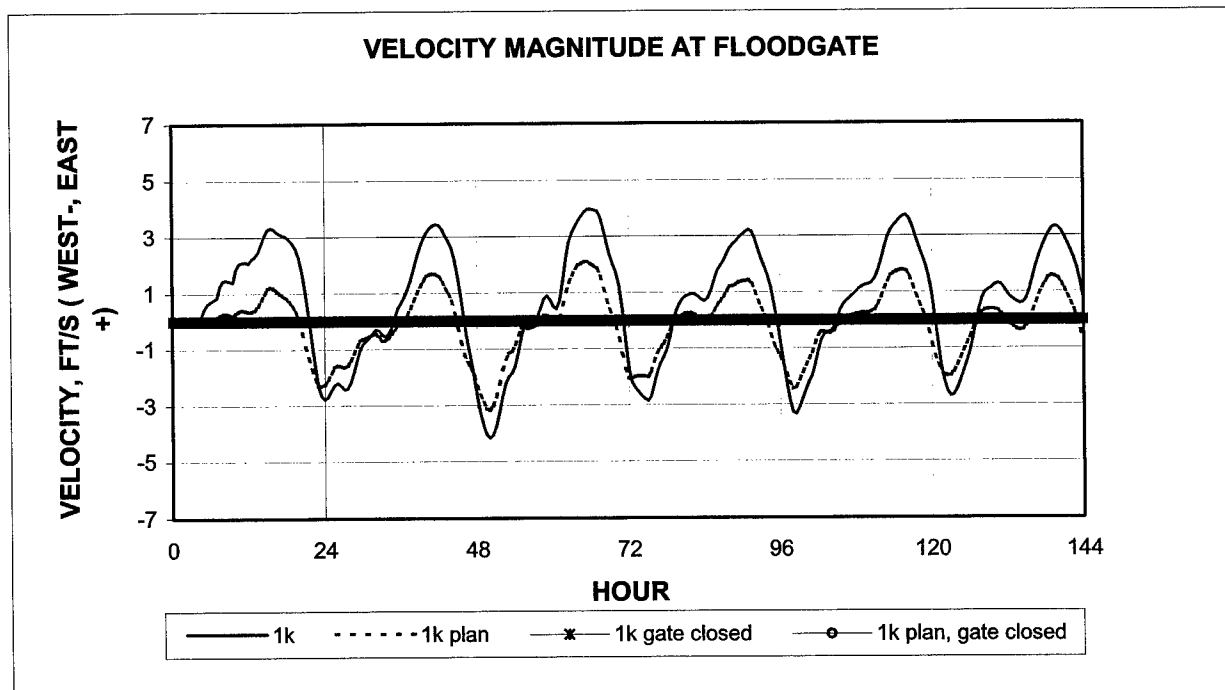
Figure 60.   Velocity at the west Brazos River floodgate for 1k discharge (Velocity is in feet per second, to convert to meters per second, multiply by 0.3048)
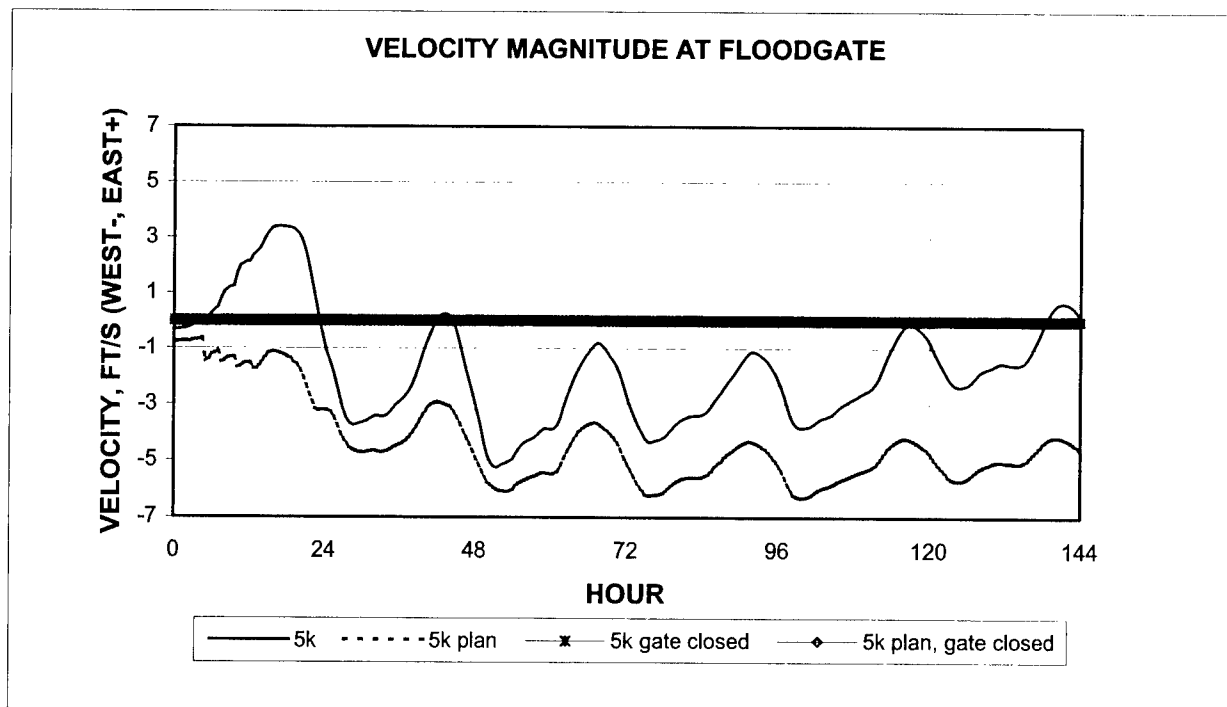
Figure 61. Velocity at the west Brazos River floodgate for 5k discharge (Velocity is in feet per second, to convert to meters per second, multiply by 0.3048)
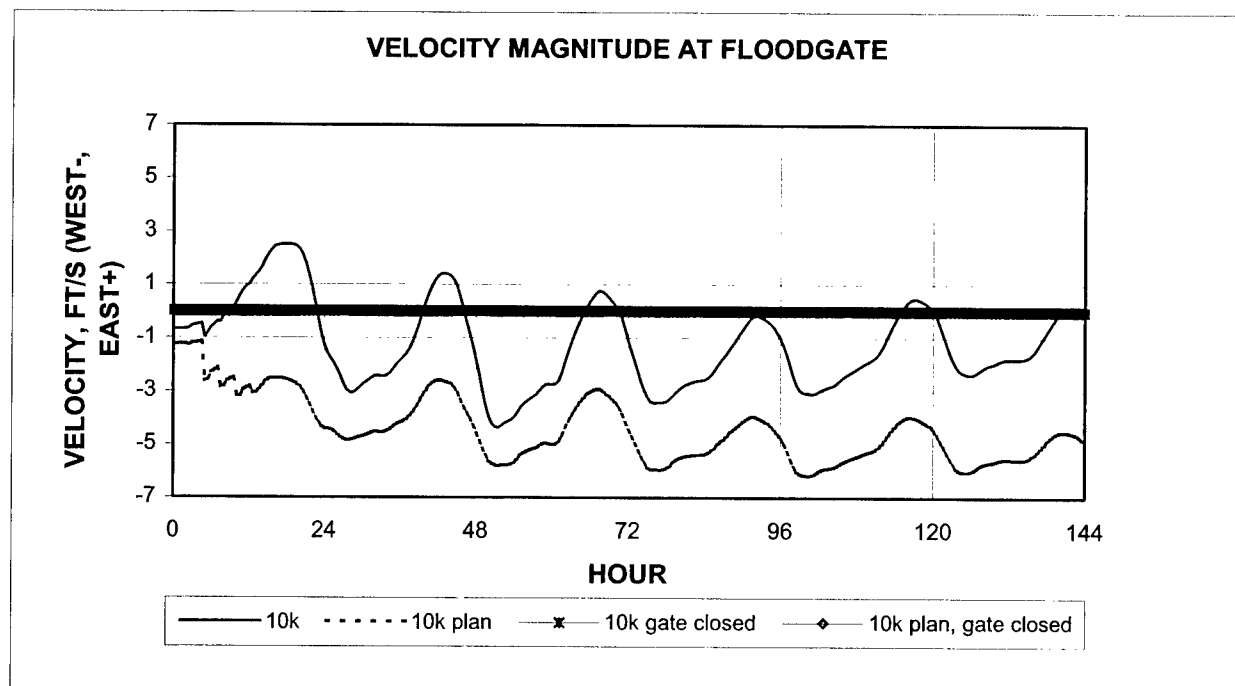
Figure 62. Velocity at the west Brazos River floodgate for 10k discharge (Velocity is in feet per second, to convert to meters per second, multiply by 0.3048)

VELOCITY MAGNITUDE AT FLOODGATE

Legend: 20k • • • • • 20k plan —✗— 20k gate closed —◆— 20k plan, gate closed
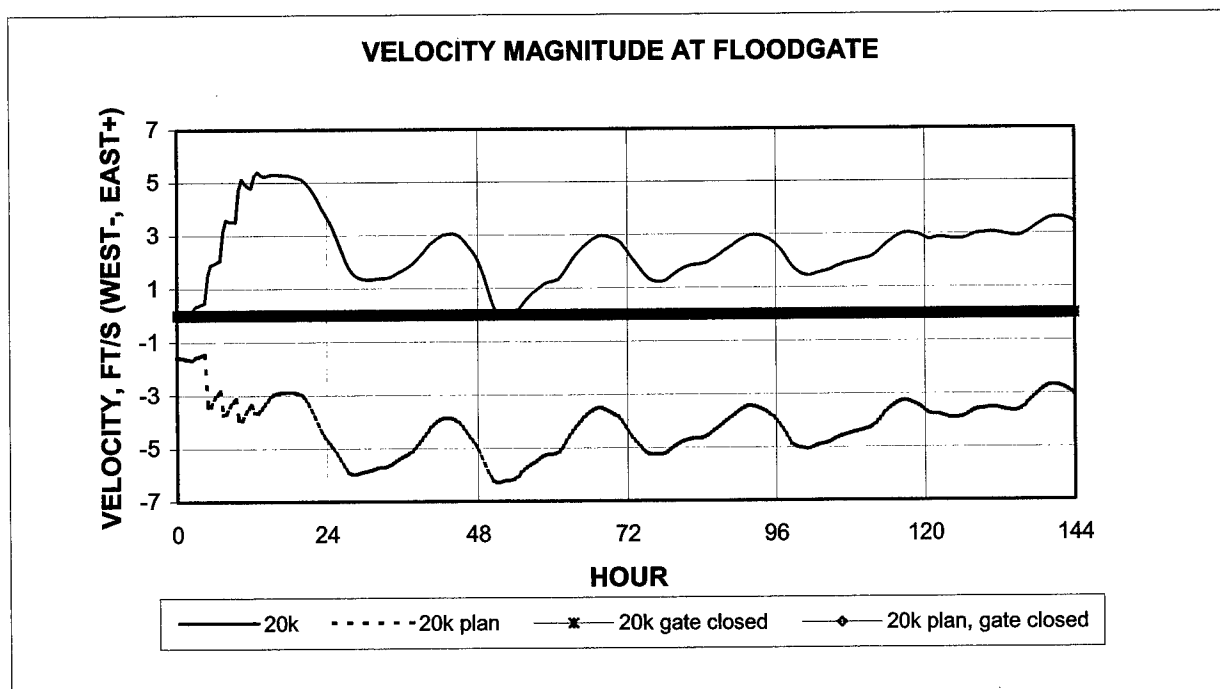
Figure 63.   Velocity at the west Brazos River floodgate for 20k discharge (Velocity is in feet per second, to convert to meters per second, multiply by 0.3048)

WATER SURFACE ELEVATION AT FLOODGATE

Legend: 1k • • • • • 1k plan —✗— 1k gate closed —◆— 1k plan, gate closed
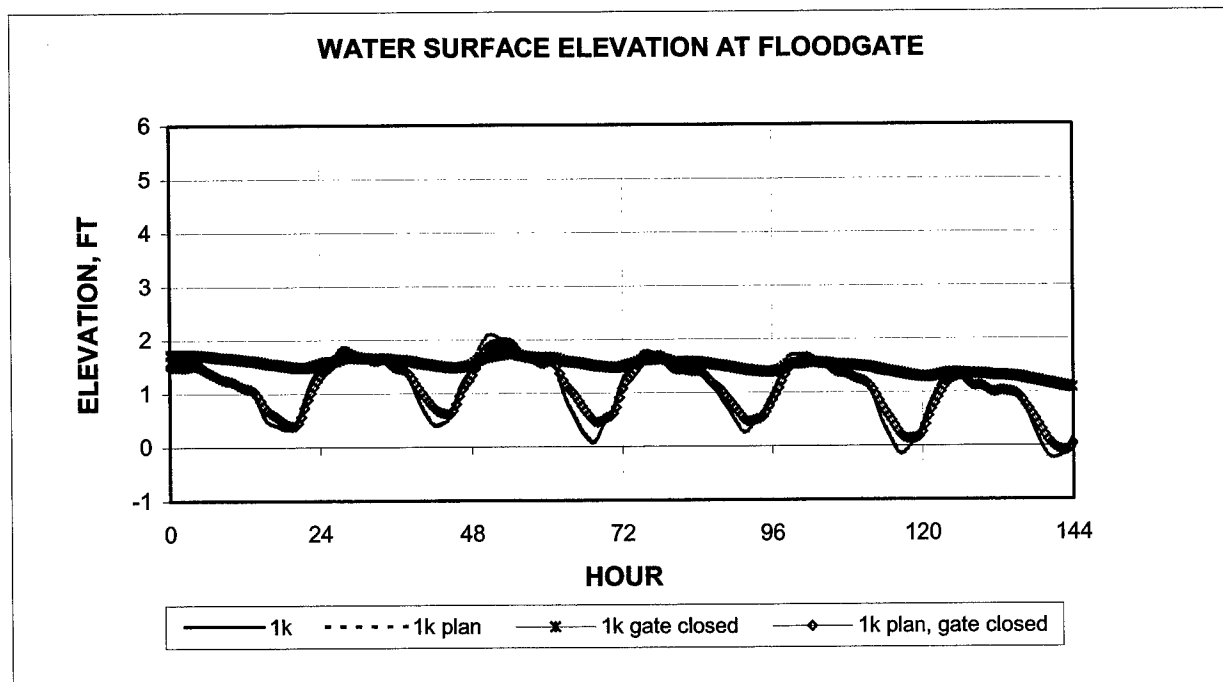
Figure 64.   Water surface elevation at the west Brazos River floodgate for 1k discharge (Elevation is in feet, to convert to meters, multiply by 0.3048)
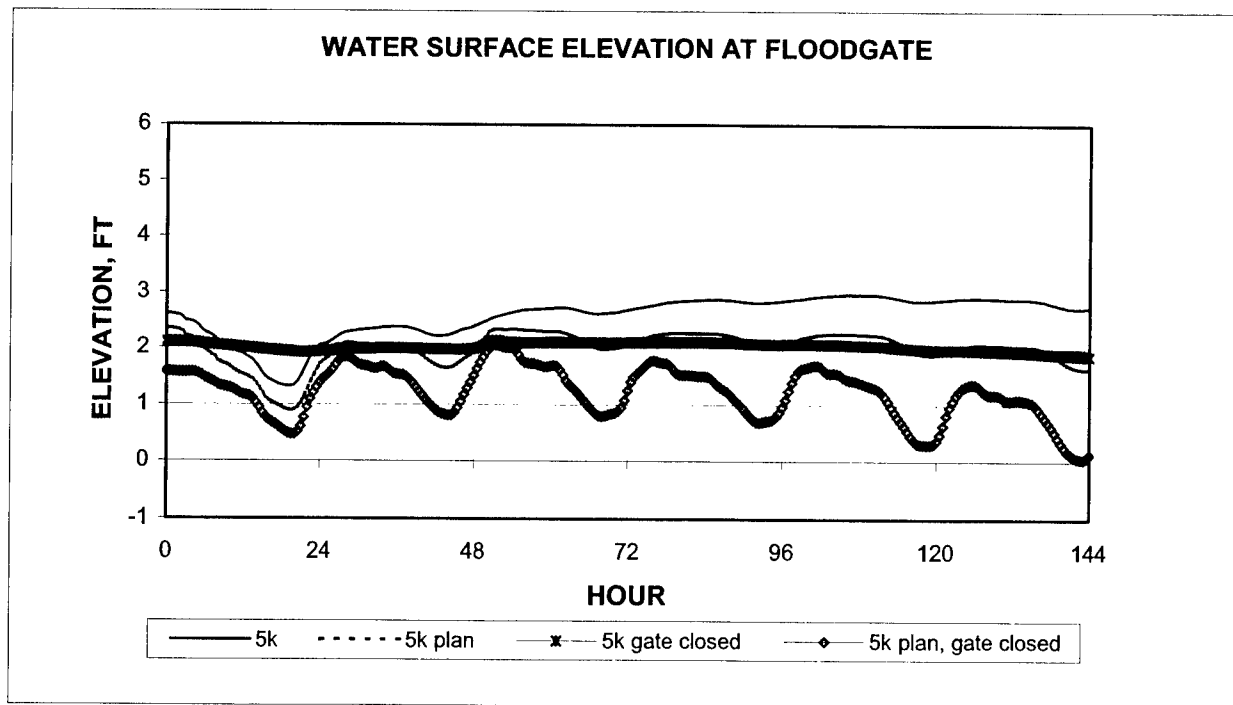
Figure 65. Water surface elevation at the west Brazos River floodgate for 5k discharge (Elevation is in feet, to convert to meters, multiply by 0.3048)
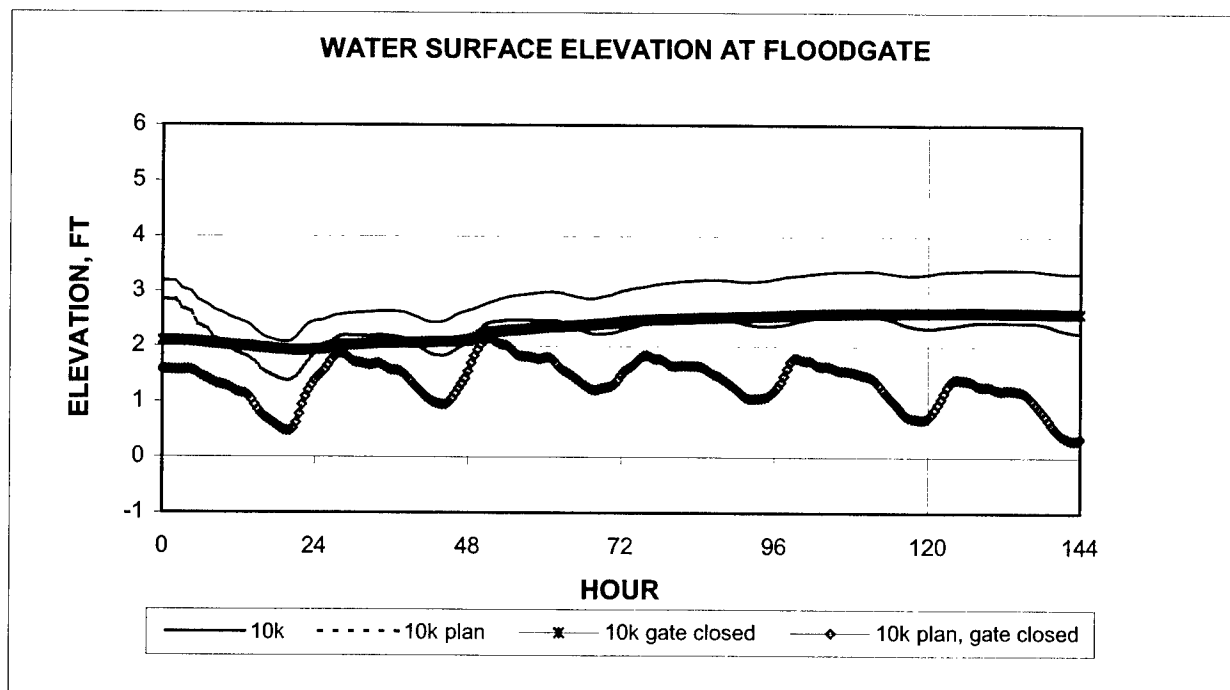
Figure 66. Water surface elevation at the west Brazos River floodgate for 10k discharge (Elevation is in feet, to convert to meters, multiply by 0.3048)

WATER SURFACE ELEVATION AT FLOODGATE
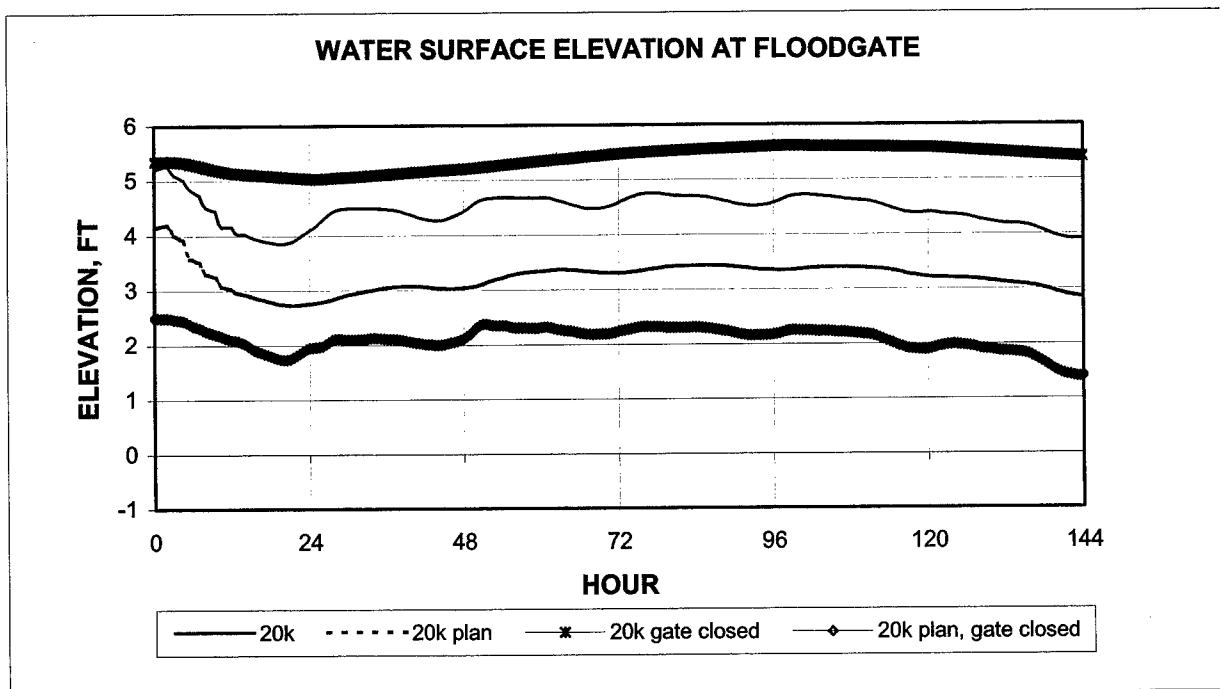
Figure 67.   Water surface elevation at the west Brazos River floodgate for 20k discharge (Elevation is in feet, to convert to meters, multiply by 0.3048)

VELOCITY MAGNITUDE AT INTERSECTION OF SAN BERNARD RIVER WITH GIWW

Figure 68.   Velocity magnitude at the intersection of San Bernard River and GIWW for 1k discharge. (Velocity is in feet per second, to convert to meters per second, multiply by 0.3048)

Figure 69.   Velocity magnitude at the intersection of San Bernard River and GIWW for 5k discharge.
(Velocity is in feet per second, to convert to meters per second, multiply by 0.3048)
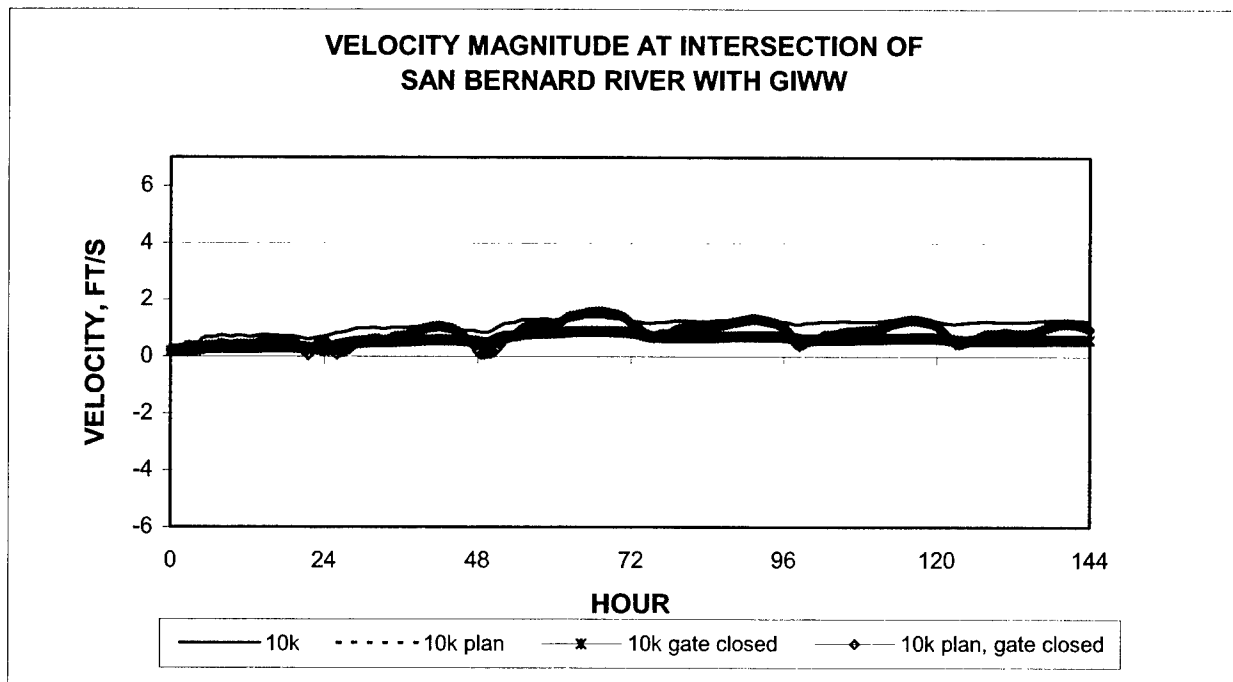
Figure 70.   Velocity magnitude at the intersection of San Bernard River and GIWW for 10k discharge.
(Velocity is in feet per second, to convert to meters per second, multiply by 0.3048)

Figure 71.   Velocity magnitude at the intersection of San Bernard River and GIWW for 20k discharge. (Velocity is in feet per second, to convert to meters per second, multiply by 0.3048)

Figure 72.   Velocity direction at the intersection of San Bernard River and GIWW for 1k discharge

VELOCITY DIRECTION AT INTERSECTION OF SAN BERNARD RIVER WITH GIWW
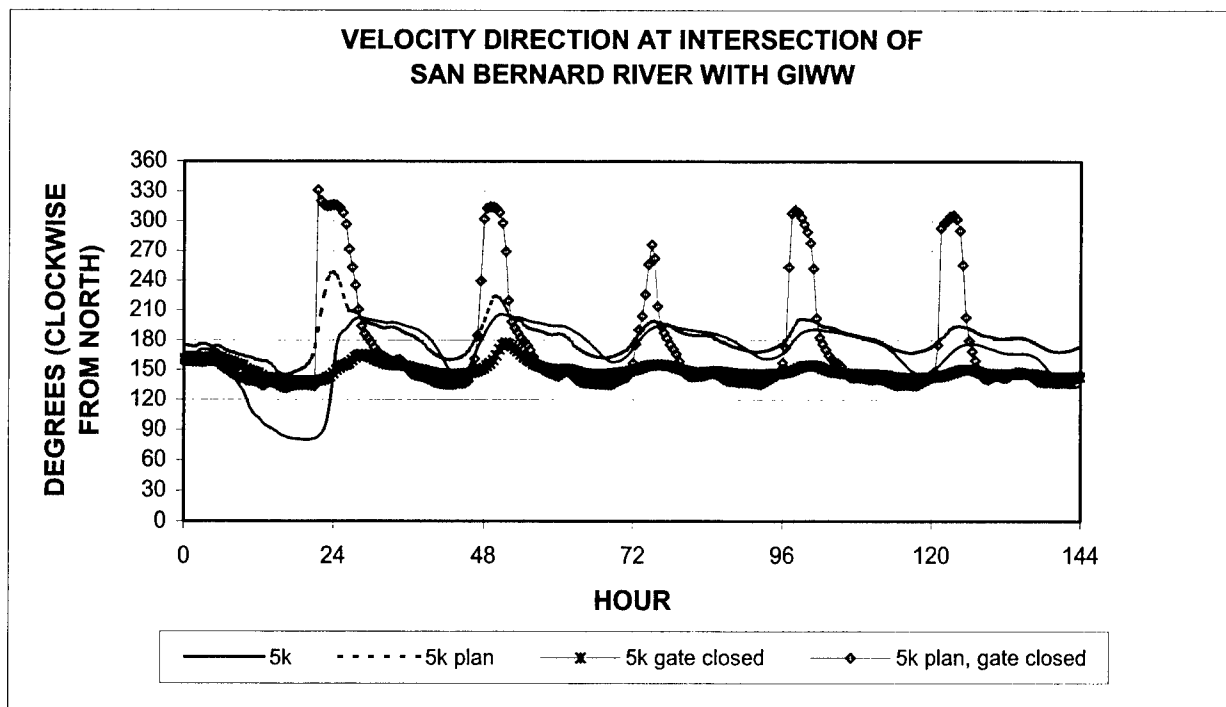
Figure 73.   Velocity direction at the intersection of San Bernard River and GIWW for 5k discharge

VELOCITY DIRECTION AT INTERSECTION OF SAN BERNARD RIVER WITH GIWW
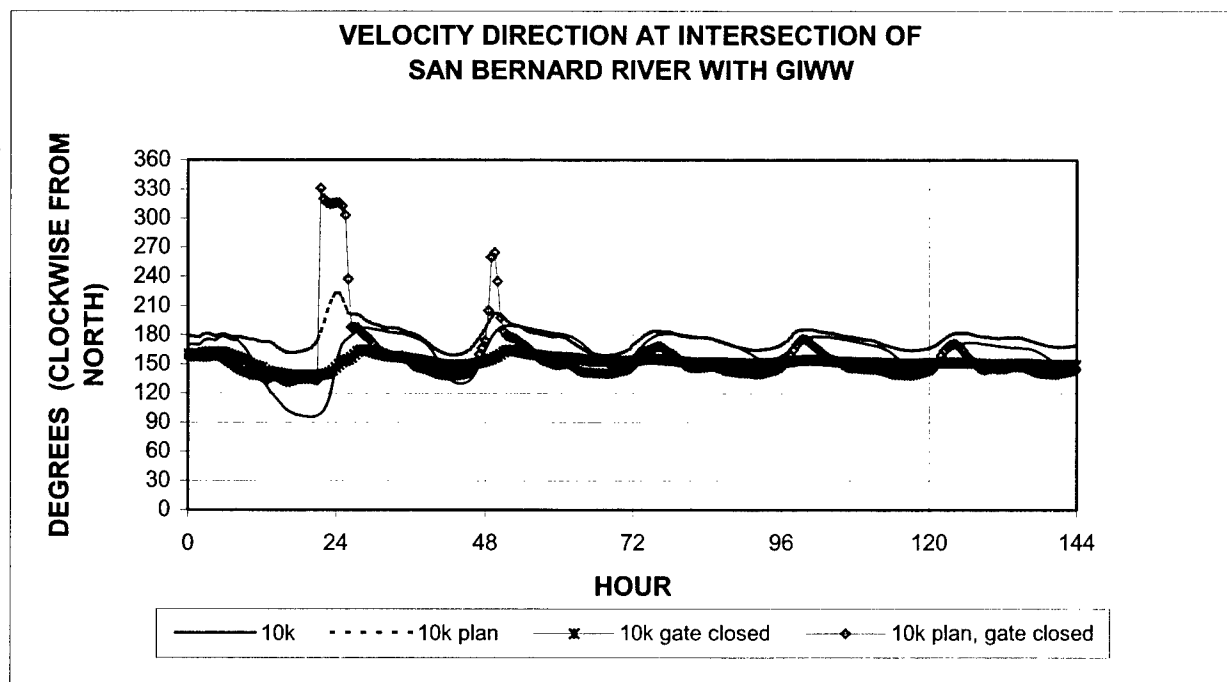
Figure 74.   Velocity direction at the intersection of San Bernard River and GIWW for 10k discharge

VELOCITY DIRECTION AT INTERSECTION OF
SAN BERNARD RIVER WITH GIWW
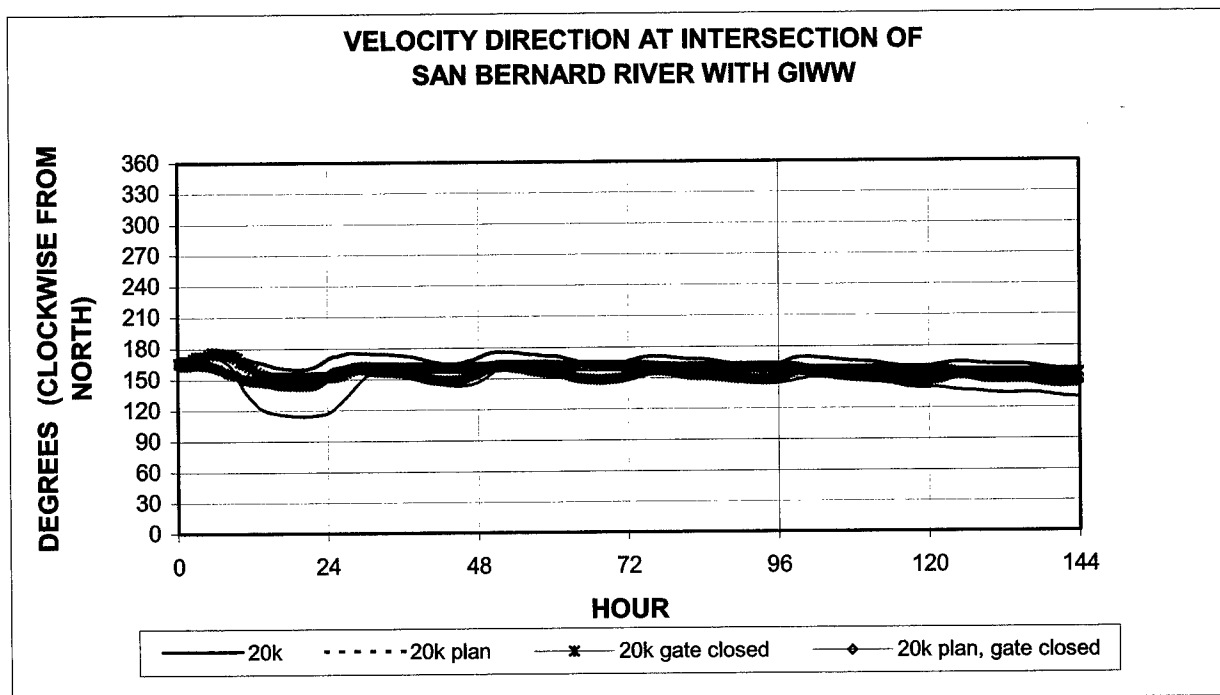
Figure 75. Velocity direction at the intersection of San Bernard River and GIWW for 20k discharge

WATER SURFACE ELEVATION AT INTERSECTION OF
SAN BERNARD RIVER WITH GIWW
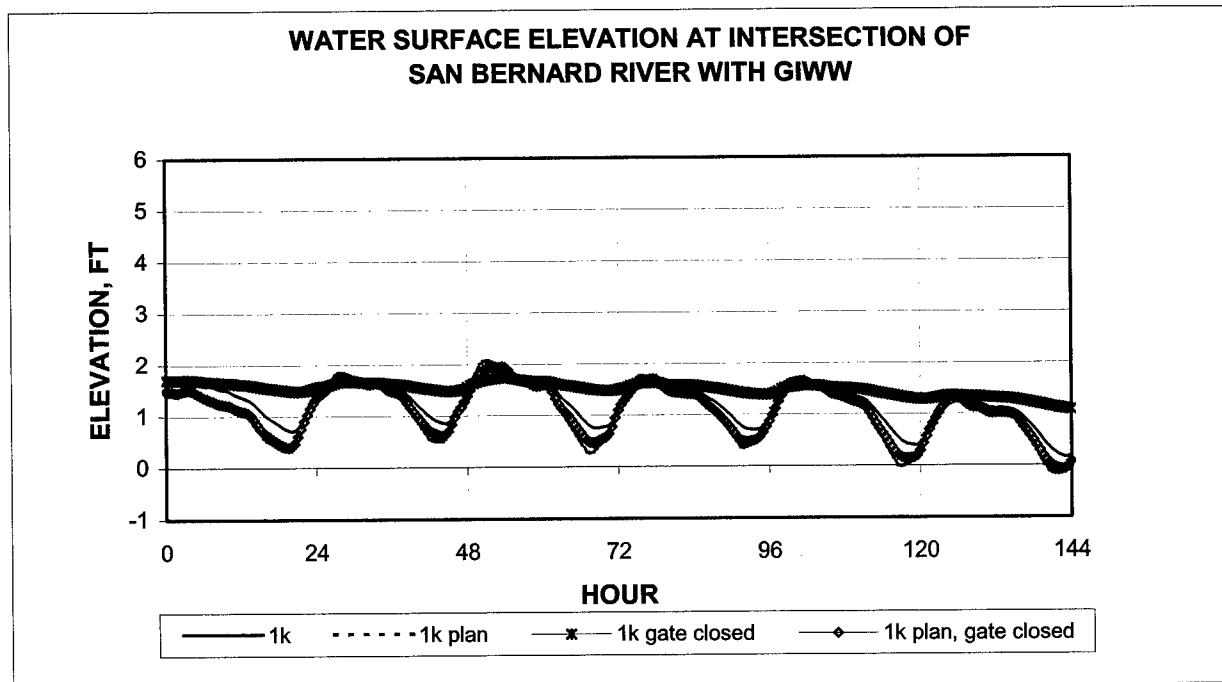
Figure 76. Water surface elevation at the intersection of San Bernard River and GIWW for 1k discharge. (Elevation is in feet, to convert to meters, multiply by 0.3048)
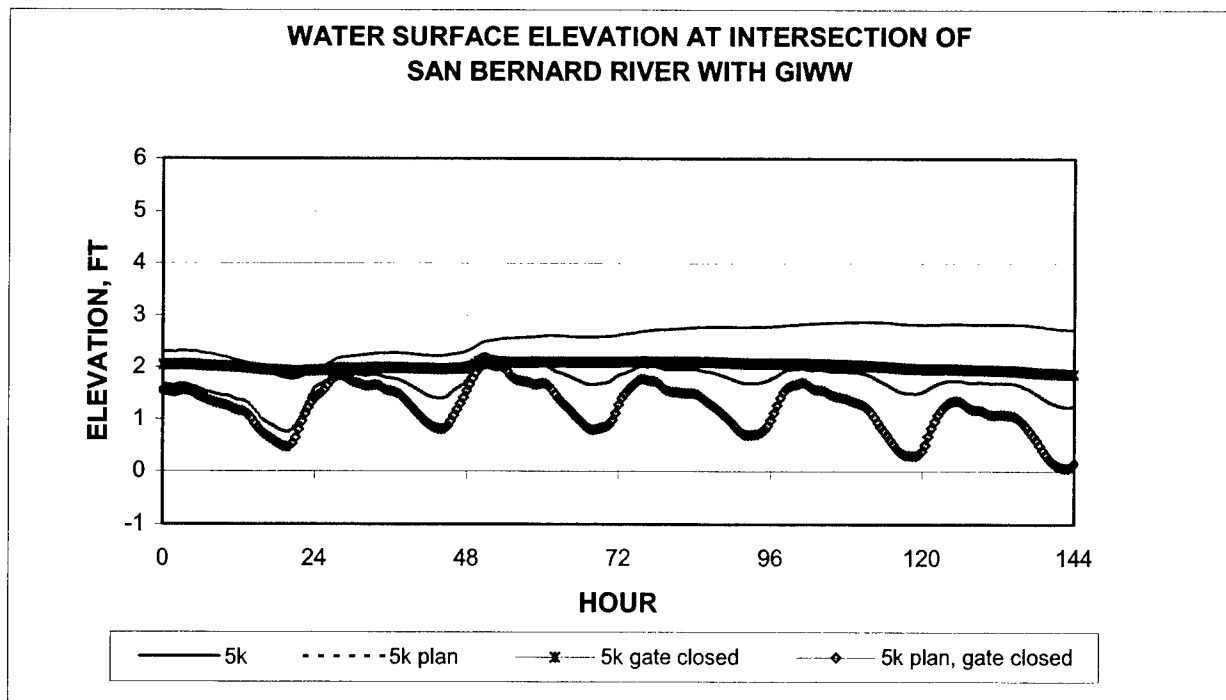
Figure 77.　Water surface elevation at the intersection of San Bernard River and GIWW for 5k discharge. (Elevation is in feet, to convert to meters, multiply by 0.3048)
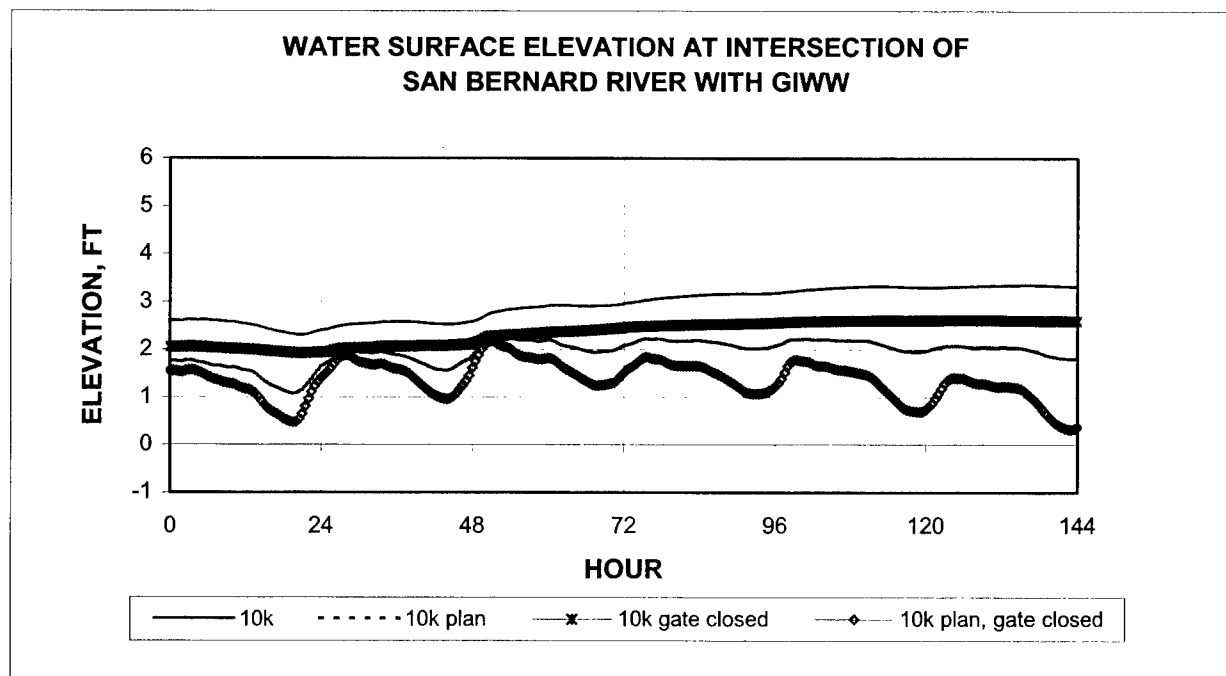
Figure 78.　Water surface elevation at the intersection of San Bernard River and GIWW for 10k discharge. (Elevation is in feet, to convert to meters, multiply by 0.3048)

WATER SURFACE ELEVATION AT INTERSECTION OF SAN BERNARD RIVER WITH GIWW
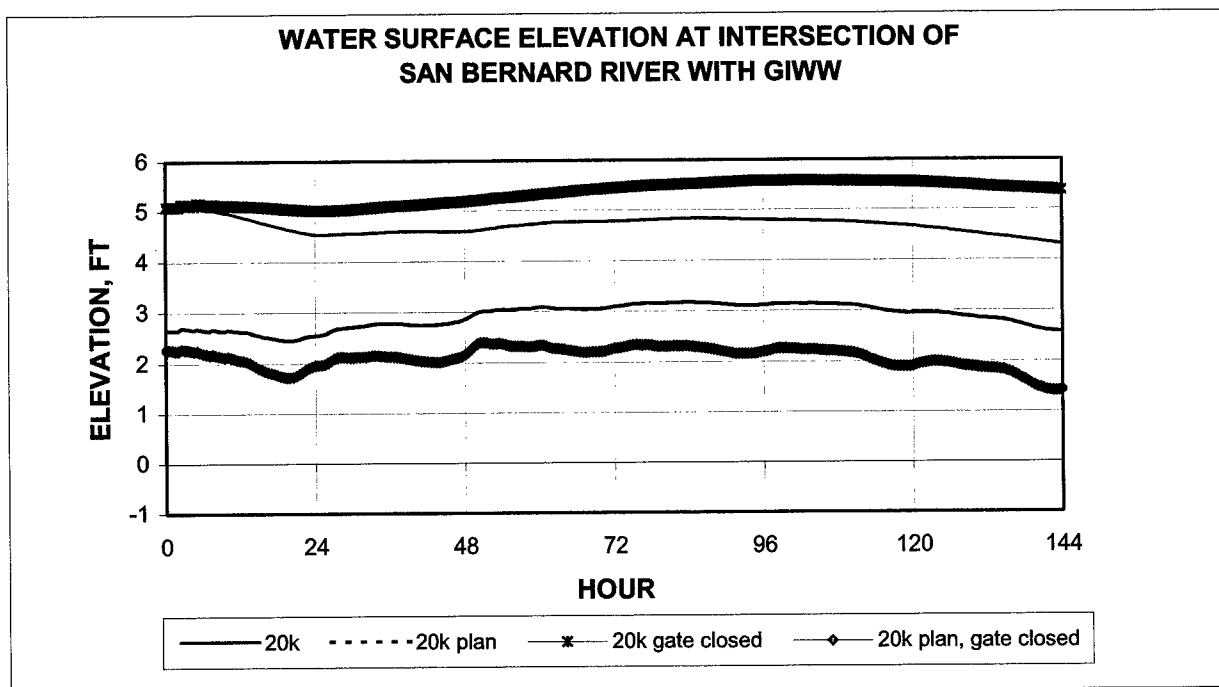
Figure 79.   Water surface elevation at the intersection of San Bernard River and GIWW for 20k discharge. (Elevation is in feet, to convert to meters, multiply by 0.3048)
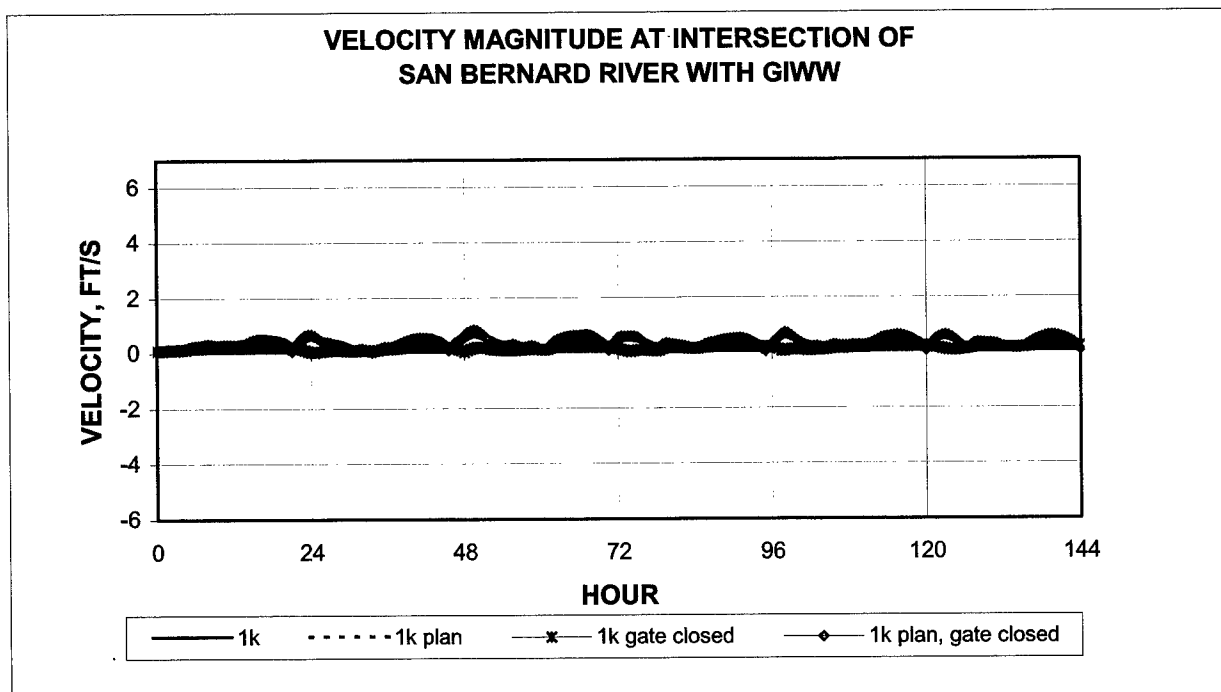

VELOCITY MAGNITUDE AT SAN BERNARD RIVER OUTLET
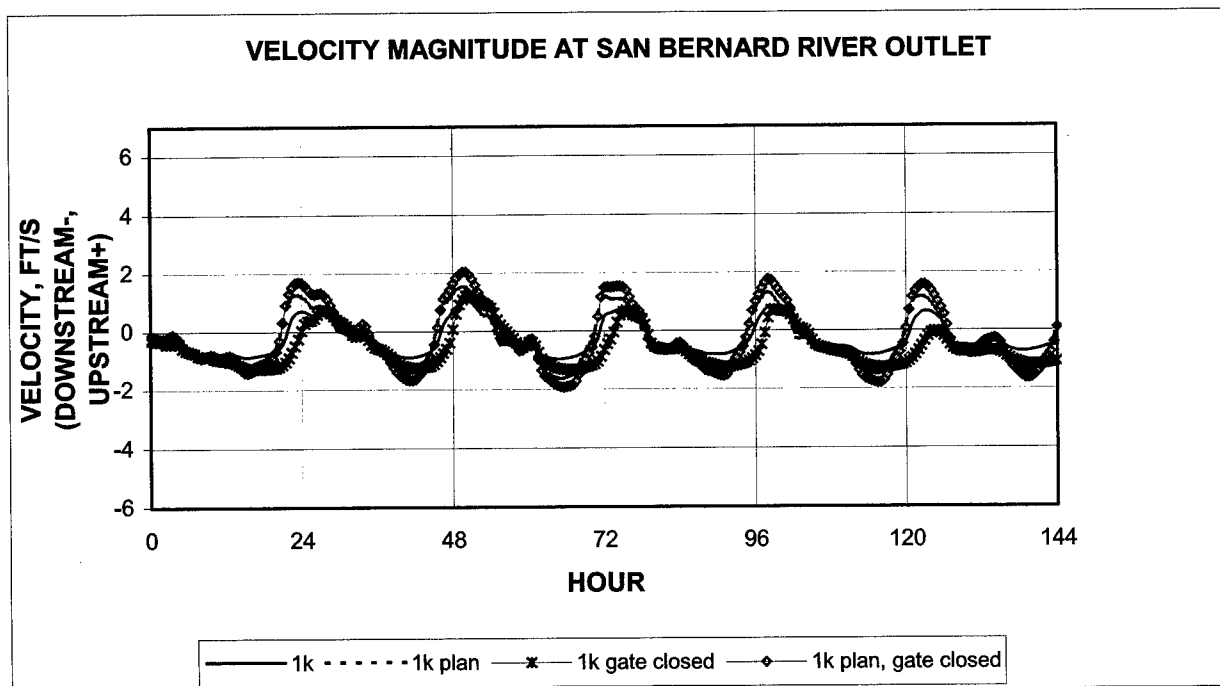
Figure 80.   Velocity magnitude at the San Bernard River outlet for 1k discharge. (Velocity is in feet per second, to convert to meters per second, multiply by 0.3048)

VELOCITY MAGNITUDE AT SAN BERNARD RIVER OUTLET
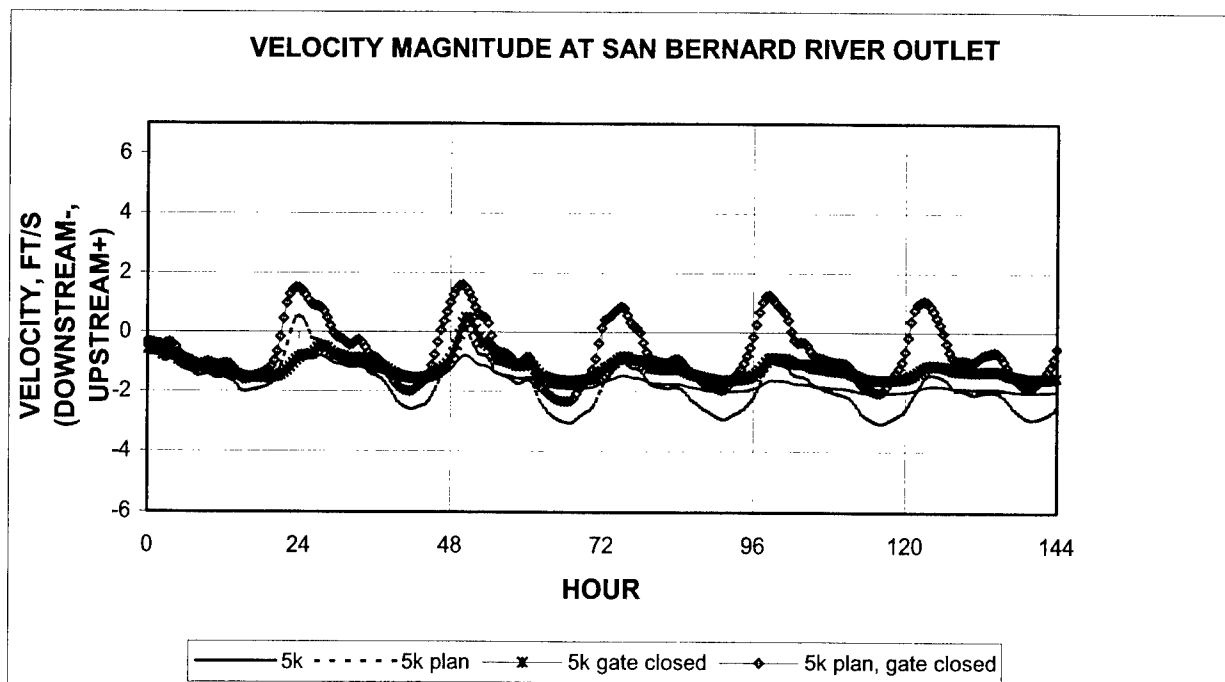
Figure 81.   Velocity magnitude at the San Bernard River outlet for 5k discharge. (Velocity is in feet per second, to convert to meters per second, multiply by 0.3048)

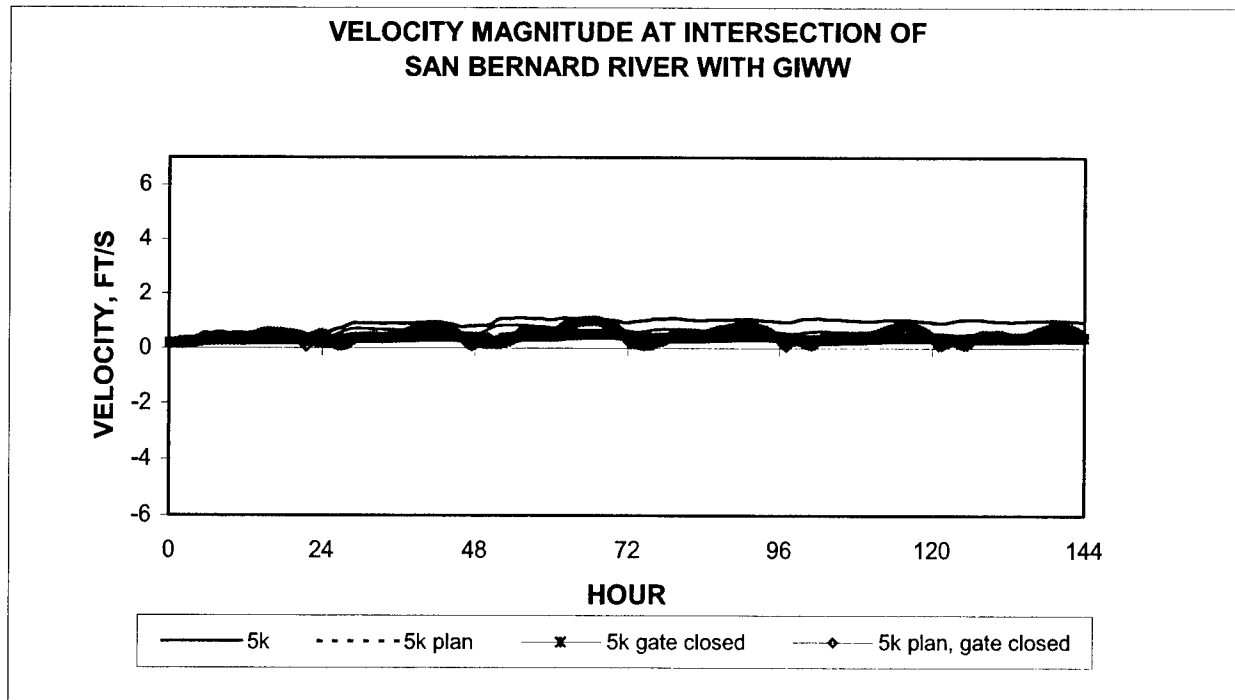## VELOCITY MAGNITUDE AT SAN BERNARD RIVER OUTLET
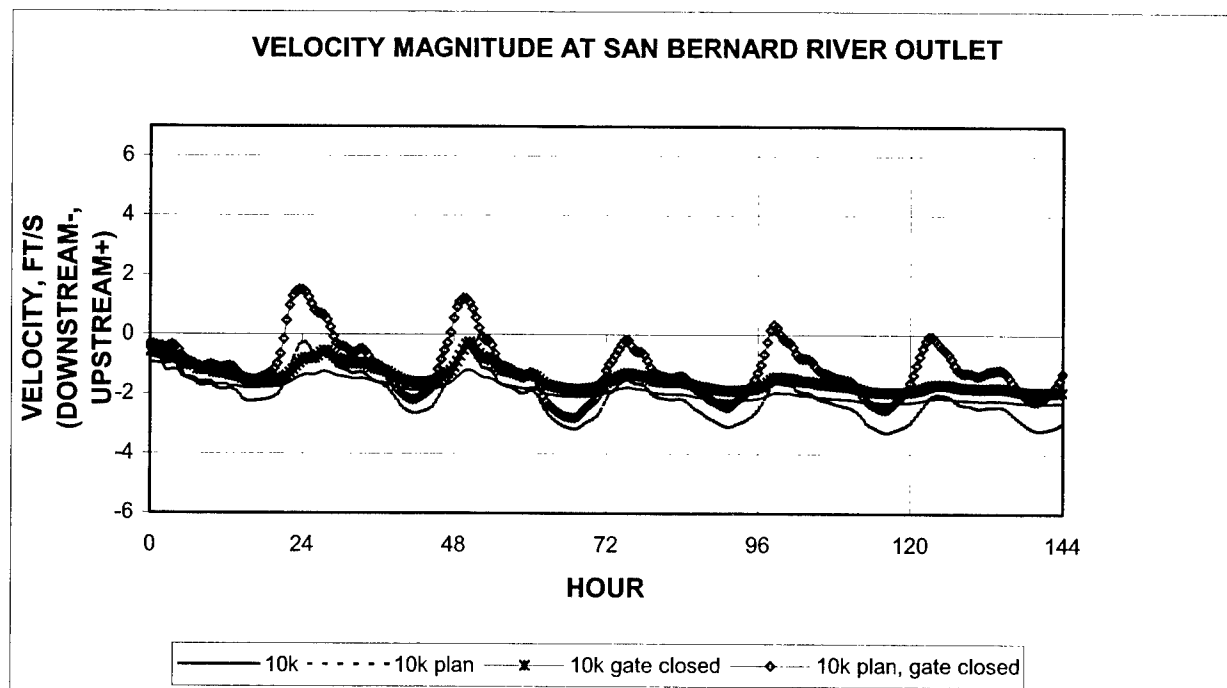
Figure 82.   Velocity magnitude at the San Bernard River outlet for 10k discharge. (Velocity is in feet per second, to convert to meters per second, multiply by 0.3048)
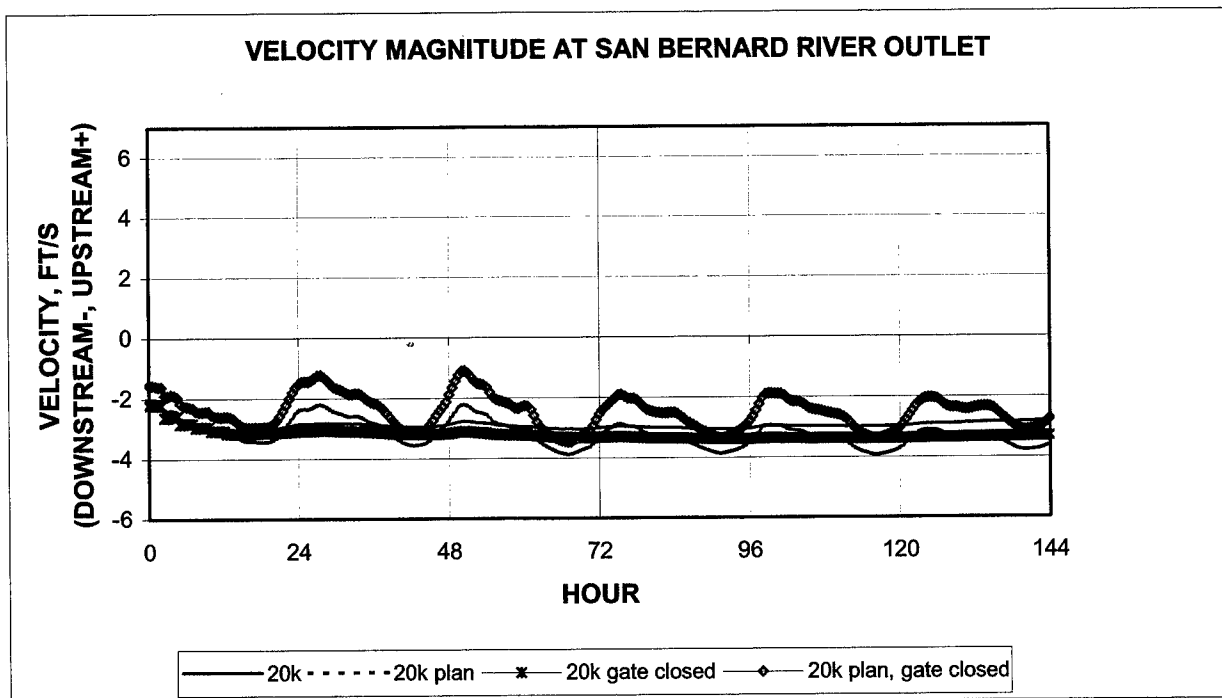
Figure 83.   Velocity magnitude at the San Bernard River outlet for 20k discharge. (Velocity is in feet per second, to convert to meters per second, multiply by 0.3048)
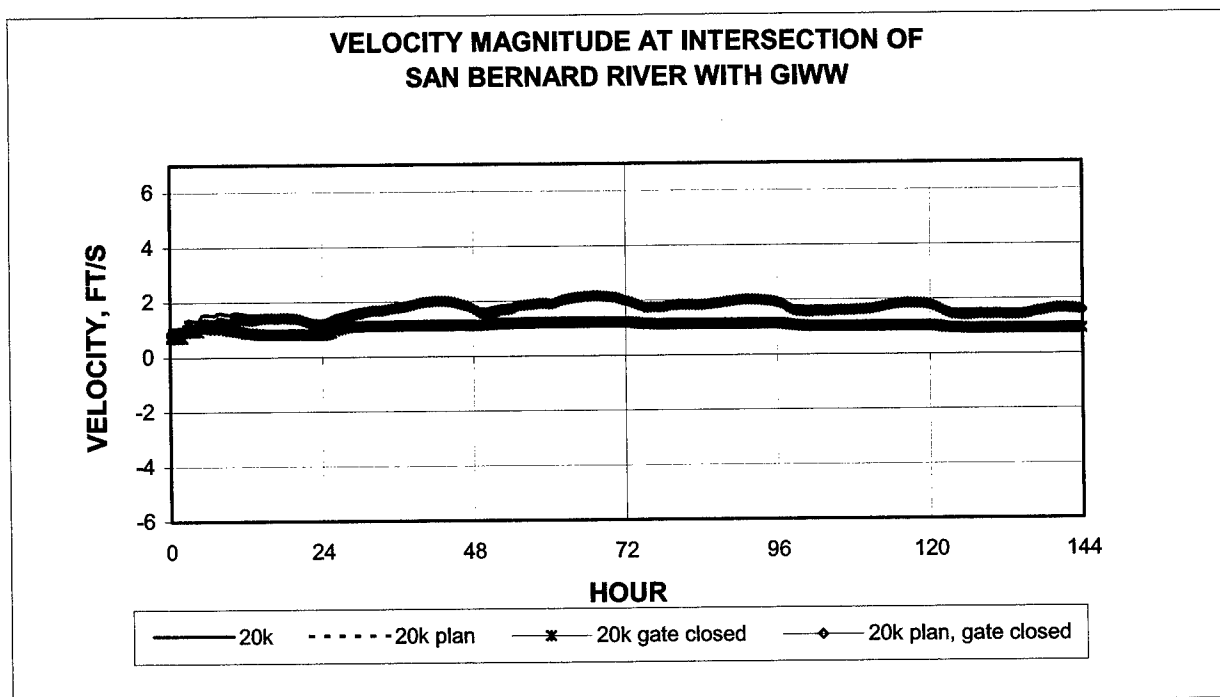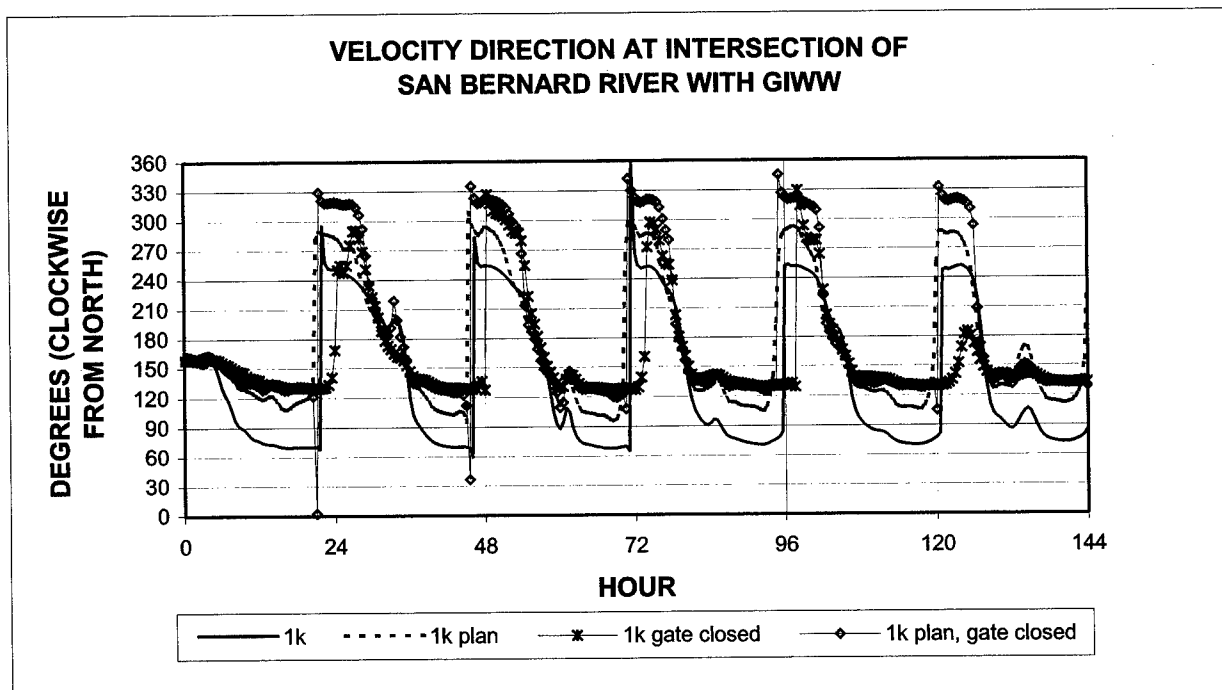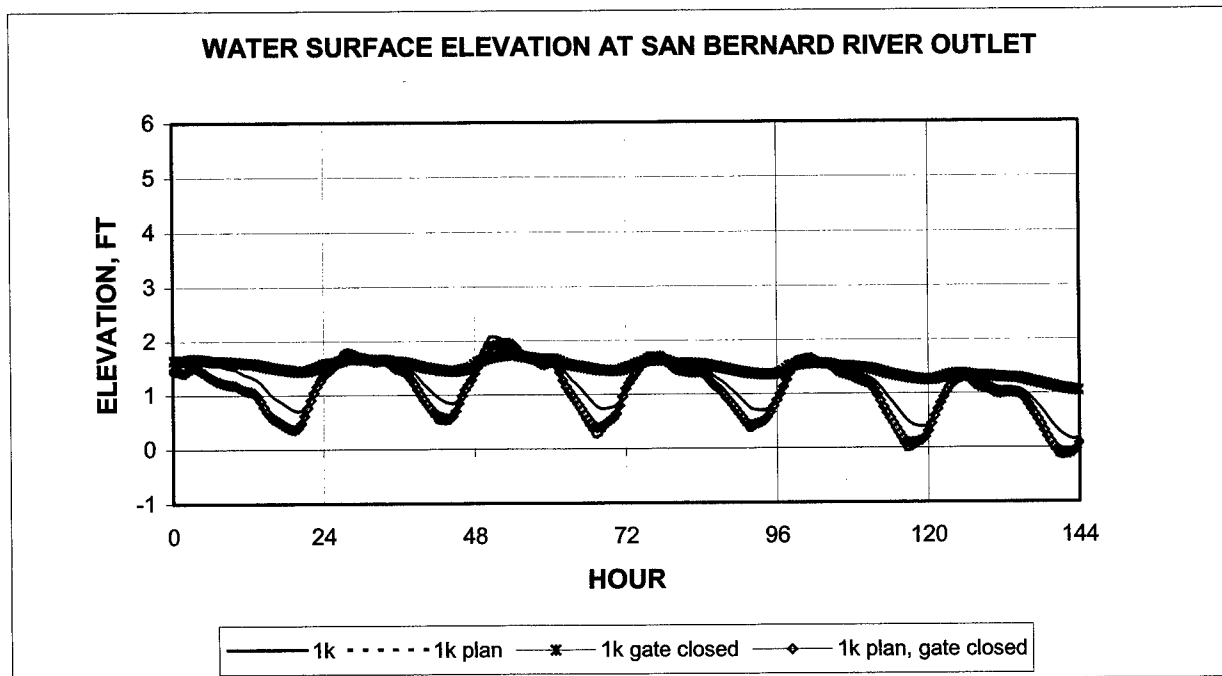

Figure 84.   Water surface elevation at the San Bernard River outlet 1k discharge. (Elevation is in feet, to convert to meters, multiply by 0.3048)

WATER SURFACE ELEVATION AT SAN BERNARD RIVER OUTLET
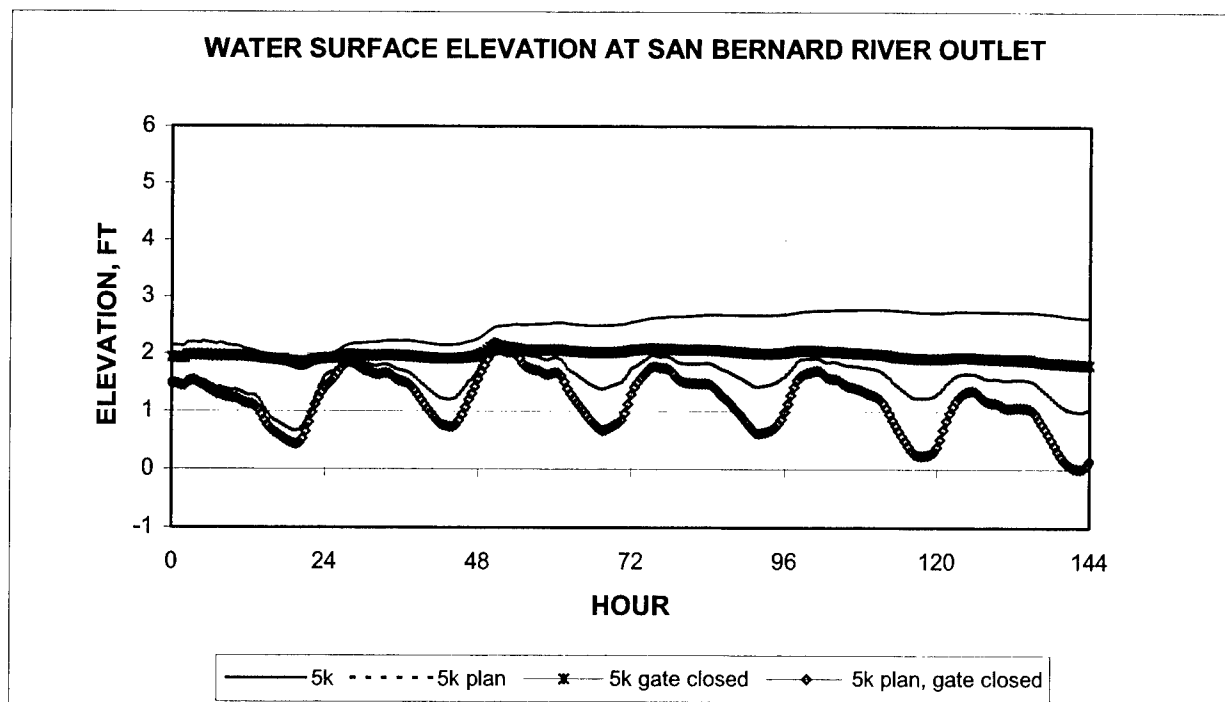
Figure 85. Water surface elevation at the San Bernard River outlet 5k discharge. (Elevation is in feet, to convert to meters, multiply by 0.3048)

WATER SURFACE ELEVATION AT SAN BERNARD RIVER OUTLET
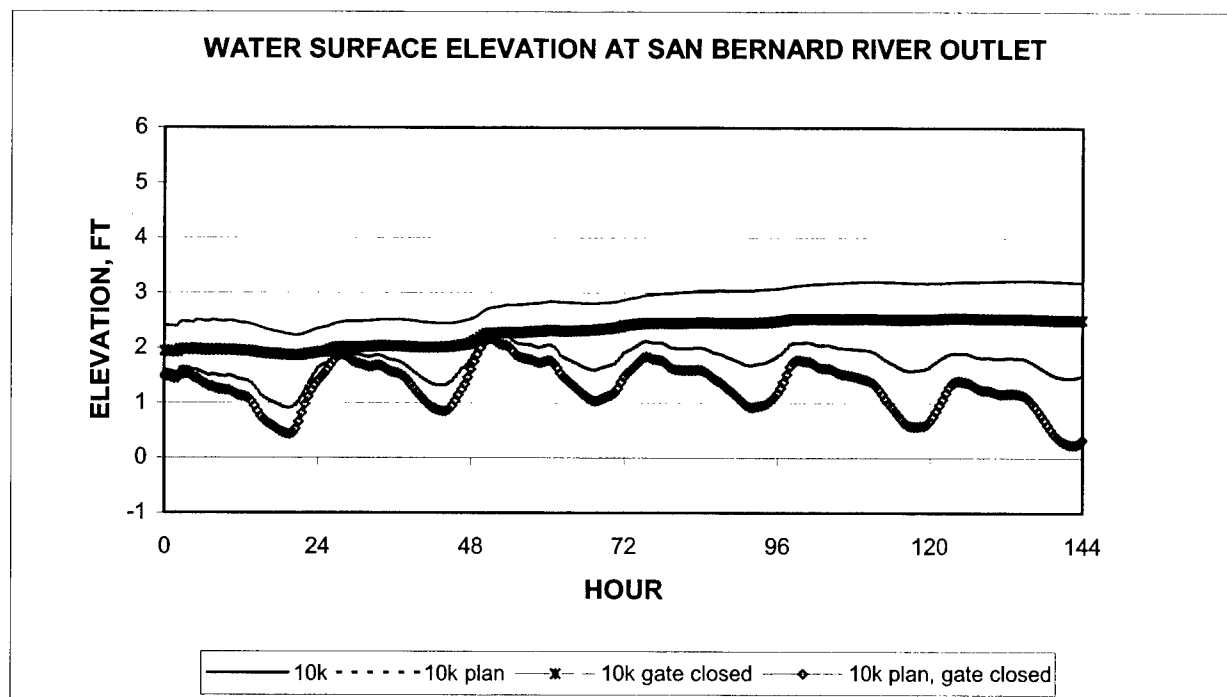
Figure 86. Water surface elevation at the San Bernard River outlet 10k discharge. (Elevation is in feet, to convert to meters, multiply by 0.3048)
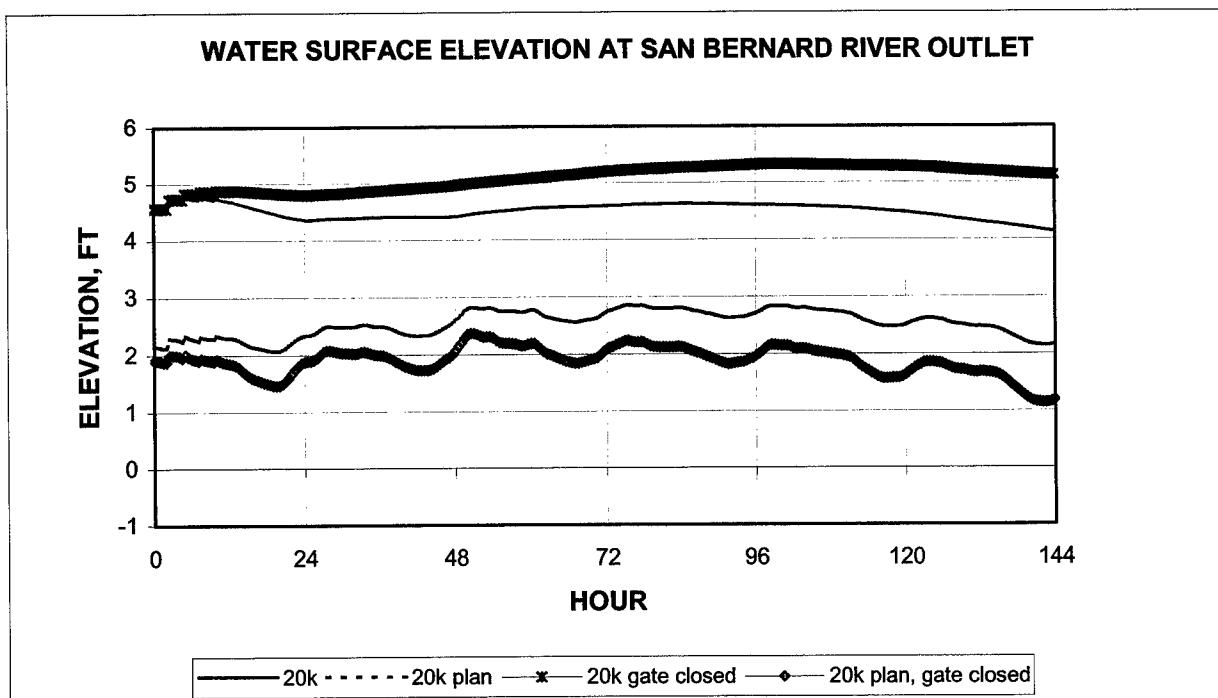
Figure 87. Water surface elevation at the San Bernard River outlet 20k discharge. (Elevation is in feet, to convert to meters, multiply by 0.3048)

Appendix A
The TABS-MD System

TABS-MDS is a collection of generalized computer programs and utility codes integrated into a numerical modeling system. TABS-MDS is capable of one-, two-, and/or three-dimensional computations; however, only the one- and two-dimensional vertically averaged capability will be discussed in this summary. The system is used for studying hydrodynamics, sedimentation, and transport problems in rivers, reservoirs, bays, and estuaries. A schematic representation of the system is shown in Figure A1. It can be used either as a stand-alone solution technique or as a step in the hybrid modeling approach. The basic concept is to calculate water-surface elevations, current patterns, sediment erosion, transport and deposition, the resulting bed-surface elevations, and the feedback to hydraulics. Existing and proposed geometry can be analyzed to determine the impact on sedimentation of project designs and to determine the impact of project designs on salinity and on the stream system. The system is described in detail by Thomas and McAnally (1985).[1]

The three basic 2-D depth-averaged components of the system are as follows:

   a. A two-dimensional model for free surface flows, RMA2.

   b. Sediment transport in unsteady 2-dimensional flows, horizontal plane, SED2D.

   c. Two-dimensional finite element program for water quality, RMA4.

RMA2 is a finite element solution of the Reynolds form of the Navier-Stokes equations for turbulent flows. Friction is calculated with Manning's equation and eddy viscosity coefficients are used to define the turbulent exchanges. A velocity form of the basic equation is used with side boundaries treated as either slip or static. The model has a marsh porosity option as well as the ability to automatically perform wetting and drying. Boundary conditions may be water-surface elevations, velocities, discharges, or tidal radiation.

---

[1] All references cited in this appendix are listed in the References section following the main text.
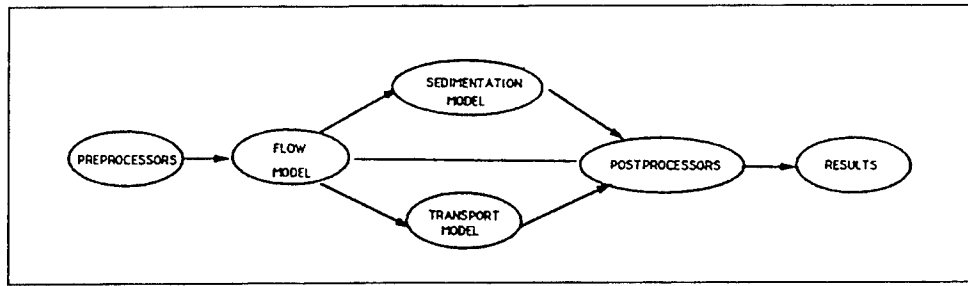
Figure A1. TABS-MD schematic

The sedimentation model, SED2D, solves the convection-diffusion equation with bed source-sink terms. These terms are structured for either sand or cohesive sediments. The Ackers-White (1973) procedure is used to calculate a sediment transport potential for the sands from which the actual transport is calculated based on availability. Clay erosion is based on work by Partheniades (1962) and Ariathurai and the deposition of clay used Krone's equations (Ariathurai, MacArthur, and Krone 1977). Deposited material forms layers and bookkeeping allows up to 10 layers at each node for maintaining separate material types, deposit thickness, and age. The code uses the same mesh as RMA2.

Consistent transport calculations including salinity are made under RMA4 using a form of the convective-diffusion equation which has general source-sink terms. Up to six conservative substances or substances requiring a decay term can be routed. The code uses the same mesh as RMA2. The model accommodates a mixing zone outside of the model boundaries for estimation of retrainment.

Pre- and Postprocessing and Analysis of TABS-MDS Models

The Surface Water Modeling System (SMS) is a comprehensive graphical user environment for performing model conceptualizations-mesh generator, statistical interpretation, and visual examination of surface water model simulations.

SMS is a pre- and postprocessor for surface water modeling and analysis in shallow open water areas such as rivers, bays, and estuaries. It includes two-dimensional finite element, two-dimensional finite difference, three-dimensional finite element and one-dimensional step backwater modeling tools. Interfaces specifically designed to facilitate the utilization of several numerical models comprise the modules of SMS. Supported models include the USACE-WES supported TABS-MD (GFGEN, RMA2, RMA4, RMA10, SED2D-WES).

Each TABS-MDS model is designed to address a specific class of problem. RMA2 calculate hydrodynamic data such as water surface elevations and flow

velocities. RMA4 tracks contaminant migration, and SED2O calculates suspended sediment concentrations, erosion, and deposition. The models support both steady-state and dynamic analyses.

The finite element mesh or cross-section entities, along with associated boundary conditions necessary for analysis, are created within SMS and then saved to model-specific files. These files are used as input to the hydrodynamic, contaminant migration, and sediment transport analysis engines. The numerical models create solution files that contain the water surface elevations, flow velocities, contaminant concentrations, sediment concentrations or other functional data at each node, cell, or section.

These files are then used to perform the analyses. Resulting solution files can be read into SMS to generate vector plots, color-shaded contour plots, time-history diagrams, and solution animation sequences.

Finite Element Modeling

The TABS-MDS numerical models employ the finite element method to solve the governing equations. To help those who are unfamiliar with the method to better understand the system, a brief description of the method is given here.

The finite element method approximates a solution to governing equations by dividing the area of interest into smaller subareas, which are called elements. The dependent variables (e.g., water-surface elevations or sediment concentrations) are approximated over each element by continuous functions which interpolate based on unknown point (node) values of the variables. An error, defined as the deviation of the governing equations using the approximate solution from the equation using the correct solution, is minimized. Then, when boundary conditions are imposed, a set of solvable simultaneous equations is created. The solution is continuous over the area of interest.

In one-dimensional problems, elements are line segments. In two-dimensional problems, the elements are polygons, either triangles or quadrilaterals. Nodes are located on the edges of elements and occasionally inside the elements. The interpolating functions may be linear or higher order polynomials. Figure A2 illustrates a quadrilateral element with eight nodes and a linear solution surface where F is the interpolating function.

Most water resource applications of the finite element method use the Galerkin method of weighted residuals to minimize error. In this method the residual, the local error in the equations use of the approximate and solution, is weighted by a function identical to the interpolating function and then minimized. Minimization results in a set of simultaneous equations in terms of nodal values of the dependent variable (e.g., water-surface elevations or sediment concentration). The time portion of time-dependent problems can be

a. Eight nodes define each element

b. Linear interpolation function
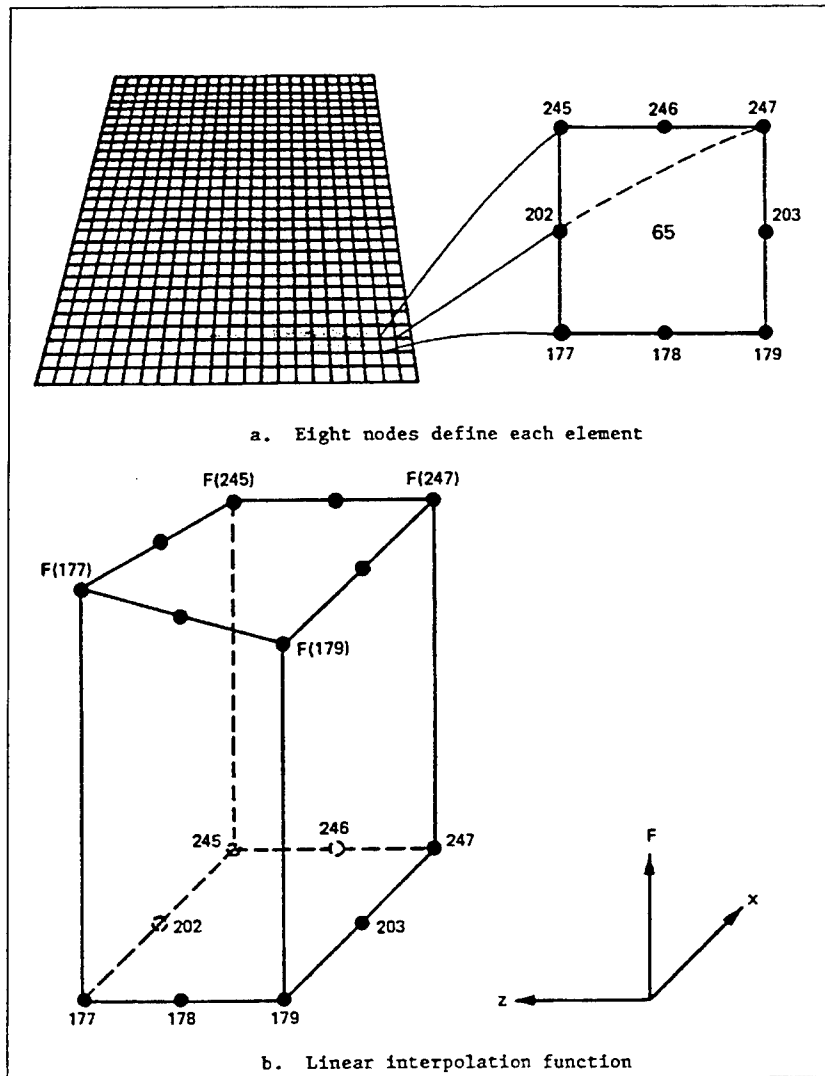
Figure A2. Two-dimensional finite element mesh

solved by the finite element method, but it is generally more efficient to express derivatives with respect to time in finite difference form.

The Hydrodynamic Model, RMA2

Applications

RMA2 is designed for far field problems in which vertical accelerations are negligible and the velocity vectors at a node generally point in the same directions over the entire depth of the water column at any instant of time. It expects a vertically homogeneous fluid with a free surface. The model will define the response to a specified horizontally inhomogeneous fluid. Both steady and

unsteady state problems can be analyzed. A surface wind stress can be imposed and the effects of the earth's rotation (Coriolis effect) can be included.

RMA2 has been applied to calculate water levels and flow distribution around islands; flow at bridges having one or more relief openings, in contracting and expanding reaches, into and out of off-channel hydropower plants, at river junctions, and into and out of pumping plant channels; circulation and transport in water-bodies with wetlands; and general water levels and flow patterns in rivers, reservoirs, and estuaries.

Limitations

RMA2 is not designed for near field problems where flow structure interactions (such as vortices, vibrations, or vertical accelerations) are of interest. Areas of vertically stratified flow are beyond this program's capability unless it is used in a hybrid modeling approach. It is two-dimensional in the horizontal plane, and zones where the bottom current is in a different direction from the surface current must be analyzed with considerable subjective judgment. It is a free-surface calculation for subcritical flow problems.

Governing equations

The generalized computer program RMA2 solves the depth-integrated equations of fluid mass and momentum conservation in two horizontal directions. The form of the solved equations is as follows:

$$h\frac{\partial u}{\partial t} + hu\frac{\partial u}{\partial x} + hv\frac{\partial u}{\partial y} - \frac{h}{\rho}\left(\varepsilon_{xx}\frac{\partial^2 u}{\partial x^2} + \varepsilon_{xy}\frac{\partial^2 u}{\partial_y^2}\right) + gh\left(\frac{\partial a}{\partial x} + \frac{\partial h}{\partial x}\right) +$$

$$\frac{gun^2}{\left(1.486h^{1/6}\right)^2}\left(u^2 + v^2\right)^{1/2} - \zeta V_a^2 \cos\psi - 2h\omega v \sin\phi = 0 \qquad (A1)$$

$$h\frac{\partial v}{\partial t} + hu\frac{\partial v}{\partial x} + hv\frac{\partial v}{\partial y} - \frac{h}{\rho}\left(\varepsilon_{yx}\frac{\partial^2 v}{\partial x^2} + \varepsilon_{yy}\frac{\partial^2 v}{\partial y^2}\right) + gh\left(\frac{\partial a}{\partial y} + \frac{\partial h}{\partial y}\right) +$$

$$\frac{gvn^2}{\left(1.486h^{1/6}\right)^2}\left(u^2 + v^2\right)^{1/2} - \zeta V_a^2 \sin\psi + 2\omega hu \sin\phi + 0 \qquad (A2)$$

$$\frac{\partial h}{\partial t} + h\left(\frac{\partial u}{\partial x} + \frac{\partial v}{\partial y}\right) + u\frac{\partial h}{\partial x} + v\frac{\partial h}{\partial y} = 0 \qquad\qquad (A3)$$

where

h = depth

U,v = x and y direction velocities, respectively

x,y,t = Cartesian coordinates and time

ρ = density of fluid

ε = eddy viscosity coefficient, for xx = normal direction on x-axis surface; yy= normal direction on y-axis surface; xy and yx = shear direction on each surface

g = acceleration due to gravity

a = elevation of bottom

n = Manning's n value

1.486 = conversion from SI (metric) to non-SI units

ζ = empirical wind shear coefficient

V_a = wind speed

ψ = wind direction

ω = rate of earth's angular rotation

ϕ = local latitude

Equations A1, A2, and A3 are solved by the finite element method using Galerkin weighted residuals. The elements may be one-dimensional lines or two-dimensional quadrilaterals or triangles and may have curved (parabolic) sides. The shape functions are quadratic for velocity and linear for depth. Integration in space is performed by Gaussian integration. Derivatives in time are replaced by a nonlinear finite difference approximation. Variables are assumed to vary over each time interval in the form

$$f(t) = f(0) + at + bt^c \qquad t_o \leq t \angle t_0 + \Delta t \qquad\qquad (A4)$$

which is differentiated with respect to time, and cast in finite difference form. Letters *a*, *b*, and *c* are constants. It has been found by experiment that the best value for *c* is 1.5 (Norton and King 1977).

The solution is fully implicit and the set of simultaneous equations is solved by Newton-Raphson nonlinear iteration.

Sediment Transport Model, SED2D

Applications

SED2D can be applied to clay and/or sand bed sediments where flow velocities can be considered two-dimensional (i.e., the speed and direction can be satisfactorily represented as a depth-averaged velocity). It is useful for both deposition and erosion studies and, to a limited extent, for stream width studies. The program treats two categories of sediment: noncohesive, which is referred to as sand here, and cohesive, which is referred to as clay.

Limitations

Both clay and sand may be analyzed, but SED2D considers a single, effective grain size for each and treats each separately. Fall velocity must be prescribed along with the water-surface elevations, x-velocity, y-velocity, diffusion coefficients, and for clay sediment, bed density, critical shear stresses for erosion, erosion rate constants, and critical shear stress for deposition.

The program does not compute water-surface elevations or velocities; therefore these data must be provided. For complicated geometries, the numerical model for hydrodynamic computations, RMA2, is used. However, at this time SED2D can only accept a two-dimensional network.

Governing equations

SED2D solves the depth-integrated convection-dispersion equation in two horizontal dimensions for a single sediment constituent. For a more complete description, see Appendix G of Thomas and McAnally (1985). The form of the solved equation is

$$\frac{\partial C}{\partial t} + u\frac{\partial C}{\partial x} + v\frac{\partial C}{\partial y} = \frac{\partial}{\partial x}\left(D_x\frac{\partial C}{\partial x}\right) + \frac{\partial}{\partial y}\left(D_y\frac{\partial C}{\partial y}\right) + \alpha_1 C + \alpha_2 = 0 \quad (A5)$$

where

C = concentration of sediment

u = depth-integrated velocity in x-direction

D_x = dispersion coefficient in x-direction

V = depth-integrated velocity in y-direction

D_y = dispersion coefficient in y-direction

α_1 = coefficient of concentration-dependent source/sink term

α_2 = coefficient of source/sink term

The source/sink terms in Equation A5 are computed in routines that treat the interaction of the flow and the bed. Separate sections of the code handle computations for clay bed and sand bed problems.

Sand transport

The source/sink terms are evaluated by first computing a potential sand transport capacity for the specified flow conditions, comparing that capacity with the amount of sand actually being transported, and then eroding from or depositing to the bed at a rate that would approach the equilibrium value after sufficient elapsed time.

The potential sand transport capacity in the model is computed by the method of Ackers and White (1973), which uses a transport power (work rate) approach. It has been shown to provide superior results for transport under steady-flow conditions (White, Milli, and Crabbe 1975) and for combined waves and currents (Swart 1976). Flume tests at the U.S. Army Engineer Research and Development Center (ERDC), have shown that the concept is valid for transport by estuarine currents.

The total load transport function of Ackers and White is based upon a dimensionless grain size

$$D_{gr} = D\left[\frac{g(s-1)}{v^2}\right]^{1/3} \tag{A6}$$

where

D = sediment particle diameter

s = specific gravity of the sediment

v = kinematic viscosity of the fluid

and a sediment mobility parameter

$$F_{gr} = \left[\frac{\tau^{1n}\tau^{(1-n)}}{\rho g D (s-1)} \right]^{1/2}$$
(A7)

where

τ' = total boundary shear stress = $\rho g R S$

where

R = hydraulic radius

S = slope of water surface

n = a coefficient expressing the relative importance of bed-load and suspended-load transport, given in Equation A9
Note:

$n = 1$ for fine sediments

$n = 0$ for coarse sediments

τ = boundary surface shear stress

The surface shear stress is that part of the total shear stress which is due to the rough surface of the bed only, i.e., not including that part due to bed forms and geometry. It therefore corresponds to that shear stress that the flow would exert on a plane bed.

The total sediment transport is (in Kg/m^3) expressed as an effective concentration

$$G_P = C_A \left[\frac{F_{gr}}{A} - 1 \right]^m \frac{sD}{h} G \left[\frac{r}{t} U \right]^n$$
(A8)

where U is the average flow speed, and for $1 < D_{gr} \leq 60$

$$n = 1.00 - 0.56 \log D_{gr} \tag{A9}$$

$$A = \frac{0.23}{\sqrt{D_{gr}}} + 0.14 \tag{A10}$$

$$\log C_a = 2.86 \log D_{gr} - \left(\log D_{gr}\right)^2 - 3.53 \tag{A11}$$

$$m = \frac{9.66}{D_{gr}} + 1.34 \tag{A12}$$

For $D_{gr} < 60$

$$n = 0.00 \tag{A13}$$

$$A = 0.17 \tag{A14}$$

$$C_a = 0.025 \tag{A15}$$

$$m = 1.5 \tag{A16}$$

Note the C_a has units consistent with G_p (kg/m^3 for SED2D).

Equations A6-A16 result in a potential sediment concentration G_p. This value is the depth-averaged concentration of sediment that will occur if an equilibrium transport rate is reached with a limited supply of sediment. The rate of sediment deposition (or erosion) is then computed as

$$R = \frac{G_p - C}{t_c} \tag{A17}$$

where

C = present sediment concentration

t_c = time constant

For deposition, the time constant is

$$t_c = \text{larger of} \left\{ \begin{array}{l} \Delta t \\ or \\ \dfrac{C_d h}{V_s} \end{array} \right. \tag{A18}$$

and for erosion it is

$$t_c = \text{larger of} \begin{cases} \Delta t \\ or \\ \dfrac{C_e h}{U} \end{cases}$$ (A19)

where

Δt = computational time-step

C_d = response time coefficient for deposition

V_s = sediment settling velocity

C_e = response time coefficient for erosion

The sand bed has a specified initial thickness which limits the amount of erosion to that thickness.

Cohesive sediments transport

Cohesive sediments (usually clays and some silts) are considered to be depositional if the bed shear stress exerted by the flow is less than a critical value τ_d. When that value occurs, the deposition rate is given by Krone's (1962) equation:

$$S = \begin{cases} -\dfrac{2V_s}{h} C \left(1 - \dfrac{\tau}{\tau_d}\right) & \text{for } C < C_c \quad \text{(A20)} \\[4mm] -\dfrac{2V_s}{h C_c^{2/3}} C^{5/3} \left(1 - \dfrac{\tau}{\tau_d}\right) & \text{for } C > C_c \quad \text{(A21)} \end{cases}$$

where

S = source term

V_s = fall velocity of a sediment particle

h = flow depth

C = sediment concentration in water column

τ = bed shear stress

τ_d = critical shear stress for deposition

C_c = critical concentration = 300 mg/ℓ

If the bed shear stress is greater than the critical value for particle erosion τ_e, material is removed from the bed. The source term is then computed by Ariathurai's (Ariathurai, MacArthur, and Krone 1977) adaptation of Partheniades' (1962) findings:

$$S = \frac{P}{h}\left(\frac{\tau}{\tau_e} - 1\right) \text{ for } \tau > \tau_e \tag{A22}$$

where P is the erosion rate constant, unless the shear stress is also greater than the critical value for mass erosion. When this value is exceeded, mass failure of a sediment layer occurs and

$$S = \frac{T_L \rho_L}{h\Delta t} \text{ for } \tau > \tau_s \tag{A23}$$

where

T_L = thickness of the failed layer

ρ_L = density of the failed layer

Δt = time interval over which failure occurs

τ_s = bulk shear strength of the layer

The cohesive sediment bed consists of 1 to 10 layers, each with a distinct density and erosion resistance. The layers consolidate with overburden and time.

Bed shear stress

Bed shear stresses are calculated from the flow speed according to one of four optional equations: the smooth-wall log velocity profile or Manning equation for flows alone; and a smooth bed or rippled bed equation for combined currents and wind waves. Shear stresses are calculated using the shear velocity concept where

$$\tau_b = \rho u_*^2 \tag{A24}$$

where

τ_b = bed shear stress

u_* = shear velocity

and the shear velocity is calculated by one of four methods:

a. Smooth-wall log velocity profiles

$$\frac{\overline{u}}{u_*} = 5.75 \log\left(3.23 \frac{u_* h}{\nu}\right) \qquad \text{(A25)}$$

Equation 25 is applicable to the lower 15 percent of the boundary layer when

$$\frac{u_* h}{\nu} > 30$$

where $\overline{u}$ is the mean flow velocity (resultant of u and v components)

b. The Manning shear stress equation

$$u_* = \frac{(\overline{u}n)\sqrt{g}}{CME\ (h)^{1/6}} \qquad \text{(A26)}$$

where *CME* is a coefficient of 1 for SI (metric) units and 1.486 for English units of measurement.

c. A Jonsson-type equation for surface shear stress (plane beds) caused by waves and currents

$$\mathbf{u_*} = \sqrt{\frac{1}{2.}\left(\frac{f_w u_{om} + f_c \overline{u}}{u_{om} + \overline{u}}\right)\ (\overline{u} + u_{om})^2} \qquad \text{(A27)}$$

where

f_w = shear stress coefficient for waves

u_{om} = maximum orbital velocity of waves

f_c = shear stress coefficient for currents

d. A Bijker-type equation for total shear stress caused by waves and current

$$U_* = \sqrt{\frac{1}{2} f_c \overline{u}^2 + \frac{1}{4} f_w u_{om}^2} \qquad \text{(A28)}$$

Solution method

Equation A5 is solved by the finite element method using Galerkin weighted residuals. Like RMA2, which uses the same general solution technique, elements are quadrilateral and may have parabolic sides. Shape functions are quadratic. Integration in space is Gaussian. Time-stepping is performed by a Crank-Nicholson approach with a weighting factor (θ) of 0.66. A front-type solver similar to that in RMA2 is used to solve the simultaneous equations.

The Water Quality Transport Model, RMA4

Applications

The water quality model, RMA4, is designed to simulate the depth-average advection-diffusion process in most water bodies with a free surface. The model is used for investigating the physical processes of migration and mixing of a soluble substance in reservoirs, rivers, bays, estuarines, and coastal zones. The model is useful for evaluation of the basic processes or for defining the effectiveness of remedial measures. For complex geometries the model utilizes the depth-averaged hydrodynamics form RMA2.

The water quality model has been applied to define the horizontal salinity distribution; to trace temperature effects from power plants; to calculate residence times of harbors or basins; to optimize the placement of outfalls; to identify potential critical areas for oil spills or other pollutants spread; to evaluate turbidity plume extent; and to monitor other water quality criterion within game and fish habitats.

Limitations

The formulation of RMA4 is limited to one-dimensional (cross-sectionally averaged) and two-dimensional (depth-averaged) situations in which the concentration is fairly well mixed in the vertical. It will not provide accurate concentrations for stratified situations in which the constituent concentration influences the density of the fluid. In addition, the accuracy of the transport model is dependent on the accuracy of the hydrodynamics (e.g., as supplied from RMA2 or another flow solution).

Governing equations

The ERDC-CHL version of RMA4 is a revised version of RMA4 as developed by King and Rachiele (1989). The generalized computer program solves the depth-integrated equations of the transport and mixing process. The form of the equations solved is:

$$h\left(\frac{\partial c}{\partial t} + u\frac{\partial c}{\partial x} + v\frac{\partial c}{\partial y} - \frac{\partial}{\partial x}D_x\frac{\partial c}{\partial x} - \frac{\partial}{\partial y}D_y\frac{\partial c}{\partial y} - \sigma + kc\right) = 0 \qquad \text{(A29)}$$

where

h = water depth

c = constituent concentration

t = time

$u, v,$ = velocity components

D_x, D_y = turbulent mixing coefficients

k = first order decay

σ = source/sink of constituent

Note that the basic governing equation for RMA4 is the same as for the sediment transport model, SED2D. The difference between the two models lie in the source/sink terms.

Equation A29 is solved by the finite element method using Galerkin weighted residuals. As with the hydrodynamic model, RMA2, the transport model RMA4 handles one-dimensional segments or two-dimensional quadrilaterals or triangles with the option for curved sides. Spatial integration of the equation is performed by Gaussian techniques and the temporal variations are handled by nonlinear finite differences, consistent with the method described for RMA2.

The boundary conditions for RMA4 are specified in several optional ways. The boundary concentration may be specified absolutely at a certain level regardless of the flow direction; the concentration can be specified to be applied only when the water is leaving the model; or a mixing zone may be specified just beyond the model boundary to provide the possibility of re-entertainment of constituent into the model that may have crossed the boundary earlier. For a more detailed description of the constituent transport model, RMA4, see King and Rachiele (1989).

Within the one-dimensional formulation of the model, there is a provision for defining the constituent concentration mixing and transport at control structures as they may have been specified in RMA2. These allow for either a flow-through condition, as for example for a wier type flow, or for a mixing chamber type of flux, which would be appropriate for a navigation lock.

Note: An annotated Bibliography of selected TABS-MD applications is available at: http://chl.wes.army.mil/software/tabs/docs.htp.

REPORT DOCUMENTATION PAGE

Public reporting burden for this collection of information is estimated to average 1 hour per response, including the time for reviewing instructions, searching existing data sources, gathering and maintaining the data needed, and completing and reviewing this collection of information. Send comments regarding this burden estimate or any other aspect of this collection of information, including suggestions for reducing this burden to Department of Defense, Washington Headquarters Services, Directorate for Information Operations and Reports (0704-0188), 1215 Jefferson Davis Highway, Suite 1204, Arlington, VA 22202-4302. Respondents should be aware that notwithstanding any other provision of law, no person shall be subject to any penalty for failing to comply with a collection of information if it does not display a currently valid OMB control number. PLEASE DO NOT RETURN YOUR FORM TO THE ABOVE ADDRESS.

1. REPORT DATE (DD-MM-YYYY)	2. REPORT TYPE	3. DATES COVERED (From - To)
September 2001	Final report	

4. TITLE AND SUBTITLE	5a. CONTRACT NUMBER
Study of Complex Flows in the Lower San Bernard River, Texas	5b. GRANT NUMBER
	5c. PROGRAM ELEMENT NUMBER

6. AUTHOR(S)	5d. PROJECT NUMBER
Jose A. Sanchez, Trimbak M. Parchure	5e. TASK NUMBER
	5f. WORK UNIT NUMBER

7. PERFORMING ORGANIZATION NAME(S) AND ADDRESS(ES)	8. PERFORMING ORGANIZATION REPORT NUMBER
U.S. Army Engineer Research and Development Center Coastal and Hydraulics Laboratory 3909 Halls Ferry Road Vicksburg, MS 39180-6199	ERDC/CHL TR-01-24

9. SPONSORING / MONITORING AGENCY NAME(S) AND ADDRESS(ES)	10. SPONSOR/MONITOR'S ACRONYM(S)
U.S. Army Corps of Engineers Washington, DC 20314-1000	
	11. SPONSOR/MONITOR'S REPORT NUMBER(S)

12. DISTRIBUTION / AVAILABILITY STATEMENT
Approved for public release; distribution is unlimited.

13. SUPPLEMENTARY NOTES

14. ABSTRACT

The San Bernard River, TX, joins the Gulf of Mexico between the mouths of the Colorado River and the Brazos River. The Gulf Intracoastal Waterway (GIWW) intersects all three rivers. Two floodgates have been provided on the Brazos River and a navigation lock has been provided on the Colorado River for preventing sediment influx from rivers into the GIWW. The 6.45-km- (4-mile-) long segment between the Brazos River and the San Bernard River is the focus of the study.

The barge navigators have complained that they experience a strong west to east current through the Brazos west gate, which is related to tides and river discharge. Shallow lakes and marshlands connected to the rivers complicate the hydraulic conditions due to storage and release of floodwater. This report describes the field data collection and its analysis as well as the numerical model study. The main objectives of the study were to construct a verified, working numerical model of the relevant water bodies that are hydraulically connected and to examine the effect of a new San Bernard River outlet to the sea on improving flow conditions.

The model reasonably reproduced prototype trends in water-surface elevation, velocities, and discharges. In general, providing a new outlet is favorable for navigation through the Brazos west floodgate during low flow conditions, but some adverse effects are shown during high flow events. Factors such as the frequency of high flow events, the operation of the floodgates, the drop of water surface elevation throughout the system, and the cost of keeping the new outlet open should be considered at the time of acceptance or rejection of the proposed plan.

15. SUBJECT TERMS

Floodgates	Numerical hydrodynamic model	San Bernard River field data
Navigation difficulties	San Bernard River	Texas Inlet

16. SECURITY CLASSIFICATION OF:			17. LIMITATION OF ABSTRACT	18. NUMBER OF PAGES	19a. NAME OF RESPONSIBLE PERSON
a. REPORT	b. ABSTRACT	c. THIS PAGE			19b. TELEPHONE NUMBER (include area code)
UNCLASSIFIED	UNCLASSIFIED	UNCLASSIFIED		142	